1-1-2020

Application Of Cellulose Nanocrystals For Stabilizing Liquid-Liquid And Liquid-Gas Interfaces In Brines

Sanjiv Parajuli

APPLICATION OF CELLULOSE NANOCRYSTALS FOR STABILIZING LIQUID-LIQUID AND LIQUID-GAS INTERFACES IN BRINES

A Dissertation
Presented in partial fulfillment for requirements
for the Doctoral degree
in Engineering Science with Emphasis in Chemical Engineering
The University of Mississippi

Sanjiv Parajuli

May 2020

ABSTRACT

Cellulose nanocrystals and their interactions with different surfactants in high ionic strength brine were studied to produce stable liquid-liquid interface (emulsions) and gas-liquid (foams) for potential application in underground CO_2 storage, enhanced oil recovery, and biodegradation of crude oil at marine oil-spill sites. Three different but related studies were carried out to complete these objectives.

Interfacial and surface properties of cellulose nanocrystals (CNC) and surfactants were studied in high ionic strength (I) brines and correlated to the stability of Pickering emulsions and foams. Bis-(2-hydroxyethyl) cocoalkylamine (CAA), dodecyltrimethylammonium bromide (DTAB) and Octyl-β-D-glucopyranoside (OGP) were adsorbed onto CNC in American Petroleum Institute (API) brine (I=1.9 M), synthetic seawater (SSW), with I=0.65 M and NaCl solutions of different ionic strength. Raman spectroscopy indicated that hydroxyl groups on the CNC surface interact with all surfactants in high ionic strength media and ionic interactions still played a role at the very large ionic strengths studied herein. Contact angle measurements indicated that CAA increased the wettability of CNC by API and SSW in dodecane; DTAB, on the other hand, decreased wettability. Emulsion stability studies revealed that ionic strength, wettability, adsorption energy, and oil content strongly affect emulsion stability, more so than surfactant adsorption. DTAB increased the stability of dodecane in SSW emulsions. Emulsions stable for over 21 months were prepared with an oil volume fraction of ϕ_o=0.75. Adsorption of CAA onto

CNC limits the migration of both CNC and CAA to the dodecane/brine interface, while DTAB adsorption has the opposite effect.

The extent of biodegradation of C15-C20 aliphatic hydrocarbons in crude oil by *Serratia marcescens* after 5 days of incubation was improved from 1-12% to 6-19% by emulsifying crude oil using cellulose nanocrystals (CNC) and no added surfactant. Surface and physicochemical properties of prepared emulsions such as water salinity, presence of divalent ions and CNC concentration affect the extent of biodegradation due to their influence in emulsion stability. Stable oil in water (O/W) emulsions containing ϕ_o=0.05 were prepared with cellulose nanocrystals (CNC) at concentrations Stability studies showed a greater extent of droplet coalescence at CNC concentrations higher than 0.8 wt % for emulsions prepared in API. Coalescence was more significant in high ionic strength solutions and the presence of divalent ions compared to monovalent ions at the same ionic strength.

Stable scCO2 emulsions and foams with the CO_2 volume fraction of 0.75 were prepared at 25^{o}C and 70^{o}C respectively using CNC suspensions in API brine in the presence and absence of DTAB. The results showed that CNC suspension can stabilize scCO_2 emulsions and foams that were resistant to creaming and macroscopic coalescence over 24 hours. DTAB containing emulsions as foams showed creaming at 25^{o}C and creaming and macroscopic bubble coarsening at 70^{o}C. The stability studies of heptane and PFO emulsions at 25 and 70^{o}C showed heptane (comparatively polar oil) formed stable emulsions at both temperatures and PFO (comparatively non-polar oil) did not form stable emulsions with either CNC or CNC+DTAB conjugates present

in brine. CNC suspensions lowered γ_{ow} between heptane and brine, however, it did not alter γ_{ow} between PFO and brine suggesting CNCs preferentially adsorb onto the heptane-brine interface. The presence of CNC increased γ_{ow} between heptane and DTAB-brine solution indicating the adsorption of DTAB onto CNC surface. Excess stress of heptane emulsions showed CNC stabilized emulsions had higher excess stress at a lower shear rate, whereas, DTAB+CNC stabilized emulsions had higher excess stress at higher shear rate. Heptane emulsions prepared using CNC only produced larger droplets but showed no droplet coalescence over 24 hours, whereas, CNC+DTAB stabilized emulsions produced finer droplets but showed droplets coalescence.

DEDICATION

This work is dedicated to my wonderful wife Jyoti Nepal, my father Rajeev Parajuli, my mother Shanti Parajuli and my brother Dr.Sajeev Parajuli.

ACKNOWLEDGMENTS

I would like to take this opportunity to express my deepest and heartfelt gratitude to my advisor Dr. Esteban Ureña-Benavides for the trust he has shown in me as I explored my way through my doctoral program and supported me each time I dwindled. It goes without saying that, this dissertation would not be complete without your help and guidance. I am indebted to your mentorship, guidance, and have and will continually drive me upwards in both personal and professional life and career. I would also like to thank my committee members Drs John O'Haver, Brenda Prager, and Davita Watkins for their continuous and valuable insights and inputs to help me complete my project goals. You were ever-present and willing to help me find answers as I tried to overcome a hurdle or pave a new path during this project.

My sincere thanks to all the collaborators, colleagues, students who have helped me during this course. I would like to mention Austin Dorris, Dr. Nathan Hammer, Omaima Alazzam, Dr, Linda Motta, Dr. Mei Wang, Purnendu Sharma, and Dr. Murthy helping me at various stages of my research project either via mentoring, collaboration or both. My gratitude to Chad Middleton, Andres Rodrigues, Maren O'Haver, Sangeet Adhikari, Dariel Wicks, William Moyer, Kevin Green, Leeta Prater and Trey Heath who have spent a countless number of hours in the lab to help me generate data of highest caliber.

Last but not least, I thank all my family for their support and especially my wonderful wife Jyoti Nepal for the endless encouragement, recommendations, guidance and an enormous amount of patience required to stand the writing of this dissertation.

TABLE OF CONTENT

LIST OF FIGURES

LIST OF TABLES

CHAPTER 1
Fundamental Aspects of Nanocellulose Stabilized Pickering Emulsions and Foams

1. INTRODUCTION

Cellulose has recently been investigated as a major constituent of advanced materials, not only because of its unique physical and chemical properties but also for its potential renewability, low cost and relatively low toxicity to humans and the environment.[1,2] It can be renewable if the rate of consumption is kept at or below the rate of natural regeneration. It is one of the most abundant polymeric bio-based natural resources in the world with an annual production of 1.5×10^{12} tons, isolated from the cell wall of higher plants, tunicates, and some microorganisms such as bacteria, fungi, and algae.[3,4]

Despite being used for multiple purposes for over 150 years, structural properties at nanoscales have been unveiled relatively recently. Since 1951, when Rånby provided the first electron microscopy images of nanocrystalline cellulose,[5] the interest in nanocelluloses have increased in fields including structural materials, electronics, catalysis, and emulsions.[6–8] Despite being very hydrophilic, it has been found that nanocellulose can migrate to and assemble at fluid-fluid (liquid/liquid and gas/liquid) interfaces to stabilize them.[9–12] In addition to the fact that nanocellulose can stabilize the fluid-fluid interface, the surface of nanocellulose are highly reactive due to the presence of superficial hydroxyl groups and can be easily modified to

impart desirable properties. [13,14] These have been researched to produce stable Pickering.emulsions and foams using cellulose nanocrystals (CNCs) and cellulose nanofibers (CNFs). Even though a large body of research exists on applications of, and conditionsconducive to, CNC and CNF stabilized emulsions and foams, there are limited thorough discussions on the fundamental mechanisms and aspects that provide stability to such systems. In this review article, we summarize some of the key factors affecting the Pickering stabilization of fluid-fluid interfaces as a whole. We then report on the state of the art of interfaces stabilized by modified and unmodified CNCs and CNFs, as well as key stabilization mechanisms proposed throughout existing literature.

2. NANOCELLULOSE: CHEMICAL AND PHYSICAL PROPERTIES

Cellulose is composed of β-D-glucopyranose units linked by (1→4) glycosidic bonds and each glucopyranose units are corkscrewed 180° with respect to its neighbors with each of its repeat units referred to as cellobiose.[4] Intermolecular hydrogen bonding between hydroxyl groups and oxygen of adjacent molecules favor parallel stacking of cellulose chains to form a fibrillar structure. These structures consist of regions of high crystallinity, often referred to as nanocrystalline cellulose as well as regions with the distorted surface, often referred to as cellulose fiber.[15,16] Cellulose fibers, when subjected to mechanical treatments (ball milling, high-pressure grinding), break down into smaller structural units of cellulose that consist of both crystalline and amorphous regions, referred to as cellulose nanofiber (CNF). Controlled acid hydrolysis of the cellulose fibers yielded in a highly crystalline form of cellulose often referred to as cellulose nanocrystal or crystalline nanocellulose (CNC).[17,18] CNF and CNC vary significantly in terms of their structure and crystallinity, these variations arise from reasons such as preparation method and cellulose source (Figure 1-1). Wood pulp and sugarcane bagasse

derived CNC exhibit needle-like structures with an average length of 151 ± 39 nm, CNF, on the other hand, have complex, highly-entangled, web-like structure. XRD studies revealed CNCs have higher crystallinity than CNF.[19,20] Irrespective of their source and crystallinity, both CNF and CNC expose hydroxyl groups on their surface, which render them with surface reactivity. Such reactivity of CNF and CNC has been used for 1) chemical modification of nanocellulose surfaces via esterification, polymer grafting, oxidation and 2) non-covalent surface modifications such as adsorption. [21,22]

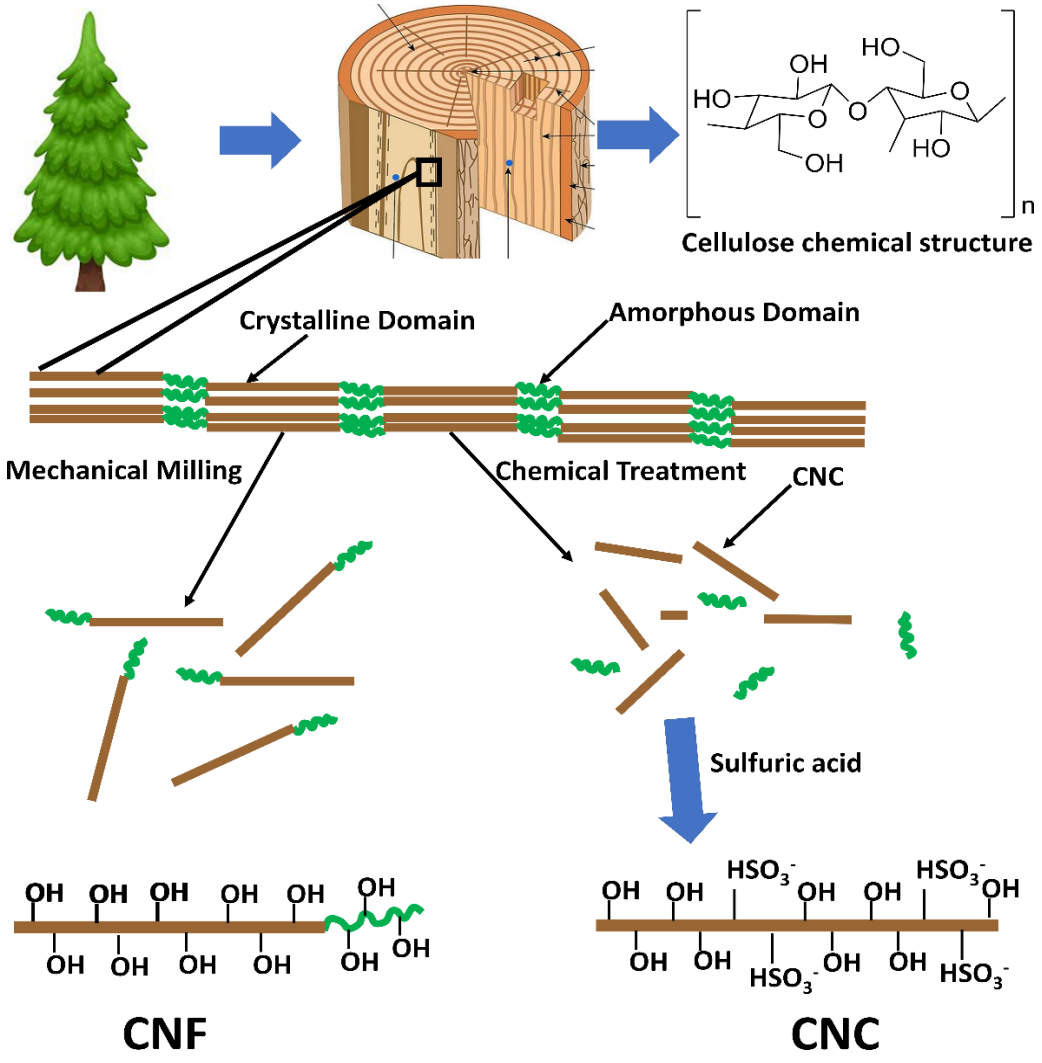

Figure 1-1 Schematic diagram of the preparation of CNCs and CNFs from wood pulp along with their chemical and morphological structures

CNF and CNC exhibit other desirable properties such as low density, chirality, high surface area, ease to functionalize and thermo-mechanical performance. These properties have been utilized to explore the potential application of nanocelluloses in the development of biosensors,[23] optical/electronic devices,[24] drug delivery systems,[25,26] anti-microbial food applications, [27] and nanocomposites for advanced materials.[28,29] Although nanocellulose (both crystals and fibers) are hydrophilic, a detailed study of the crystalline structure of mildly hydrolyzed cellulose Iβ and cellulose II, indicated that the 200 crystalline plane is preferentially etched. Consequently, C-H moieties are exposed at this surface, rendering hydrophobic properties to it. [30–32] The presence of both hydrophilic and hydrophobic moieties implies that CNC and CNF can migrate to and stabilize interfaces, even though they are considered non-surface active. This surface property of CNC/CNF has been extensively studied and used to stabilize the liquid-liquid and liquid-gas interface. Thus crystalline and fibrillar forms of nanocelluloses have also been used to prepare hydrogels, aerogels, foams, and emulsions.[33,34] Solid nanoparticle stabilized Pickering emulsions and foams find applications in multiple industries including food, pharmaceutical, cosmetic, agriculture, environmental and energy sectors.[14,35] While fundamental properties of Pickering emulsions are similar to traditional surfactant-stabilized emulsions, the mechanisms involved in stabilization of Pickering emulsions and foams are significantly different. Unlike surfactants, nanoparticles do not significantly reduce the interfacial tension between two fluids to favor and stabilize emulsion/foam droplets; rather nanoparticles migrate and adsorb irreversibly to the fluid interface and arrange themselves to form a rigid structure that prevents coalescence.[36,37] The energy requirement (ΔE_{ads}) for desorption of spherical nanoparticles having a radius (r) can be estimated using the equation given below.

$$\Delta E_{ads} = \pi r^2 \gamma_{OW}(1 \pm cos\theta)^2 \qquad (1)$$

where γ_{ow} is interfacial tension and θ is a three-phase contact angle. It has been estimated that the desorption of particles from the fluid-fluid interface requires energy in the order of 10^5 k_BT, while desorption of surfactant generally required on energy in the order of a few hundred k_BT, this indicates that Pickering emulsions are generally more stable than surfactant stabilized emulsions. [38,39] For the rod-shaped particles such as CNC, the adsorption energy can be estimated assuming they are cylindrical with length L and radius rand is given by equation (2).[40]

$$\Delta E_{rod} = 2rL\gamma_{OW}(\theta_{ow}\cos\theta_{ow} - \sin\theta_{ow}) + \gamma_{OW}r^2\cos\theta_{ow}\,[2\theta_{ow} - \sin(2\theta_{ow})] \quad (2)$$

In equation 2, ΔE_{rod} is adsorption energy for rod-shaped particles θ_{ow} is the contact angle, γ_{ow} interfacial tension. In addition to these parameters rheology, and intermolecular interactions also play a crucial role in the stability of the particle-stabilized interface.

In this review, advances in the understanding of nanocellulose stabilized liquid-liquid and liquid-gas interfaces, and the influence of surface modification on interface stability are discussed. After a brief introduction to mechanisms of interfacial stability, the behavior of modified and unmodified CNC and CNF at liquid-liquid interfaces will be discussed, followed by a discussion on aspects of nanocelluloses at liquid-gas interfaces.

3. FACTORS AFFECTING PICKERING STABILIZATION OF THE INTERFACE

Several factors (Figure 1-2) affect the ability of nanoparticles in general to stabilize the liquid-liquid and gas-liquid interfaces. Some of these factors will be discussed in detail in the following sections.

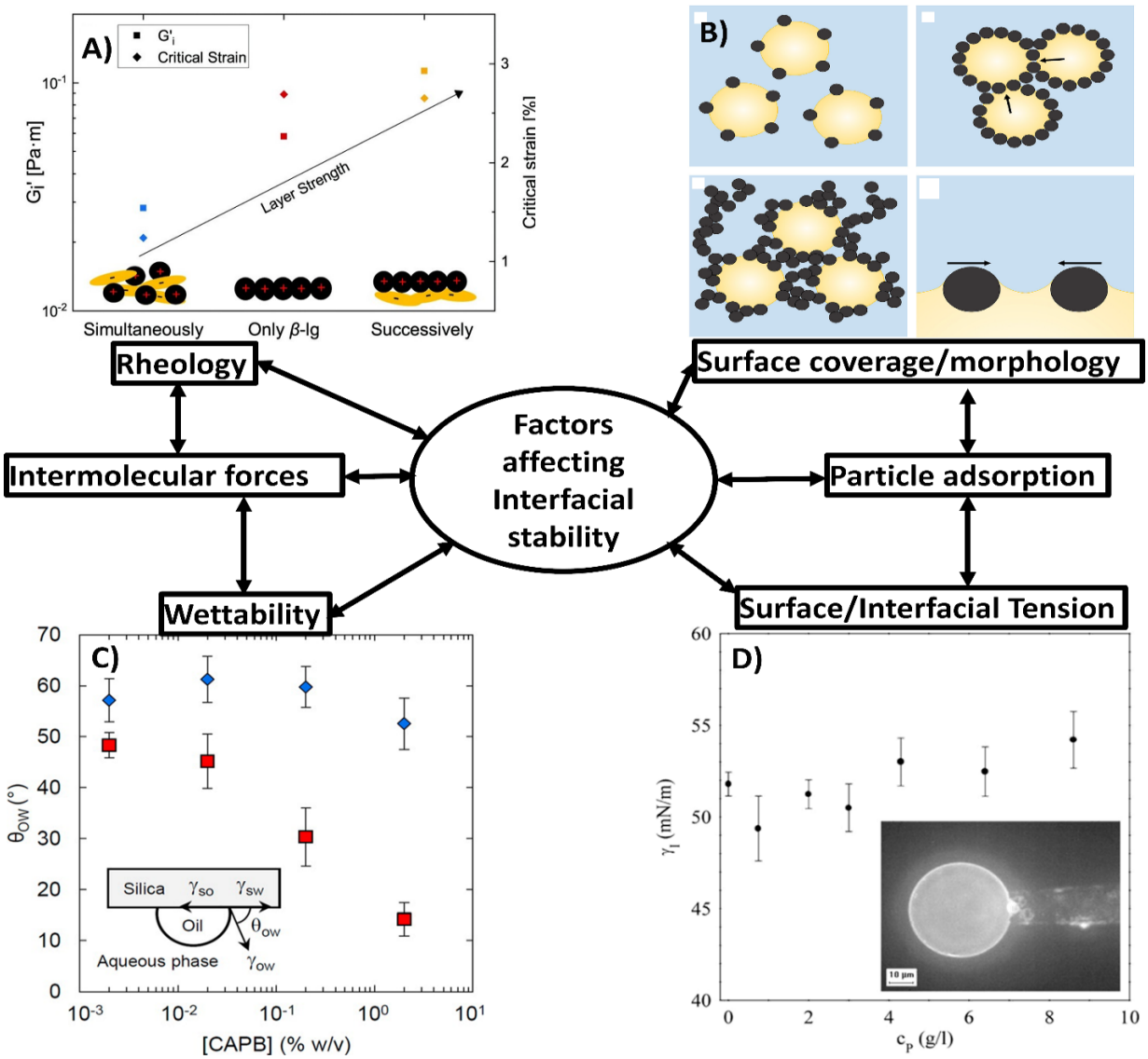

Figure 1-2: Properties of different interfaces stabilized by nanoparticles and nanofibers. A) the schematic of equilibrium interfacial storage modulus (G_i') and critical strain of the protein-polysaccharide layer. Reproduced from Ref. *[41]* with permission from the Royal Society of Chemistry. B) Schematic representation of Pickering particles (lipids) at the surface and/or in the continuous phase of O/W emulsions. Reprinted from *[38]* Copyright (2018), with permission from Elsevier. C) Static contact angles (θ_{ow}) of captive dodecane droplets in surfactant solution on hydrophilic silicon wafers versus initial concentration of surfactant in DI water (◊) and SSW (□). The inset of the figure shows a schematic diagram of the oil/aqueous-phase/silica contact angle. Reprinted with permission from *[42]*. Copyright (2014) American Chemical Society." D) The γ_{ow} of isooctane droplets stabilized by silanized particles versus particle concentration with inset showing particle-coated droplet in a micropipette. Reprinted with permission from*[43]*. Copyright (2003) American Chemical Society.

3.1. Rheology

One of the key factors affecting the stability of Pickering emulsions and foams is the mechanical properties of the fluid/fluid interface, especially the interfacial elasticity and viscosity. The increment in viscosity and elastic properties of Pickering interfaces (Figure 1-2A) is often attributed to two factors: coating of droplets with solid particles and aggregation of particles in the continuous phase. Measurements of interfacial viscosity along with other rheological properties can be critical in designing a stable fluid-fluid interface, as they provide information about the morphology and dynamics at the interphase. [44,45] Based on the interfacial deformation pattern and stresses used, two distinct types of interfacial rheology measurements are often carried out:

3.1.1. Interfacial dilatational rheology

The interfacial dilatational modulus (E) relates the variation of the interfacial area (A), to the corresponding dilatational stresses. It is often measured via pendant drop tensiometry by applying a dilatational perturbation to the relative drop area, while simultaneously recording the interfacial tension (γ). The dilatational modulus is then found by the direct application of equation 2.

$$E = \frac{d\gamma}{d \ln A} \qquad (2)$$

From equation 2 it can be seen that for a stable interface, where there is a minimal change in surface area, the dilatational viscoelasticity is a large number compared to the unstable interface, where the relative area variation is more prominent.

For measurements carried out using the oscillating drop method, a sinusoidal variation of the area is applied such that

$$\Delta A/A_0 = (\Delta A/A_0)_{max} \sin(2\pi\nu t) \qquad (3)$$

Where $\Delta A = A - A_0$, and A_0 is the reference interfacial area. The perturbation results in a harmonic variation of the interfacial tension

$$\Delta\gamma = (\Delta\gamma)_{max} \sin(2\pi\nu t + \phi) \qquad (4)$$

The subscript 'max' represents the amplitude of the oscillation, ϕ is the phase shift between the area and the interfacial tension signals and ν is the frequency. These equations are often expressed in terms of angular frequency $\omega = 2\pi\nu t$.[46,47]

Oscillatory surface dilatational measurements are also useful in finding the dilatational storage modulus (E') and loss modulus (E"). The storage modulus is equal to the pure elastic contribution and the loss modulus corresponds to viscous contributions. They are calculated as

$$E' = (\Delta\gamma)_{max} \left(\frac{A_0}{\Delta A}\right)_{max} \cos\phi \qquad (5)$$

$$E'' = (\Delta\gamma)_{max} \left(\frac{A_0}{\Delta A}\right)_{max} \sin\phi = \omega\eta_d \qquad (6)$$

where η_d is the interfacial dilatational viscosity [48,49]

3.1.2. Interfacial shear rheology

Interfacial shear rheology involves inducing shear at the interface without changing the shape/area of the interface. Analogous to dilatational rheology, an oscillatory shear test performed at an angular frequency ω, and strain amplitude ε_0, results in a shear deformation (ε) given by

$$\varepsilon = \varepsilon_{max} \sin(\omega t) \qquad (7)$$

The corresponding shear rate ($\dot{\gamma}$) is

$$\dot{\gamma} = \dot{\gamma}_{max} \cos(\omega t) \qquad (8)$$

The shear stress (τ) is shifted with respect to the strain by a phase angle ϕ

$$\tau = \tau_{max} \sin(\omega t + \phi) \qquad (9)$$

Based on these equations the interfacial shear storage (G') and loss (G") moduli are given by

$$G' = \frac{\tau_{max}}{\varepsilon_{max}} \cos \phi \qquad (10)$$

$$G" = \frac{\tau_{max}}{\varepsilon_{max}} \sin \phi \qquad (11)$$

Pickering interfaces are shown to have elastic properties at low strain with G' dominating G", however, as the strain is increased they exhibit plastic properties indicated by a slight drop in G' and increase in G".[50,51] Large values of G' relative to G" are indicative of a rigid interfacial layer.

3.2. Morphology and assembly of particles at interfaces

The morphology of nanoparticles, their concentration, the surface coverage, and aggregation state significantly affect the stability of the fluid-fluid interface. It has been well established that nanoparticles migrate to the interface of fluids they are partially wetted by and align themselves to form a compact structure (Figure 1-2B) that helps stabilize emulsions and foams, generally without lowering interfacial tension. The properties of these mechanical barriers at the interface can be studied in terms of surface coverage and morphology.[52] Until recently most of the Pickering emulsions were prepared using spherical particles, however, it was found that ellipsoidal particles can form a more compact monolayer at the interface as compared to spherical particles leading to the formation of an interfacial monolayer with a higher elastic modulus and hence a more stable interface.[52,53] The roughness of solid particle surface also affects their ability to stabilize interface, silica nanoparticles that exhibited rough surfaces were incapable of stabilizing emulsions prepared using water as aqueous phase and isooctane/octanol as the organic phase. The reduced surface contact might be the reason for the reduced ability of rough surfaces to stabilize droplets.[43]

Besides the morphology of the solid particles, the surface coverage of the interface by the

particles is also an important parameter influencing the stability of the interface. It has been identified that surface coverage of droplets by particles is important for stabilization of oil/water or gas/water interface.[38] The surface coverage (C) is defined as the ratio of a theoretical maximum surface area susceptible to coverage by particles(S_M) to the total surface area displayed at the interface (S_I).[54,55]

$$C = \frac{S_M}{S_I} \qquad (9)$$

For cuboid nanoparticles having a length (l), width (w), height (h) and density (ρ) and mass (m)

$$S_M = N_p \times l \times h = \frac{m}{h\rho} \qquad (10)$$

Where N_p is the number of particles

And for droplet size having a Sauter mean radius (r) and Sauter mean diameter of (d_{32})

$$S_I = \frac{3V_{oil}}{r} \qquad (11)$$

Combining, (9), (10), and (11) we get

$$C = \frac{md_{32}}{6h\rho V_{oil}} \qquad (12)$$

Low surface coverage resulted in the coalescence of emulsion droplets stabilized by colloidal particles.[38,54] It has been further identified that a critical degree of surface coverage is attained in a system where the number of particles is not sufficient to cover entire interface, during such process, the droplets will coalesce rapidly until the critical coverage is attained.[56] However, it has also been proposed that if multiple layers of nanoparticles exist at the interface, further adsorption can lead to droplet coalescence.[40,57]

3.3. Surface/Interfacial tension

Lowering of interfacial tension between two fluids is critical for surfactant-stabilized droplets. Adsorption of surfactant at interface favors droplets formation due to low interfacial

tension, besides, they also prevent coalescence and Ostwald ripening.[58] Solid unmodified nanoparticles, however, do not generally lower interfacial tension between two fluids (Figure 1-2D), they rather form a mechanical barrier at the interface thereby preventing coalescence of the droplets.[43] In systems containing insoluble dispersed particles where measurement techniques such as Du Nuoy ring and Wilhelmy plates do not provide accurate results due to kinetics of particle migration to the interface, it is a common practice to use methods such as axisymmetric drop shape analysis, in addition to capillary force, drop weight and maximum bulk pressure measurements are often used to measure interfacial tension (γ_{ow}) between two immiscible fluids using the Young-Laplace equation.

$$\Delta p_0 = \Delta \rho g h - \gamma_{ow}\left(\frac{1}{R_1} + \frac{1}{R_2}\right) \qquad (13)$$

Where Δp is Laplace pressure, and R_1 and R_2 are radii of curvature of a pendant drop and ρgh is the hydrostatic pressure. Surface and interfacial tension play a critical role in facilitating the formation of droplets and bubbles. Equation 14 shows that the free energy of droplet formation (ΔG_{drop}) is controlled by γ_{ow} and temperature (T).

$$\Delta G_{drop} = A_{OW}\gamma_{OW} + n_p(\Delta E_{ads} - T\Delta S_{ads}) \qquad (14)$$

In the equation above, A_{ow} is the interfacial area, n_p is the number of particles and ΔE_{ads} is the adsorption energy of particles and fluid-fluid interface. The effect of the entropy term (ΔS_{ads}) in the equation is expected to be relatively small for large particles. It should be noted that ΔE_{ads} is can be further expanded (See equation 1) to reveal that it depends on the wettability of particles by the fluids, indicating that interfacial tension, particle concentration, and wettability are factors the govern droplet formation.

There is little evidence that indicates interfacial tension between two fluids is affected by the adsorption of unmodified nanoparticles at the interface of two fluids. Bare silica does not

lower the surface/interfacial tension between air/water and trichloroethylene (TCE)/water, however, a coating of these nanoparticles with sulfonated polystyrene resulted in a decrease in interfacial tension between TCE/water indicating that the grafted polymer penetrated the oil/water interface.[59,60] Nanoparticles grafted with hydrophobic polymers increases the hydrophobicity of nanoparticles, at the interface the hydrophobic polymer arrange themselves such that they are partitioned towards the oil phase while the nanoparticles are partitioned towards the aqueous phase such alignment of polymer-grafted nanoparticles also reduce the surface tension.[61,62]

3.4. Adsorption/ wettability

Adsorption of nanoparticles at the fluid interface is a single phenomenon critical to stabilizing Pickering emulsions and foams. The nanoparticles adsorb at the interface to form a monolayer, they form a rigid mechanical structure that prevents the fluid-fluid interface from coalescing thereby improving the stability of emulsions and foams. The stability due to adsorption primarily arises from the high energy required (ΔE_{ads}) for desorption of nanoparticles from the interface as indicated by Equation (1).[42,63–65] As mentioned earlier, physical properties (shape, size) and surface chemistry of nanoparticles are crucial in determining adsorption/ wettability of nanoparticles and hence their ability to stabilize the fluid-fluid interface.[66] Particles can be used to stabilize both O/W and W/O interfaces provided that both fluids partially wet the surface of the particles, however, the type of emulsion/foam stabilized by the particle depends on the wettability of particles. Wettability of a particle can be calculated by the measurement of the three-phase contact angle (Figure 2C) between particle, organic, and aqueous phase, as shown in Equation 1. These contact angle values can be used to estimate the relative position of the particles at the interface.[54,55]

$$\cos\theta = \frac{\gamma_{po} - \gamma_{pw}}{\gamma_{ow}} \quad (1)$$

Where γ_{po} is interfacial tension between particle and oil phase, γ_{pw} is interfacial tension between particle and water and γ_{ow} is interfacial tension between oil and water and θ is the three-phase contact angle. Particles that have contact angle in the range of $0^o \leq \theta \leq 90^o$ and hence are inherently hydrophilic stabilize interfaces O/W interfaces, whereas hydrophobic particles with contact angle ranging from $90^o \leq \theta\ 180^o$ stabilize W/O interfaces. [66–70]

3.5. Intermolecular and surface forces

The stability of the fluid-fluid interface is governed by intermolecular forces (IMFs) and forces between surfaces and fluid. The stability of the interface is governed by the colloidal stability of particles. It should be noted that the interactions listed are not exhaustive and it is outside the scope of the current study to discuss each of these interactions in detail. This article will only discuss these forces very briefly in a qualitative manner and serve to provide a brief introduction to the subject. IMF and surface forces acting on colloidal systems can be broadly categories into

1. DLVO interactions
    a. Van der Waals forces
    b. Electrostatic double-layer forces
2. Non-DLVO interactions
    a. Hydration forces
    b. Hydrophobic interactions
    c. Depletion forces
3. Capillary forces

3.5.1. DLVO interactions

DLVO interactions have been used to successfully explain the properties of many colloidal systems, emulsions, and foams.[71,72] Van der Waals interactions are short-range attractive forces that arise due to the oscillation of electron clouds. The strength of van der Waal's attraction is affected by the dielectric properties of colloidal particles and background medium. [72–75] Electrostatic double-layer interactions occur due to the formation of non-homogenous charge distribution around the surface of colloidal particles that have a surface charge. The layer of charge is often called double layer and the width of the layer (Debye length) depends on the concentration of electrolytes in the medium. Debye length (λ_D) is measured using equation (16) and is dependent on the electric permittivity of medium (ε), the concentration of an i^{th} component in bulk solution (C_i) and valency of i^{th} electrolytes present in the solution (Z_i) [72–78]

$$\lambda_D = \sqrt{\left(\frac{e^2}{\varepsilon\varepsilon_0 k_B T}\sum_i C_i Z_i^2\right)} \qquad (16)$$

Where e is the charge of an electron, ε_0 is dielectric constant, k_B is Boltzmann constant, and T is the temperature. Van der Waals forces and electrostatic double-layer forces are often also reported as DLVO forces. Hence, DLVO theory can be used to explain the stability of aqueous colloidal suspension as an interaction between van der Waals force and repulsive electrostatic double-layer force.[72] Electrostatic double-layer pressure between two charged surface, wherein there are no interactions between counterions and the surface, can be estimated using contact value theorem expressed in equation (17), where P(D) is double repulsive pressure at distance D, k is Boltzmann constant, T is temperature ρ_s and ρ_m are ionic densities at surface and midplane respectively.

$$P(D) = kT[\rho_s(D) - \rho_s(\infty)] = kT[\rho_m(D) - \rho_m(\infty)] \qquad (17)$$

3.5.2. Non-DLVO interactions

As the proximity between two surfaces reduces to the nanometer range, the theory of DLVO forces often fails to describe the interactions between 2 surfaces. At such proximity, another set of short-range forces dominates DLVO forces. These short-range forces are often described as non-DLVO forces and can be attractive, repulsive, or oscillatory. Solvation of solutes/ particles in the aqueous phase can be affected by properties of both solvent and surfaces, at short range solvation (hydration if water) interaction arises between particles and extended surfaces. Equation 10 can be extended to estimate repulsive solvation pressure is given by equation (18). [79]

$$P(D \to 0) = -\rho(\infty)kT \qquad (18)$$

While the solvation force discussed earlier can be oscillatory depending on the separation, solvation forces can also be monotonically repulsive or attractive depending on the properties of solvent and surfaces. If the solvent in consideration is water hydration forces can act as repulsive forces whereas hydrophobic interactions can act as attractive forces.[80] Yet another non-DLVO force that could play an important role in colloidal stabilization of systems consisting of particles and polymer/surfactants is depletion forces. These forces arise when large macromolecules are suspended in a dilute solution of non-adsorbing polymers/micelles due to the exclusion of small non-adsorbed species (depletants) from the space between two large particles when the particles are close enough. Depletion forces are equal to osmotic pressure outside the gap between two particles and can be either attractive (promotes flocculation) or repulsive (prevents flocculation) in nature depending on the distance between the particles, concentration of depletant.[81–84] Derjaguin approximation (Equation 19) is often used to quantify depletion forces (f_s) between particles of radius R, separated by the distance h and have

osmotic pressure Π.

$$f_s(h) = -\pi R \int_{\infty}^{h} \Pi(h')dh' \qquad (19)$$

3.5.3. Capillary forces

Capillary forces are caused by the formation of the thin film at the curved interface between fluids. The curvature at the interface generated due to surface/interfacial tension of the fluids creates capillary pressure that is used as a measure of the stability of the film which in turn is correlated stability of the interface (emulsions/foams). Maximum capillary pressure (P_c^{max}) provides the measure of the maximum pressure the thin film between the fluids can withstand before it ruptures resulting in droplet/bubble coalescence. Denkov (1992) developed a model to calculate (P_c^{max}) for the thin film between two fluids with surface tension (σ) stabilized by a monolayer of spherical particles of radius R, they found that the maximum capillary pressure can be calculated using equation 20.

$$P_c^{max} = p^* \frac{2\sigma}{R} \qquad (20)$$

Where p* is a positive dimensionless parameter that is a function of interface coverage and packing parameter of the particles at the interface.[85,86] This equation was further extended to develop equation 14 which can be used to calculate maximum capillary pressure in the film stabilized by a double layer of particles that take hexagonal packing formation.

$$P_c^{max} = p^* \frac{2\sigma}{R}(\cos\theta + z) \qquad (21)$$

In equation 21, θ is the contact angle between particle and fluids and z is a constant dependent on the arrangement of fluids in the film.[57,87] The films when initially formed are in swollen state and drain until the equilibrium is reached, the kinetics of film thinning (lamella drainage) can be characterized by an equation known as Reynolds equation (Equation 22).

$$-\frac{dH}{dt} = \frac{2H^3\Delta P}{3\mu R_f^2} \quad (22)$$

Where H is the film thickness, t is drainage time, ΔP is the pressure drop causing the film thinning, μ is bulk viscosity and R_f is the film radius.[88,89]

4. STABILIZATION OF LIQUID-LIQUID INTERFACE

Both CNCs and CNFs (modified/unmodified) have been used extensively to stabilize the liquid-liquid interface to form emulsions and emulsion gels and numerous studies have shown their ability to stabilize liquid-liquid interface. [90–94] In general, there is a consensus in the existing literature that partial wetting of nanocellulose by fluids is critical to the stabilization of the interface. However, as mentioned in earlier sections factors such as morphology, surface activity, and intermolecular forces are also important in determining the ability of nano cellulosic particles to stabilize an interface. Unmodified CNCs/CNFs are extensively known to stabilize O/W type emulsions [37,54,95] while surface-modified nanocelluloses with increased hydrophobicity have been successfully used to prepare W/O emulsions.[96,97] The following section highlights studies that used unmodified CNC/CNF to prepare CNC Pickering emulsions along with discussions on the factors that determine the mechanisms of Pickering stabilization.

4.1. Stabilization of liquid-liquid interface by unmodified nanocelluloses

4.1.1. Rheology

Both CNC and CNF have been used to modify the rheological properties of the aqueous phase for various applications. [98–101] The tendency of CNC and CNF form H-bonding with neighboring water molecules resulting in the formation of a percolated network which causes an alteration in the rheological properties of the aqueous suspension. CNC and CNF suspensions exhibit shear-thinning, viscoelastic properties, often with enhances storage modulus in the aqueous medium. [99,101,102] In addition to the aqueous suspension, nanocellulosic material

has also been reported to improve the stability of liquid-liquid interface by altering its rheological properties and hence stabilizing the Pickering emulsions. Rheological properties of CNC and CNFs stabilized O/W emulsion prepared using hexadecane and 50 mM NaCl were examined. Visual examination of the prepared emulsions indicated that CNC stabilized emulsions were flowing whereas CNF stabilized emulsions were gel-like. The dynamic mechanical properties of the emulsions studied using small amplitude oscillatory shear (SAOS) showed G'>G" for emulsions prepared using both CNC and CNF, with G' and G" two orders of magnitude greater for CNF stabilized emulsions (Figure 1-3).[103] The increased viscoelastic properties were attributed to the interconnections that strongly strengthen the emulsions. Furthermore, large amplitude oscillatory shear (LAOS) studies of the CNC stabilized emulsions were carried out to study properties variation in relation to droplet size and size distribution, and stability. Strain sweep measurements were carried out up to 100%. The results indicated that after deformation, CNC stabilized emulsions showed the ability to return to their original state. CNF emulsions, on the other hand, showed improved mechanical stability but were unable to their original state after deformation. The authors suggest that the disruption of CNF fibers and potential desorption of CNF from the interface after deformation could potentially explain the results. [104] CNF stabilized emulsions also shows a prominent increase in viscosity [105,106] due to the formation of a percolated network of its fibers in the aqueous phase, this results in the entrapment of the droplets within the network which promotes emulsion stability by limiting the droplet collision and coalescence.

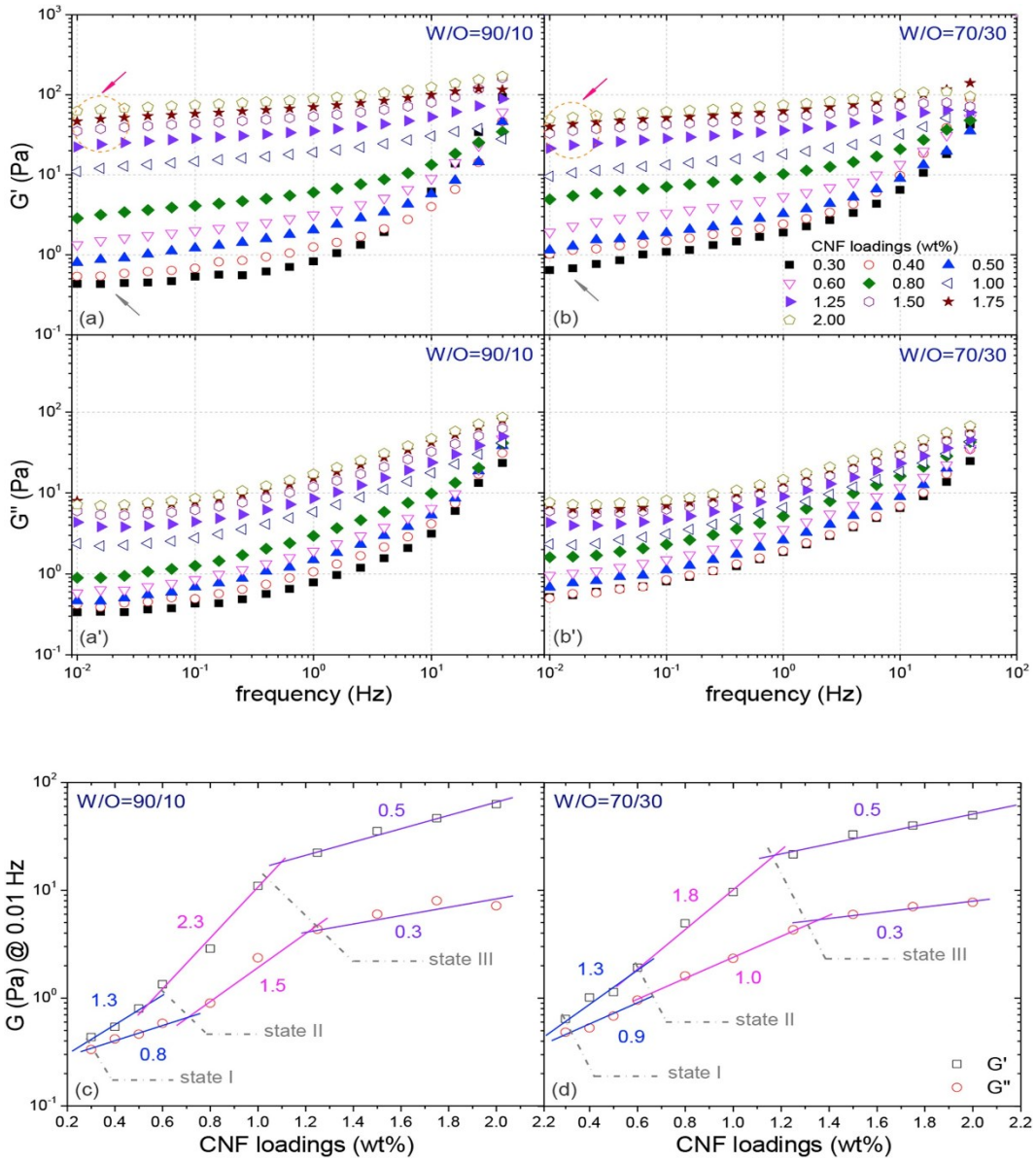

Figure 1-3: Dynamic moduli for the emulsions with the W/O ratio of (a, a') 90/10 and (b, b') 70/30. The CNF loading dependences of low-frequency dynamic moduli for these two emulsion systems are summarized in (c) and (d). Reprinted from, [*[103]*] Copyright (2019), with permission from Elsevier.

4.1.2. Particle adsorption, concentration and surface coverage

Particle adsorption can affect the extent of their ability to stabilize an interface. It has been found that a monolayer of ellipsoidal particles exhibits high surface modulus and produce more elastic monolayer, and more yield structured orientation than spherical particles. [107,108]

These findings suggest that features such as the rod-like shape of CNC along with its high aspect ratio can be exploited to prepare the stable liquid-liquid interface. Kalashnikova et al. first reported the use of CNC obtained from hydrolysis of bacterial cellulose by hydrochloric acid to stabilize hexadecane/styrene emulsions in DI water. The concentration of bacterial cellulose nanocrystals (BCN) affected the stability of emulsions to creaming and droplet size. It was found that the average droplet diameter decreased with an increase in BCN concentration, however, at BCN concentration ≥ 2 g/L the emulsions droplets plateaued with no effect of BCN concentration on droplet size beyond this concentration. The organization of BCN at the interface was studied in terms of surface coverage, it was found that at low BCN concentration droplets showed identical surface coverage of 60% minimum required for the formation of stable emulsions. At a higher concentration of BCN, the surface coverage increased with an increase in BCN concentration. It should be noted that the surface coverage calculations are based on the area covered by individual BCN, while in reality, aggregates are likely to be formed at the interface implying that the calculated values are likely an overestimate of actual coverage. In addition to surface coverage, the authors postulate that a thin cross-section of BCN (7nm) allows for a certain degree of flexibility, with the curvature of BCN and hence its organization at the interface limiting the size of the droplets formed by BCN (Figure 1-4). Other studies have also identified the surface coverage and limited coalescence as important factors guiding stability of CNC based Pickering emulsions.[53,109,110] The structure of the oil-water interface stabilized by charged and uncharged cotton CNC was studied in hexadecane/styrene droplets using small-angle neutron scattering. It was found that the thickness of the CNC stabilized interface (7nm for charged and 18nm for uncharged) did not change with the increase in CNC concentration or addition of 5 mM (for desulfated CNC) to 50mM (for sulfated) NaCl into the aqueous phase

(Figure 4-g). It was suggested that the CNC adsorb at the interface as a monolayer and that the organization of CNCs at the interface is such that they interact with oil phase-only via their hydrophobic (2 0 0) plane (Figure 1-5A).[32,53]

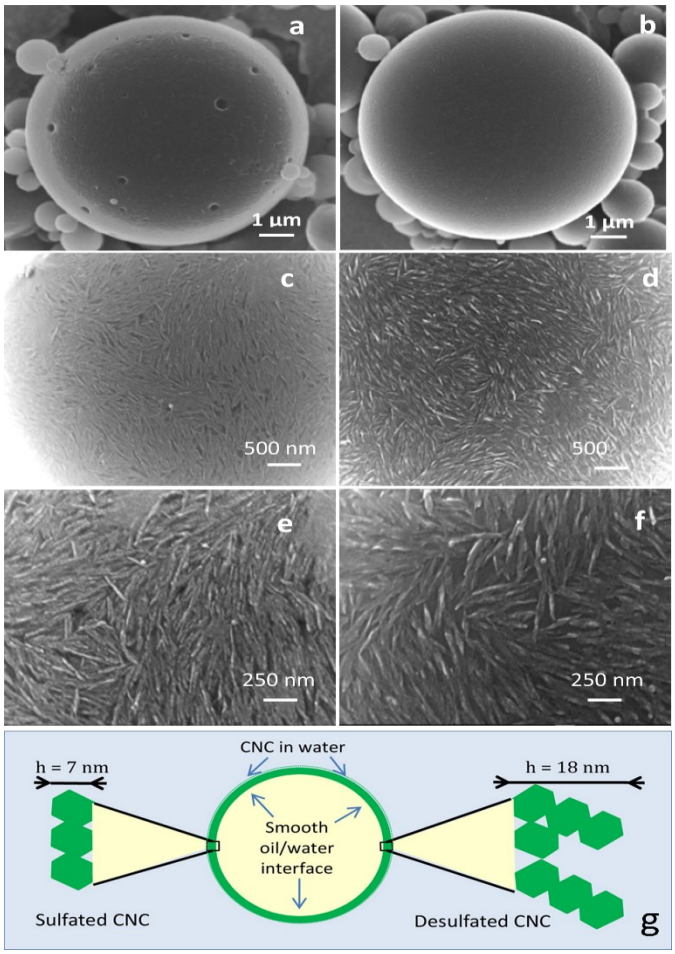

Figure 1-4: Morphology of CNC stabilized styrene emulsions (a, b), orientation of CNC at the oil-water interface (c-f) and the schematics of CNC packing and orientations based on small-angle neutron scattering. Adapted with permission from *[109]*. Copyright (2016) American Chemical Society

4.1.3. Intermolecular and surface forces

Forces acting to stabilize the liquid-liquid interface can be broadly categorized as intermolecular forces acting between the nanocellulose particles and the forces acting to drive adsorption of CNC/CNF at the interface. The forces thus acting in the Pickering stabilization of the interface will primarily depend on the surface properties of the nanocellulose, and

components present at the interface. It is thus often the case that forces responsible for Pickering stabilization be are discussed on a case by case basis, but few important forces have been discussed in the literature. Electrostatic double-layer forces and van der Waals forces between the charged surface sulfated CNC are discussed frequently in studies that use CNC to stabilize emulsions. Cotton derived sulfated CNC (0.1 wt%) with a surface charge density of larger than 0.03 e/nm^2 were unable to stabilize the hexadecane in water emulsion, however, neutralization of surface charge by HCl resulted in the formation of stable emulsions. It was further observed that the average droplet diameter of emulsions decreased with a decrease in surface charge. The electrostatic repulsion between charged CNC limits their adsorption to the oil-water interface thereby diminishing their ability to stabilize the emulsions. [32] Varanasi et al., however, stabilized canola oil and hexadecane emulsions using unmodified CNC (1 wt%) with the surface charge density of 0.11 e/m^2. The authors argue that at high enough CNC concentration, they start to form aggregates due to H-bonding between themselves and water molecules, these aggregates have a higher force of attraction that dominates the repulsive force between CNC and interface, resulting in adsorption of the aggregates. [111] The addition of electrolytes to the aqueous suspension screens the surface charge, this results in van der Waals force of attraction, inter and intramolecular H-bonding and hydrophobic interactions between nanocelluloses being more dominant than the electrostatic repulsion causing the CNC to form aggregates, which facilitates the stabilization of emulsions. [106,111]

In a different study, O/W emulsions containing 10 wt% sunflower oil in 0.16 wt% NaCl solution were prepared using the combination of unmodified CNC and non-adsorbing CNF using a two-step sequential addition method. CNC stabilized Pickering emulsions were first prepared and then followed by the addition of CNF at varying concentrations. The authors suggest that the

addition of CNF within induces depletion forces resulting in the flocculation of emulsion droplets (~2μm), with the extent of flocculation increasing with increasing CNF concentration until a critical CNF concentration (0.2 wt%). Furthermore, at CNF concentration higher than 0.3 wt% the authors attributed the emulsion stability to the formation of emulsion gels due to the formation of the CNF network in the medium. The findings thus indicate that at intermediate concentration range, CNF can improve the stability CNC Pickering emulsions by depletion forces, while at higher CNF concentration the stabilization mechanism could be due to the formation of emulsion gels. [112]

4.1.4. Adsorption and wettability

Adsorption and wettability are yet another key factors that affect their ability to stabilize the liquid-liquid interface. CNC and CNF are not surface active but can adsorb to many oil-water interfaces and thereby stabilizing it. CNC exhibits an excellent ability to adsorb to the interface. Wide-angle X-ray spectroscopy of CNCs indicates that crystalline planes of the CNC are not identical and consist of a flat hydrophobic plane (2 0 0) which imparts amphiphilic properties to CNC (Figure 1-5A). [32] Furthermore, it has been suggested that CNCs orient themselves at the interface along their length and interact with the oil phase via their hydrophobic plane.[53] Despite being very hydrophilic due to the presence of a free hydroxyl group on their surface, and relatively small water contact angle (θ=22^o) for unmodified CNC and water contact angle of 62^o for transesterified CNCs they do adsorb to the oil-water interface (Figure 1-5B).[113–115] Unmodified CNF, on the other hand, exhibits a relatively larger water contact angle (θ=53^o) [116], however, the mechanism by which they adsorb to the interface has not been properly understood. Interestingly, despite small water contact angles, both CNC and CNF have been successfully used to stabilize different kinds of liquid-liquid interfaces, especially when the

charges on the surface are screened either by the addition of electrolytes or by adjustment of pH.[117] Since both CNC and CNF in their unmodified state have contact angle less than 90° they align themselves more towards the aqueous phase, the emulsions stabilized by these nanocelluloses always have oil as a discrete phase and aqueous suspension as the continuous phase in an emulsion they stabilize. It should be noted that measuring static contact angle on CNC/CNF films is very challenging due to the absorption of water molecules by the films resulting in film swelling and continuous decrease in measured contact angle. Furthermore, the values of the measured angle differ based on the method used for film formation, cellulose type, and surface modifications. [118]

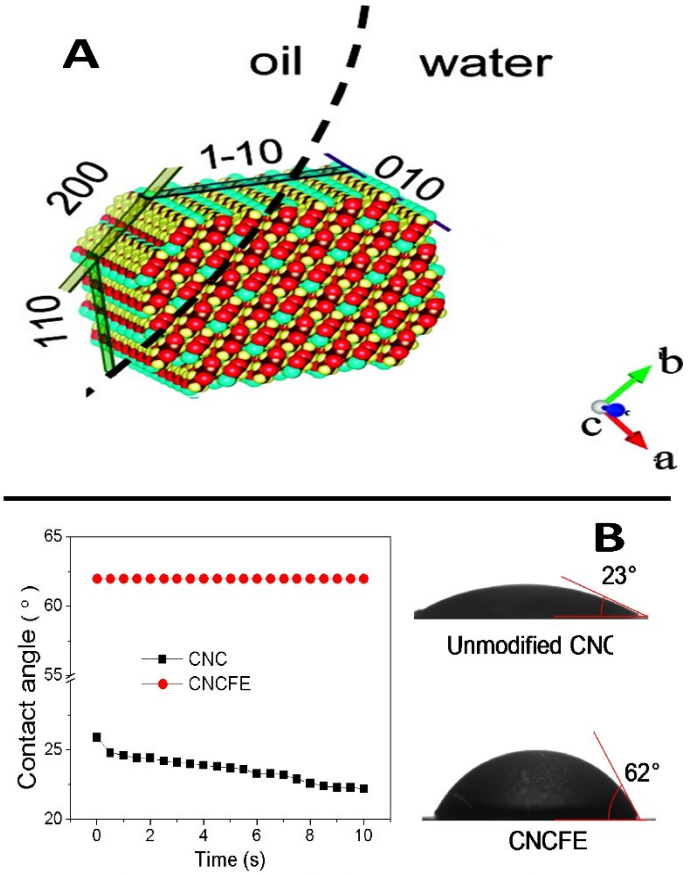

Figure 1-5: A) Schematic diagram depicting the orientation of CNC at the hexadecane-water interface via its (2 0 0) hydrophobic plane. Reprinted with permission from *[32]*. Copyright (2012) American Chemical Society. B) Water contact angle (θ_{ow}) of unmodified and modified CNC. Reprinted from *[115]*, Copyright (2017), with permission from Elsevier.

The discussions above clearly indicate that multiple factors are involved in the Pickering stabilization of liquid-liquid interface by CNC and CNF. While enhanced rheological properties determine the improvement in viscoelastic properties of the interface, it is adsorption and wettability that determine whether a given interface can be stabilized by unmodified nanocelluloses. Furthermore, the concentration of nanocellulose also has a profound impact on their ability to stabilize and enhance the stability of interface along with surface charge density of the particles. While the importance of surface charge density on the ability of nanocellulose to stabilize the liquid-liquid interface might be debatable, studies point out that screening of surface charge allows for interface stabilization at a significantly lower concentration. While intermolecular and surface interactions driving interface stabilization varies from one system to another, it can be concluded that forces such as electrostatic double-layer repulsion between charged particles, van der Waals force of attraction, H-bonding between nanocelluloses and depletion forces are extensively discussed in the literature involving nanocellulose stabilized emulsions. Interestingly, to the best of the authors' knowledge, no study has discussed capillary forces while discussing nanocelluloses stabilized interfaces despite it being discussed for other inorganic nanoparticles. [119,120]

4.2. Stabilization of liquid-liquid interface by modified nanocelluloses

CNC and CNF in their unmodified form have been used to stabilize liquid-liquid interfaces, especially when the charges on the surface have been screened by either the addition of electrolytes, adjustment of the pH, or modification of synthesis protocol but are limited in functionality. [54,117] Superficial hydroxyl groups of these nanocelluloses provide sites for surface reactions that can modify surface properties of the nanocellulose. The modifications, in general, are usually performed to increase hydrophobicity, responsiveness to external stimuli

such as pH, temperature, and magnetic field. [10,121,122] Unmodified CNC/CNF generally stabilizes O/W type emulsions, hence surface modifications are also desired to prepare W/O type or multiple emulsions using CNC.[96] Numerous studies in recent years have used various modifications of nanocellulose to enhance their ability to stabilize the liquid-liquid interface. Chemical modification of the CNC/CNF surface takes the form of polymer grafting, tempo mediated oxidation, cationization, esterification, and non-covalent surface chemical modifications.[4] The following section will discuss some key factors that govern Pickering stabilization by modified CNC and CNF.

4.2.1. Rheology

Similar to the studies comprising of unmodified CNC/CNF, rheological properties of emulsions prepared using modified nanocelluloses are studied to examine the viscoelastic and flow properties of the emulsions. Chemical modifications performed on the CNC surface increase viscosity of the emulsions prepared, primarily due to the formation of nanocellulose network in the aqueous phase and in general, surface modified nanocellulose emulsions exhibit gel-like behavior. [121,123–125] Interestingly, it was found that the addition of acetic acid or NaCl to rapeseed oil emulsions prepared using tempo oxidized CNF (T-CNF) resulted in a loss of viscosity. The authors argue that the stabilization of the T-CNF network in the aqueous phase is driven by electrostatic repulsion between the CNF particles, the addition of acid/ electrolytes screen the negative charge on the surface causing the network to collapse and hence destabilizing of emulsions. [126] It can be argued that screening of surface charge by electrolytes can promote inter-fiber interactions resulting in the formation of a stronger network, however, the authors argue that the addition of electrolytes or protonation of carboxyl groups on the T-CNF surface can result in irreversible aggregation and collapse of nanocellulose network. In addition to

increasing viscosity, surface modification of nanocelluloses also improves the viscoelastic properties of emulsions they stabilize. [127,128] Pandey et al. performed desulfation of CNC using acid (a-CNC) and base (b-CNC) treatment to reduce the surface charge density of CNC and prepared emulsions using dodecane in DI water. The flow behavior of emulsions was studied as a function of time in linear viscoelastic (LVE) region. The results indicated that all emulsions showed gel-like behavior and G' values were higher for both a-CNC and b-CNC compared to unmodified charged CNC (Figure 1-6a,1-6b). Furthermore, for a-CNC storage modulus (G') increased between 1 day and day 7 and then plateaued whereas for b-CNC the value of G' decreased between day 1 and day 7 before it plateaued. It is suggested that the increase in G' observed in a-CNC emulsions in partly due to the strengthening of the droplet network due to short-range interactions, while the drop seen in b-CNC emulsions are due to the coalescence of droplets resulting in a decrease in the number of droplet contact points. Strain sweep of emulsions prepared using the CNC showed similar rheological behavior after day 1, however, after day 7, for emulsions consisting of more than 5 mg_{CNC}/ml_{oil} showed weak strain overshoot in loss modulus. It has been discussed that such weak overshoot can be correlated to bond breaking and rearrangement in attractive emulsion droplets. [127,129,130]

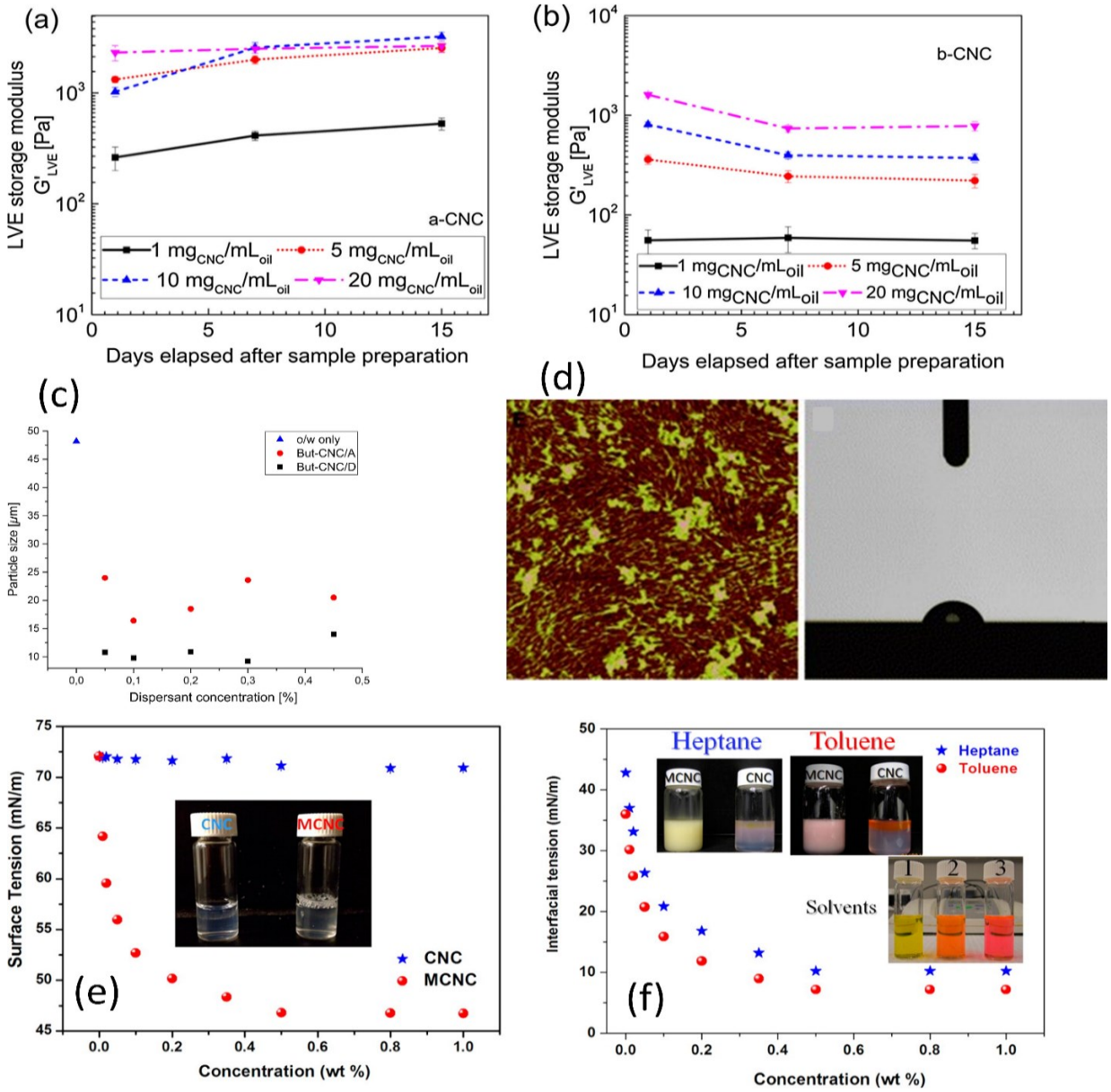

Figure 1-6: Factors affecting the stability of liquid-liquid interfaces by modified nanocelluloses. (a) LVE storage modulus for a-CNC stabilized emulsions, and (b) b-CNC stabilized emulsions after different aging times. Reprinted from *[127]*, Copyright (2018), with permission from Elsevier. (c) Oil droplet size in o/w emulsions as a function of the concentration of bifunctionalized CNC. Reprinted from *[131]*, Copyright (2016), with permission from Elsevier. (d) AFM image of the model surface of STAC-modified CNCs rinsed with Toluene (left) and water droplet on STAC modified CNC film for contact angle measurement (right). Republished with permission of RSC, from *[114]*; permission conveyed through Copyright Clearance Center, Inc. (e) Surface tension as a function of CNC concentration (star-unmodified CNC, circle-modified CNC) with pictures of 0.1wt% CNC at pH 12 and (f) γ_{ow} (star-heptane/water; circle-toluene/water) at different concentrations of PDMAEMA-g-CNC (pH 12). Reprinted with permission from *[132]*. Copyright (2014) American Chemical Society.

4.2.2. Particle morphology, concentration and surface coverage

The size and the crystallinity of CNC and CNF can be altered to a certain extent during the commonly used reactions to modify their surface properties. Slight shortening of the length, widening of the particles due to increased short-range particle interactions and decrease in crystallinity have been reported, while in other cases, the crystallinity remains unaffected. [131,133,134] A more critical factor governing the stability of the liquid-liquid interface is the concentration of modified nanocellulose used for stabilization of interface. Desulfation of CNC results in stabilization of the dodecane-water interface as minimal surface charge results in diminished electrostatic repulsion between the fluid-fluid interface, aggregation of particles and their adsorption at the interface. In a trend similar to desulfated BCN, D[3,2] of hydrophobic nanocellulose stabilized emulsions decrease with increasing nanocellulose concentration and finally plateau beyond a critical concentration (Figure 1-6c).[124,131,135] 0.5 wt % poly[NIPAM] grafted CNC were able to stabilize 71% of heptane emulsions in DI water whereas the equivalent concentration of unmodified CNC was unable to stabilize the emulsions.[10] Polystyrene grafted CNCs (PS-CNC) produced stable emulsions in toluene and water at a concentration of 0.3 wt% and above, with droplet size decreasing with an increase in the concentration of PS-CNC and plateaued at the PS-CNC concentration of 0.5 wt%. Selective grafting of polystyrene at one end of the CNC imparts amphiphilic behavior to the CNC driving CNC portioning at the oil-water interface. Surface coverage at maximum D[3,2] indicated that for more polar hexadecane 50% coverage of interface by CNC was sufficient to stabilize the emulsions with a smaller diameter (4 μm) compared to 140% coverage required for less polar toluene (diameter = 14 μm). [135] Nanocellulose surfaces have also been modified using simple physical adsorption of surfactants and water-soluble polymers onto the CNC surface.

[40,136,137] Pretreatment of CNC with hydroxyethyl cellulose (HEC) or methylcellulose (MC), formed more stable emulsions and finer droplets than either CNC or polymers. The authors argue that 75% of the oil-water interface is covered by polymer-coated CNC based on the assumption that all CNC adsorb to the interface and the thickness of the polymer layer at the interface is 10nm. [136] These studies indicate that the surface modification of nanocelluloses enhances their ability to stabilize the liquid-liquid interface. The concentration and size of the nanocelluloses dictate emulsion droplets size at a lower concentration, and beyond certain critical concentration, the droplet size becomes independent of nanocellulose concentration.

4.2.3. Surface and interfacial tension

Surface and interfacial tension are two forces that are significantly affected by surface modification of nanocelluloses. Since both CNC and CNF in their natural state are highly hydrophilic, most of the nanocelluloses surface modifications (except deposition of iron oxide particles) involve increasing the hydrophobicity of the particles without altering their physical properties. Such hydrophobic modifications often result in CNC/CNF exhibiting surface-active properties by altering the surface and interfacial tension of the gas-liquid or liquid-liquid interface. [132,136,138,139] Studies have shown, surface modifications such as polymer PDMAEMA grafting, succinylation, and carboxylation results in both CNF and CNC decreasing of the surface/interfacial tension between two fluid components by adsorbing at the interface (Figure 1-6e,1-6f). [132,138] Surface tension between air and an aqueous suspension of modified CNF and CNC were examined using a force tensiometer. The results indicated both modified and unmodified nanocelluloses altered the surface tension, with the addition of succinate and carboxylate functional groups onto CNF and CNC surfaces respectively altering it to a greater extent. Furthermore, it was found that at concentrations above 0.1 wt% the surface tension

increased until the value of unmodified nanocellulose.[138] These observations are contrary to other findings that suggest that unmodified CNF/CNCs do not affect the surface tension between fluids. [40,136,139] Du Nuoy ring method is commonly not used to measure surface/interfacial tension of nanoparticle dispersion due to the long-time required for particles to migrate and adsorb to the interface and due to concerns regarding adsorption of hydrophilic particles to the ring itself. While it is plausible to assume that modified nanocelluloses with increased hydrophobicity are likely to be surface-active and migrate to the interface quicker, the adsorption of particles to the ring should be considered when analyzing surface tension measurements. The impact of physical adsorption of polymers and surfactants on the surface and interfacial tension between fluids has been studied. It has been found that polymers such as hexamethyl cellulose (HEC) and methylcellulose (MC) did not affect interfacial tension on their own and neither did CNC. Adsorption of these polymers onto the CNC surface, however, lowered the interfacial tension between dodecane and CNC suspension with increasing polymer concentration and plateaued at the interfacial value corresponding to pure polymers. [136] In the case of surfactants, adsorption of surfactants onto CNC surface resulted in surface tension vs surfactant concentration shifting to higher concentration and increasing the critical micelle concentration of surfactants in solutions. Such impacts have been very prominent in some conditions and were absent in others,[40,139] it is not clear at this moment about the factors causing such observations.

4.2.4. Adsorption and wettability

Similar to the surface and interfacial tension, one of the major impacts of surface modifications of nanocelluloses is alterations in the wettability of these particles by water. The hydrophilic nature of CNCs/CNFs implies that the measured water contact angle (WCA)

between the unmodified particles and DI water is θ=22° for spin-coated CNC films and θ=53° for CNF coatings.[113,114,116] Surface modification by physical adsorption of surfactants and quaternary ammonium salts to the CNC surface increased hydrophobicity and static contact angle between CNC films and water (Figure 1-6d). [40,114,139] Furthermore, it was found that the contact angle between unmodified CNC films and surfactant solutions increases with an increase in the concentration of surfactant solutions and plateaus/decreases beyond the CMC of surfactant solution in the presence of CNC. [139] Interestingly, adsorption of pH-sensitive non-ionic surfactant Bis-(2-hydroxyethyl) cocoalkylamine (CAA) onto the CNC surface in high ionic strength aqueous phase resulted in a decrease in three-phase contact angle between dodecane-surfactant solution and CNC films resulting in catastrophic destabilization of emulsions upon addition of surfactant CAA.[40] Chemical modification of CNC/CNF using methods such as polymer grafting and esterification also results in an increase in contact angle between modified nanocelluloses and water. [113,123,138,140] It has been reported that surface functionalization of CNF with stearic acid increased its water contact angle from 53° to 112°, such surface-functionalized CNF was used to produce stable Pickering emulsions (both O/W and W/O). [140] Similarly, the addition of succinate group to CNF surface resulted in a slight increase in contact angle from 66° to 71° post surface modification. In the same study, carboxylation of the CNC surface was carried out which did not significantly change the contact angle between CNC films and water. It was found that surface-modified CNC/CNF was more efficient in producing stable emulsions of marine diesel oil with finer droplets as compared to less stable emulsions with unmodified CNC/CNF.[138]

4.2.5. Intermolecular and surface forces

The forces acting on the liquid-liquid interface to stabilize them are predominantly

governed by the nature of surface modifications at the interface. The addition of hydrophobic moieties to the nanocellulose surface depletes electrostatic repulsions between two particles which results in aggregation of CNC/CNF and enhancement of the surface activity of the nanocellulose. [10,123,125] The aggregation in the aqueous phase, in turn, is driven primarily by interparticle H-bonding, hydrophobic interactions and van der Waals force of attraction.[106,117,127] It has been discussed that for CNC grafted with polymers such as poly (NIPAM), the ionic strength affects the solvation of polymers in the aqueous phase and hence their ability to stabilize the emulsions. Such observation indicates that solvation forces are important intermolecular forces that can affect the stability of the liquid-liquid interface in the presence of nanocelluloses. Finally, as mentioned earlier due to the anisotropy of CNCs/CNFs, it has been found that nanocelluloses are more effective depleting agents than the spherical nanoparticles and can induce depletion flocculation at a much lower concentration. Three different range of concentration of CNC and CNF were correlated to depletion stabilization. It was established that at intermediate concentration range, highly flocculated droplets were formed due to CNF induced depletion interaction. At lower CNF concentration no droplet flocculation was observed and at higher concentration (beyond critical stabilization concentration) the droplets were independent of CNF concentration and the mechanisms driving emulsion stability were established as depletion interaction and emulsion gelation. [127,141]

5. STABILIZATION OF GAS-LIQUID INTERFACE

There is a limited number of studies that describe the Pickering stabilization of air-liquid interface by nanocellulosic materials.[14] The interest in stabilization of Pickering foams by CNC/CNF is increasing, however, because nanocelluloses stabilized foams can be used for a multitude of applications. While the forces responsible for stabilization of air-liquid interfaces

are generally similar to the liquid-liquid interfaces, few parameters define air-liquid interfaces more adequately. We will briefly discuss these parameters before discussing other factors described in the literature that determine the stability of CNC/CNF stabilized air-liquid interfaces.

Gas-liquid interfaces take the form of thin films and foams with the CNC/CNFs adsorbed at each face of the films such that hydrophobic planes of nanocelluloses oriented towards the gas-phase. The central liquid tends to drain out and the film begins to drain out and thin until the repulsive force between the adsorbed particles is dominant to stabilize the film against collapse. This pressure arising due to the repulsive forces is termed as *disjoining pressure* and is a critical parameter determining foam stability. It should be noted, however, that the rate of liquid drainage is higher at the edges compared to the lamellar part. This phenomenon can be explained by the Laplace equation (equation 23), which implies that around the edges the pressure (P^{β}) is lower than the pressure in the lamellar region (P^{α}) due to higher radius curvature (r) at the edges. This pressure gradient is a driving force for the drainage of liquid from the lamellar region to the edges of the film. [76]

$$P^{\alpha} - P^{\beta} = \frac{2\gamma}{r} \qquad (23)$$

Analogous to Ostwald ripening in the emulsions, diffusion of gas from smaller to larger bubbles as a result of Laplace pressure results in the coarsening of foam which is often described as another mechanism of foam instability. [142,143] Thus, factors contributing to foam instability can be categorized as film drainage, bubble coarsening, and coalescence.

Both CNCs and CNFs have been used to stabilize wet foams with varying degrees of success. To the best of our knowledge, there are no reports of the use of unmodified negatively charged CNCs to prepared wet Pickering foams, however, CNCs are frequently used to improve

the mechanical properties of dry composite foams and aerogels stabilized by polymers. [144–146] The following sections will highlight CNC/CNF stabilized wet foams and the factors affecting the foam stability will be discussed.

5.1. Stabilization of gas-liquid interface by unmodified nanocelluloses

There are no reports of unmodified CNC being used for the preparation of aqueous foams as they do not stabilize the air-water interface, in general, modified CNCs with increased amphiphilic properties, or CNFs with higher aspect ratio are used to generate aqueous foams.[12,147]

5.1.1. Rheology

Interfacial dilational (E) and interfacial shear (G) rheology can provide an estimation of viscoelastic properties of the gas-liquid interface stabilized by nanocelluloses. Examination of interfacial dilatational rheological properties of CNC suspension and air showed that surface charge affects the interfacial dilatation storage modulus (E'). In the NaCl concentration examined (0-17.5 mM), it was found that increasing electrolytes concentration resulted in an increase in E' and no significant change was observed with an increase in deformation (Figure 1-7C,1-7D). This behavior can be attributed to screening of surface change by NaCl allowing interparticle interactions without causing aggregation. At 17.5 mM, however, while an increase in E' was observed at lower deformation, at higher deformation, E' decreased. The authors argue that the result could be due to breakage in the layer orientation. Furthermore, at constant NaCl concentration, an increase in bulk CNC concentration corresponds to an increase in E' indicating coverage of the interface can be correlated to enhanced interfacial dilational storage modulus. Hence, sufficient surface coverage, as well as salt-induced charge screening, is required to form viscoelastic CNC interfacial layers. Interfacial shear modulus measurement showed a similar

trend with G' increasing with salt concentration and bulk CNC concentration.[12,148] Stocco et al. suggested that for stabilization of the wet foams (cessation of bubble coarsening), the compression (oscillatory) elastic modulus (E) should be larger than half of the surface tension of the liquid. [149] This suggests that the compression elastic modulus should be greater than 36mN/m for the stabilization of air-water foam, however, the oscillatory elastic moduli of unmodified CNCs/CNFs were measured to be less than 10 mPa.m. [150]

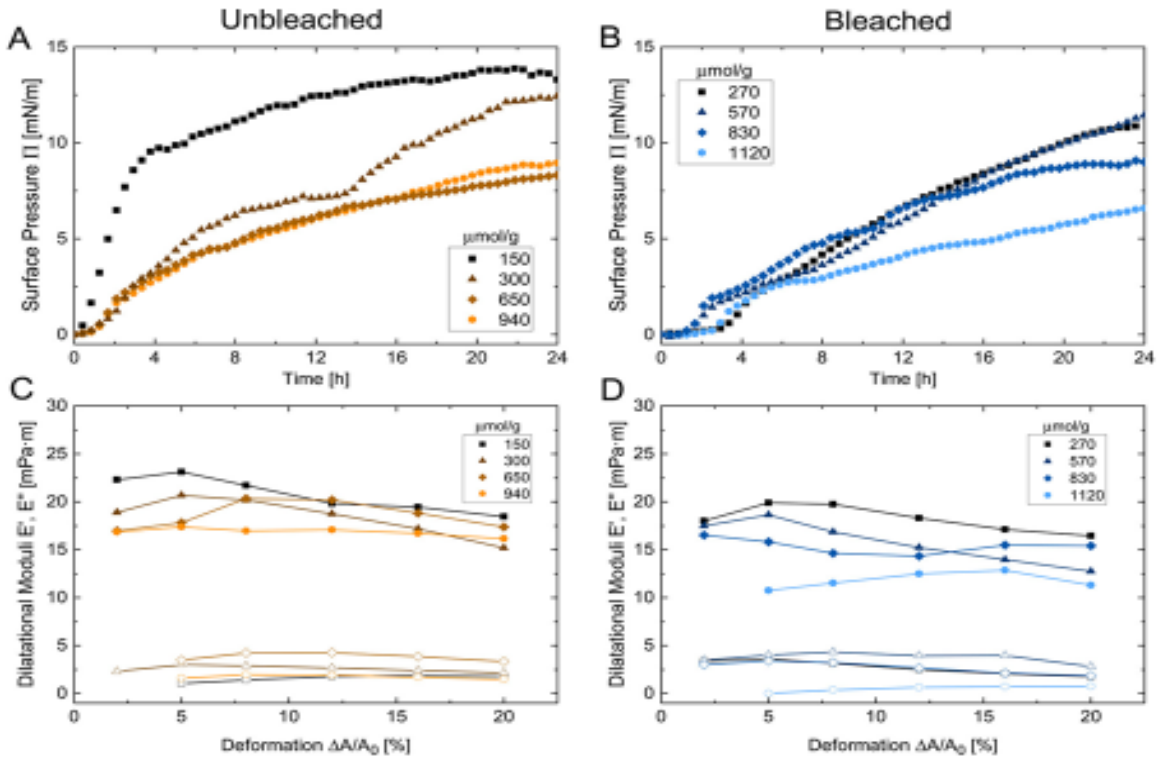

Figure 1-7: Adsorption kinetics of 0.1 wt % CNFs with varying charge densities derived from A) unbleached and B) bleached softwood pulp. The interfacial dilatational storage (E') and loss(E") modulus of C) unbleached and D) bleached CNFs. Reprinted with permission from *[147]*. Copyright (2019) American Chemical Society.

5.1.2. Particle adsorption, concentration and surface coverage

Adsorption of CNC at the air-water interface was assessed in terms of change in surface pressure (Π) defined as the difference between surface tension (γ_0) measured at t=0 and any

arbitrary time. An increase in surface pressure (Π) was reported indicating the adsorption of CNC at the air-water interface within 14 hours (Figure 1-7A,1-7B). The kinetic study of the adsorption process clearly showed an initial lag phase, followed by steady adsorption, the authors argue that lag could be attributed to the diffusion of CNCs to the interface. Furthermore, increasing the bulk concentration of CNC (upto 0.5%) and the addition of electrolytes to the solution increased Π_{max} and decreased lag phase.[12,151] These findings indicate that screening of surface charge (electrostatic repulsion) promotes CNC adsorption at the A/W interface, promotes closer packing of the particles at the interface, and increases the adsorption energy. Structural analysis of CNCs at the A/W interface was conducted using AFM and neutron reflectometry. AFM imaging of the particles indicated at 0.001 wt%, CNCs were evenly distributed in bulk but present as clusters at the interface with significantly higher surface coverage at the interface than in bulk suspension. Furthermore, neutron reflectometry of the air-D_2O interface in the presence of 0.75 wt% CNC in 20 mM NaCl revealed that the layer at the interface was merely 8±2 Å, suggesting the formation of a discontinuous interfacial layer. It should be noted that the conditions in which the study was conducted were beyond monolayer saturation conditions and favored the formation of the multilayer.[12] However, it should be noted that despite increased adsorption and surface coverage unmodified nanocelluloses were not able to produce stable foams.

5.1.3. Surface/interfacial tension and wettability

Surface tension between air and unmodified CNF suspension was measured using a pendant drop method, the results indicated that CNF was not able to lower the surface tension to promote interface stability. Unsurprisingly, surface modification of CNF with surfactants lowered the air-water surface tension and also produced stable foam. [150] An increase in

surface pressure measured in terms of change in surface tension was reported, indicating after an initial lag of 2-3 hours, the surface tension of water decreased steadily over 14 hours in the presence of CNF (Figure 1-8). [12] The impact of CNC concentration on surface tension was studied, it was found that in high salinity brines (1.9M and 0.65M) at concentration beyond 0.8 wt% presence of CNC aggregates decreased the surface tension between air and brine [40] Static contact angles between water, air and CNC films with different hydrophilicity were compared using a sessile drop method, predictably, the contact angle was higher (44.1 ± 1.5°) for more hydrophobic films compared to hydrophilic films whose contact angle was reported at 26.9 ± 1.5°.[152] These values of contact angles indicate that the wettability of unmodified CNCs by water is too high for them to stabilize the air-water interface.

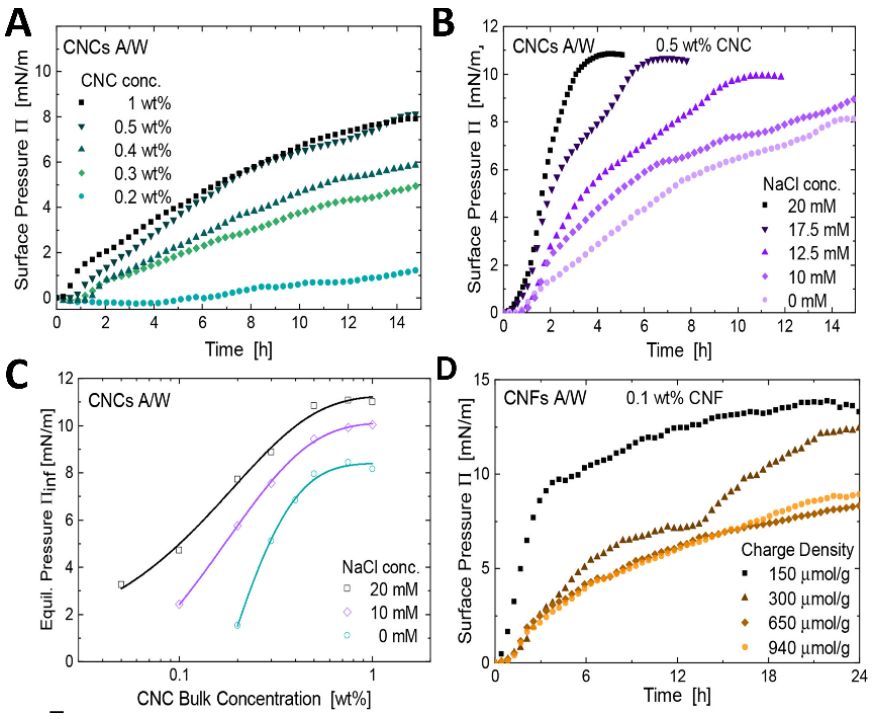

Figure 1-8: Surface pressure variation as the measure of adsorption of unmodified CNCs at air-water interfaces expressed as a function of A) time for different concentrations of CNC, B) 0.5 wt% CNC at different ionic strength, C) Adsorption isotherms for CNCs at the A/W interface compiled from the equilibrium surface pressure Π_{inf}, D) Adsorption of CNFs with varying charge density. Adapted from *[151]*, Copyright (2019), with permission from Elsevier.

5.1.4. Surface and intermolecular forces

Electrostatic repulsion between the films which results in a generation of disjoining pressure is a critical molecular force determining the stability of CNC stabilized air-liquid interface, besides, the rate of film thinning controlled by the pressure gradient between lamella and film edges are forces that determine foam stability. Screening of superficial nanocellulose charges results in van der Waals force and hydrophobic interactions between particles being dominant in the system which promotes adsorption of CNC/CNF to the interface which in turn can result in interfacial stabilization. [12,147,148]

While the studies mentioned earlier clearly indicate that unmodified nanocelluloses adsorption at the air-water interface improves the rheological properties of the interface, improves surface coverage of the interface by the CNC/CNF, and lowers the surface tension of liquid over time or at higher concentration in high ionic strength medium. It should be noted that these improvements surface properties by unmodified nanocelluloses do not translate into foam stability and surface modification is often required for CNC/CNF to prepare foams. It is not established at this moment as to why the unmodified nanocelluloses, despite improving the surface properties, are unable to produce stable foams. It could be argued that the extent of enhancement of surface properties by unmodified CNC/CNF is insufficient and hence surface hydrophobization is required for the generation of nanocellulose stabilized foams.

5.2. Stabilization of gas-liquid interface by modified nanocelluloses

Surface modified CNC and CNF have been used more effectively to stabilize the air-water interface to produce stable foams as compared to unmodified nanocelluloses. Multiple reports indicate that the surface of nanocelluloses can be modified using polymers, hydrophobic chemicals, and surfactants to improve their ability to stabilize foams. [150,153,154] In the

following section will discuss factors discussed in the literature that describes the stability of the air-water interface.

5.2.1. Rheology

Surface modified nanocelluloses exhibits improved rheological properties in comparison to unmodified nanocelluloses. [11,155,156]. Surface modified CNFs with varying length and surface charge density produced by TEMPO mediated oxidation were studied for their ability to stabilize air-water foams. The interfacial dilatational storage (E') and loss modulus (E") were examined after allowing the adsorption of CNFs to the interface. The results indicated that CNFs formed a viscoelastic interfacial layer with storage modulus dominating the loss modulus. Interestingly, it was found that the viscoelastic nature of the interface was independent of the CNF surface charge, the authors argue that the long fibril lengths favor fibril entanglement and hence the formation of the viscoelastic layer. It has been reported that the carboxylated CNCs form a viscous interfacial layer and screening of surface charge is required for CNCs to form a viscoelastic layer. It should be noted however that TEMPO-oxidized nanocelluloses on their own did not stabilize air-water foams. [147,148] Cervin et al. have discussed the rheological properties of TEMPO-oxidized CNFs and CNCs surface modified by adsorption of surfactants octylamine and decylamine in great detail. The impact of nanocelluloses with different charge densities (500, 900, and 1400 μeq/g), aspect ratios (CNF and CNCs), and the concentration of CNF on the rheological properties of the interface were compared (Figure 1-9A, 1-9B). The results indicated that the complex viscoelastic modulus of the interface stabilized by nanocellulose with a higher aspect ratio (CNF) exhibited higher complex viscoelastic modulus. The impact of charge density was studied by measuring the viscoelastic modulus of CNFs with different charge density and also by screening surface charge using salts. The result indicated an

increase in charge density from 500 to 900 μeq/g resulted in increased complex viscoelastic modulus, but further increase in the charge density to 1400 μeq/g reduced the complex viscoelastic modulus. The addition of salt also tended to increase the complex viscoelastic modulus. Finally, the complex viscoelastic modulus increased with increasing CNF concentration although there seems to be a maximum at 5 g/L where the complex viscoelastic modulus started to decrease with time. [150] Interestingly, the authors found that in instances when the complex viscoelastic modulus of the interface was greater than half the surface tension (36 mN/m in this case), in such cases the foams generated were stable, agreeing to suggestions by Stocco et al. regarding the rheological requirements for stabilization of air-water interface.

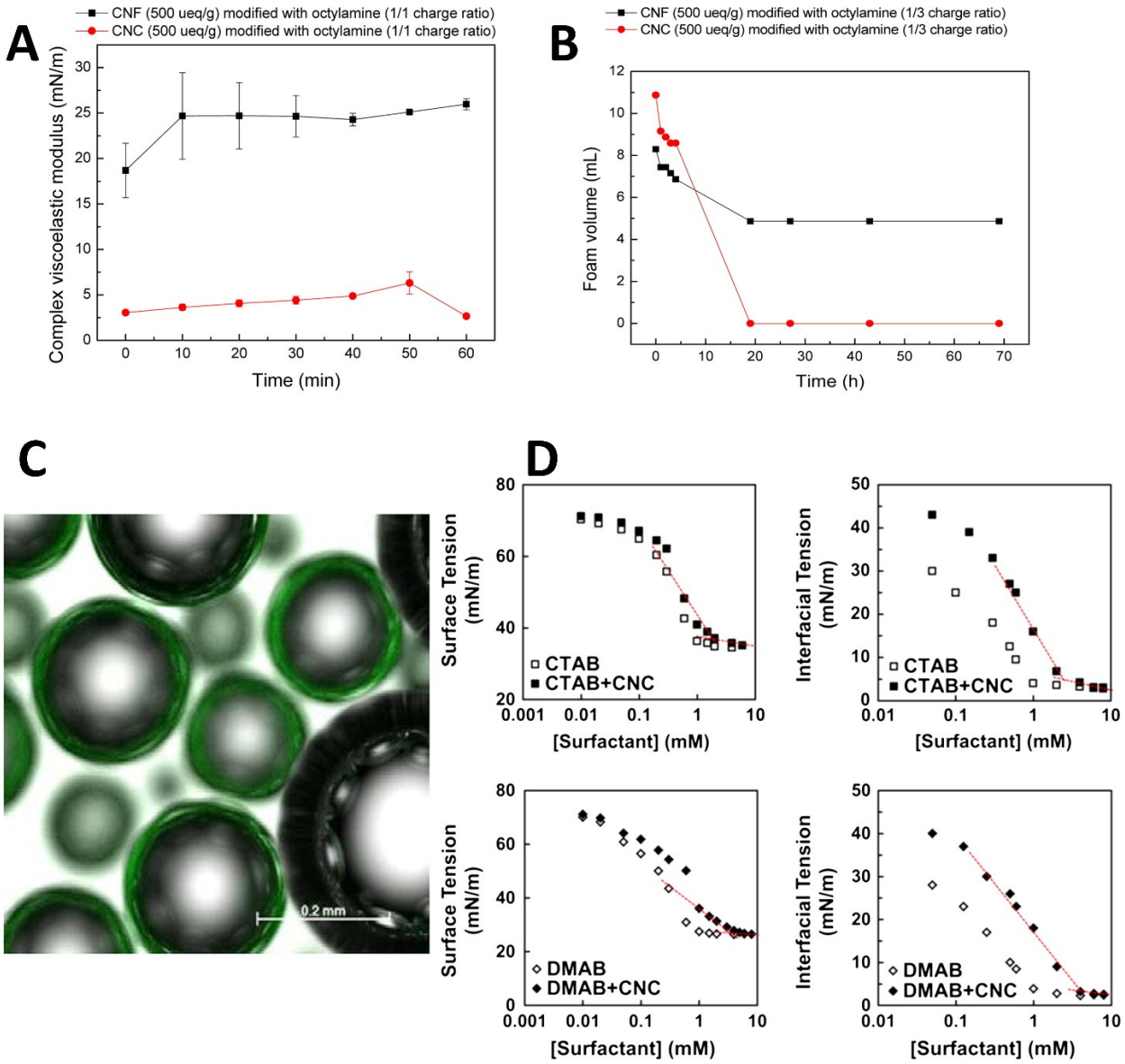

Figure 1-9: Properties of air-water interface stabilized by modified nanocelluloses. A) Complex viscoelastic modulus of CNC and CNF modified with octylamine as a function of time. B) Foam volume as a function of time for CNF and CNC. Reprinted with permission from *[150]*. Copyright (2015) American Chemical Society. C) Optical micrograph of air bubbles in water covered with fluorescently labeled octylamine-treated CNF. Reprinted with permission from *[157]*. Copyright (2012) American Chemical Society. D) The surface tension of CTAB (top) and DMAB (bottom) at room temperature; in the presence (closed symbols) and absence (open symbols) of CNC (0.25 w.%). Reprinted from *[139]*, Copyright (2015), with permission from Elsevier

5.2.2. Particle adsorption, concentration and surface coverage

Surface hydrophobization of nanocelluloses significantly alters their adsorption behavior

at the interface. While it has been established that the surface modification improves the ability of nanocelluloses to stabilize air-water interface and form stable foams, the quantitative estimation of adsorption of the modified particle at the interface is limited. However, improvement in rheological and surface properties of the air-water interface does provide evidence of improved particle adsorption. The apparent viscosity of sodium dodecyl sulfate (SDS) and CNF system increases with increase in the concentration of CNF from 0.3 to 2.5 wt%, it has been suggested that such observations can be attributed to the entanglement of the fibrils which in turn improves the stability of the air-water interface (Figure 1-9C).[158] For a given concentration of CNF, charge density determined the volume of air trapped in the foam. In addition to improving the stability of the interface, increasing the concentration of octylamine adsorbed CNF also increased the porosity of the foam and decreased the foam density. [157,159]

5.2.3. Surface tension and wettability

Surface activity and wettability of nanocelluloses can probably be considered the most affected properties of native nanocelluloses due to surface hydrophobization. Covalent modifications, polymer grafting, and surfactant adsorption affect the surface activity and wettability of nanocellulose.[160] Polymers (methylcellulose) adsorbed CNC were found to have lowered the air-water surface tension to 48 mJ/m^2, whereas the CNC alone had no impact on the surface tension of the system (Figure 1-9D).[139,154] Hiranphinyophat et al. found that CNCs modified with poly[2-isopropoxy-2-oxo-1,3,2-dioxaphospholane] (PIPP) lowered the air-water surface tension from 72 mN/m to below 45 mN/m, however, the change in surface tension with an increase in PIPP grafted CNC was minimal upto CNC concentration of 0.3 wt%, at higher concentration (0.4 wt%) slight decrease in surface tension was measured. Similar observations have been reported in other polymer grafted CNC studies.[11,161] Li et al. found that wettability

differs among CNCs with different crystalline allomorphs. CNC (I) films with lower surface charge density and needle-like structure had all hydroxyl or sulfonic groups in the equatorial region and hydrogen in axial which resulted in hydrophobic properties with a contact angle of 44.1±1.5°. CNC (II) films, on the other hand, had higher surface charge density and the molecular chains have alternating polarities stack mainly by hydrophobic forces and consequently exhibit more hydrophilic properties with the water contact angle of 26.9±1.5°.[152]

5.2.4. Capillary pressure and intermolecular forces

It has been suggested that particle assembly at the interface is necessary but not sufficient requirement for the generation of stable foams using nanoparticles. It has been argued that foam stability requires a large fraction of bubbles covered by smaller particles, have liquid with higher surface tension and a favorable contact angle between the particles and the fluids. [150] Kaptay has discussed the role of capillary pressure and the electrostatic repulsion between the films that prevent them from coalescing or coarsening. [87] It has been reported that the higher surface charge density of nanocelluloses results in the formation of thinner film at the interface and improved concentration of CNF at the interface resulting in the generation of stable air-water interface.

6. CONCLUSIONS

The ability of nanocellulosic materials to stabilize liquid-liquid and gas-liquid has been well documented and several studies have used these particles to produce emulsions and foams. The majority of these studies characterize these emulsions and foams in great detail, however, the discussions on underlying mechanisms that control the stability are often limited to individual systems. This paper has systematically discussed some key factors and mechanisms that contribute to the ability of nanocelluloses to stabilized various interfaces. Among the factors

discussed, CNC concentration, surface charge screening, surface coverage have been discussed in the literature but other factors such as wettability, interfacial tension, interfacial rheology, and intermolecular forces are not discussed in greater detail. One key conclusion of the study is that partial wetting of the particles by both phases is critical to the adsorption of these particles at the interfaces.

Recent studies have also indicated that interfacial rheological properties also play a crucial role in the stabilization of liquid-liquid and gas-liquid interfaces. Recent findings indicated that unmodified CNCs decreased the surface tension between air and water. Besides, unmodified CNC suspensions in high salinity brine were also shown to have decreased surface tension at concentrations higher than 1 wt.%. In addition to strong covalent interactions, short-range intermolecular forces such as H-bonding, Van der Waals attraction, ion-dipole interactions have been identified as potential forces that act at the nanocelluloses stabilized interfaces.

CHAPTER 2

Surface and Interfacial Interactions in Dodecane/Brine Pickering Emulsions Stabilized by Combination of Cellulose Nanocrystals and Emulsifiers

S. Parajuli, A.L. Dorris, C. Middleton, A. Rodriguez, M.O. Haver, N.I. Hammer, E. Ureña-Benavides, Surface and Interfacial Interactions in Dodecane/Brine Pickering Emulsions Stabilized by the Combination of Cellulose Nanocrystals and Emulsifiers, Langmuir. 35 (2019) 12061–12070. https://doi.org/10.1021/acs.langmuir.9b01218.

ABSTRACT

Interfacial properties of cellulose nanocrystals (CNC) and surfactants were studied in high ionic strength (I) brines and correlated to the stability of dodecane/brine Pickering emulsions. Bis-2-hydroxyethyl cocoalkylamine (CAA), dodecyltrimethylammonium bromide (DTAB) and Octyl-β-D-glucopyranoside (OGP) were adsorbed onto CNC in American Petroleum Institute (API) brine (I=1.9 M) and synthetic seawater (SSW), with I=0.65 M. Raman spectroscopy, indicated that hydroxyl groups on the CNC surface interact with all three surfactants in high ionic strength media. Ionic interactions still play a role at the very large ionic strengths studied herein. Despite all surfactants adsorbing onto CNC, only the surface tension of CAA solutions in both brines was increased by the addition of 0.5 wt.% CNC. The effect was much more prominent in API than in SSW. Contact angle measurements indicated that CAA increased the wettability of CNC by both brines in dodecane; DTAB, on the other hand, decreased wettability. Emulsion stability

studies revealed that ionic strength, wettability, adsorption energy, and oil content strongly affect emulsion stability, more so than surfactant adsorption. In API, CNC aggregates alone stabilized the emulsions better compared to samples with additional emulsifiers; the same was true in SSW for oil contents below 50% v/v. For oil contents above 50% v/v in SSW, CAA, was either detrimental or failed to improve emulsion stability. On the other hand, DTAB increased the stability of dodecane in SSW emulsions. Emulsions stable for over 21 months were prepared with oil contents of 75% v/v. Adsorption of CAA onto CNC limits the migration of both CNC and CAA to the dodecane/brine interface, while DTAB adsorption has the opposite effect.

Keywords: Cellulose nanocrystals, Interfacial tension, Surface Tension, Pickering Emulsions, Brine, Adsorption, Raman spectroscopy, Contact angle, Wettability

1. INTRODUCTION

Emulsions have applications both in daily life and in industries, and as the demand for stable formulations based on natural ingredients increases, there is a growing trend for using naturally occurring colloidal particles as stabilizers instead of surfactants.[162–164] Some of the common industrial applications of emulsions include food additives, oil-based creams, cosmetics, fertilizers, textile coatings, tertiary oil recovery, and oil spill cleanup.[165–169] Particle-stabilized (Pickering) emulsions have numerous advantages over traditional surfactant-stabilized emulsion including lower toxicity, low emulsifier content, and adjustable droplet size.[36,170–172] Emulsions prepared using only surfactants or nanoparticles have been extensively studied, but many commercial products of recent times have used a combination of surfactants and nanoparticles; therefore, it is important to understand how nanoparticles and surfactants interact, and the mechanisms by which they stabilize emulsions. This understanding contributes to the efficient design and development of emulsion-based products.[173] CNC

stabilized emulsions prepared in high salinity brines find applications in enhanced oil recovery and potential applications in oil spill cleanup operation in the marine environment.

Charged nanoparticles such as silica, clay, gold, and cellulose nanocrystals (CNC) are often used in conjunction with surfactants to stabilize emulsions.[174] Surfactants favor the formation of smaller emulsion droplets by lowering the interfacial tension between two phases; they also promote stability by preventing fluid drainage from droplets. Nanoparticles, on the other hand, do not significantly reduce the interfacial tension, but instead, migrate to and assemble at the liquid/liquid interface allowing stabilization of Pickering emulsions.[175] Pickering stabilization is a result of the nanoparticles forming a rigid structure around the droplet, which prevents droplet coalescence and Ostwald ripening.[176,177] Stabilization of emulsions by particles makes them more stable to coalescence as compared to surfactants because the energy associated with desorption of particles from the interface can be in the order of 10^3-10^4 k_BT, whereas the energy required to desorb surfactants from the interface is two to three orders of magnitude smaller. This indicates that the adsorption of nanoparticles onto interfaces can essentially be considered irreversible.[14,64,178]

Few studies exist of Pickering emulsions in high salinity brine. Worthen et al. reported improved stability of emulsified seawater/dodecane systems and CO_2 foams by a mixture of the zwitterionic surfactant caprylamidopropyl betaine and negatively charged silica nanoparticles as compared to a standalone surfactant or silica nanoparticles.[64,179] Binks et al., reported that mixtures of cationic surfactant CTAB and silica nanoparticles have synergistic effects on improving the stability of water/dodecane emulsions.[180] At low concentration (0.1 wt.%), the interaction between colloidal silica particles and non-ionic surfactant Span® 80 results in a

lowered interfacial tension, thereby enhancing the stability of paraffin oil/water emulsions. Alternatively, at higher surfactant concentration (1.8 wt.%) emulsion stability was reduced.[181] CNC produced from bacterial cellulose was first used to stabilize hexane/water emulsions through ultrasonic mixing to produce monodisperse O/W emulsions that were stable for several months.[54] Hu and co-workers used 0.3 wt.% cotton derived CNCs alongside 0.2 wt.% polymer solutions of hydroxyethyl cellulose, dextran, and methylcellulose to stabilize emulsions of water and dodecane.[182] Gestranius et al. also prepared O/W Pickering emulsions using CNF, tempo CNF, and CNC in dodecane; without using any surfactants. Emulsions prepared using CNF were stable to low shearing and an increase in temperature (up to 80^{o}C).[106] Cellulose nanocrystals (CNCs) have been used to stabilize oil in water (O/W) emulsions in low salinity aqueous phases. CNC dispersions in low salinity brine (1000 ppm NaCl) were used to enhance crude oil mobility in sandstone cores for tertiary oil recovery at elevated temperatures and variable pH. Viscosity measurements of the effluent revealed that most CNC traverses the core.[168,183,184]

Despite the outburst in research involving CNC stabilized emulsions; most studies have been conducted in low ionic strength (I) aqueous phases. Relatively little research has been done to explore the potential of CNC as emulsion stabilizers in high ionic strength brines. Furthermore, the literature indicates negatively charged particles have been used in combination with ionic and nonionic surfactants with varying degrees of success to stabilize emulsions in low ionic strength aqueous dispersions. This study attempts to elucidate the different outcomes obtained when different types of surfactants are added to Pickering emulsions. To achieve this goal, molecular interactions between CNC and surfactants in high salinity brines are studied via Raman spectroscopy, tensiometry, and adsorption measurements. The effect of those

interactions on surface/interfacial properties are correlated to the stability of emulsions stabilized by CNCs and added emulsifiers in high salinity aqueous solutions.

2. EXPERIMENTAL SECTION

2.1. Materials

Cellulose nanocrystals (11.5 wt.%), prepared from *Pinus strobus* (Northern pine) wood pulp, made by the USDA Forest Products Laboratory and distributed by The University of Maine were used as received. 99.9% reagent quality dodecane was purchased from Sigma Aldrich (St. Louis, MO) and used as received (unless otherwise specified). Dodecyltrimethylammonium bromide ≥ 90% (DTAB), Guar Gum, Octyl-β-D-glucopyranoside (OGP), calcium chloride ($CaCl_2$), sodium chloride (NaCl) and synthetic seawater (SSW) were all purchased from Sigma Aldrich and used as received. ETHOMEEN C/15®, Bis (2-hydroxyethyl) cocoalkylamine (CAA), was kindly gifted by AkzoNobel (Houston, TX) and was used as received. The chemical structures of the emulsifiers used are depicted in Appendix A Figure S1.1. American Petroleum Institute (API) brine was prepared by adding 8 wt.% NaCl and 2 wt.% $CaCl_2$ in DI water.

2.2. Characterization of CNC

AFM measurements were carried out using a Nanoscope IIIA multimode scanning probe microscope from Bruker (Billerica, MA). Topographic images obtained from AFM were processed using Gwyddion software to measure the length and height of cellulose nanocrystals. Measurement of at least 100 rod-shaped individual crystals indicated the average length of the particles was 128±43 nm and the average height was 6.4±1.8 nm, as shown in Appendix A Figure S1.2. Conductometric titration of CNCs using methods explained elsewhere[185,186] indicated an average sulfur content of 0.045±0.018 g-sulfur/g- cellulose on the surface of the CNC used in this study (Appendix A Figure S1.3).

2.3. Adsorption measurements

Adsorption of surfactants onto the CNC surface was measured using Shimadzu's total organic carbon (TOC-L CSH E100) and total nitrogen (TNM-L) analyzer. Surfactant solutions in API (I = 1.9 M) brine and SSW (I = 0.65 M) were allowed to equilibrate with 1 wt% CNC for at least 12 hours, followed by centrifugation of the suspension to separate CNC from the solution. The supernatant was carefully recovered and analyzed for the concentration of total organic carbon and total nitrogen. Equilibrium concentrations were plotted against the adsorbed concentration to generate adsorption isotherms of individual surfactants onto the CNC surface.

2.4. Raman Spectroscopy

A solid-state Horiba Labram HR Evolution Raman spectrometer (Horiba Instruments Inc, TX) using a 600 grooves/mm grating, 532-nm laser excitation, CCD camera detection, and a 100x micro-Raman objective was employed for the acquisition of Raman vibrational spectra. Vibrational Raman spectra of freeze-dried CNC dispersions in API brine and SSW were compared with the spectra of surfactants adsorbed CNC in both brines. Spectral signatures at higher wavenumber corresponding to -OH stretching were analyzed for probable interactions between CNC and surfactants. Before obtaining the spectra, surfactant solutions in brine and CNC dispersions were equilibrated for approximately 12 hours. The dispersion was then centrifuged, the pellet recovered and allowed to sit in a hardened filter paper to remove excess water by capillary action. The pellet devoid of unadsorbed surfactants was then freeze-dried to remove excess water.

2.5. Surface Tension Measurements

The surface tension vs surfactants concentration plots in API brine and SSW (without CNC in dispersion) were generated using a DuNuoy ring method after allowing the solution to equilibrate for 10 mins using a force tensiometer, Sigma 701 (Nanoscience Instruments, Phoenix,

Arizona). A surface tension vs surfactant concentration plot was also generated for each surfactant in the presence of 0.5 wt.% CNC aggregates (or flocs) in brine, using axisymmetric pendant drop analysis with an Attension Theta Tensiometer (NanoScience Instruments, Phoenix, Arizona) after equilibrating for 60 mins. Critical micelle concentration (CMC) of surfactants in brine was calculated in the presence and absence of CNC aggregates (or flocs). CMC calculated in presence of CNC is referred to as "apparent critical micelle concentration" (ACC).

2.6. Interfacial tension measurement

The interfacial tension between oil (dodecane) and an aggregated CNC dispersion in brine was measured using an optical tensiometer (NanoScience Instruments, Phoenix, AZ). Prior to the measurement of interfacial tension, n-dodecane was passed through an alumina column several times to remove impurities. The pendant drop method was used to perform axisymmetric drop shape analysis of a captive aqueous phase drop in the presence of excess oil phase and after equilibrating with excess dodecane for 60 mins, before taking measurements. Contours of the droplet's shape were fitted to the Young-Laplace equation to calculate interfacial tension.[187]

$$\Delta p = \rho g h - \gamma \left(\frac{1}{R_1} + \frac{1}{R_2}\right) \qquad (1)$$

Where Δp is the pressure difference across the interface, γ is surface/ interfacial tension, R_1 and R_2 are principal radii of curvature and the term ρgh is hydrostatic pressure.

2.7. Contact angle measurement

A thin film of cellulose nanocrystals was generated by adding a drop of 1wt.% CNC suspension in DI water onto freshly cleaved mica surface and drying overnight in a vacuum oven at 50ºC. The RMS roughness of the CNC film was measured using AFM to confirm the uniformity of the surface and was smaller than the height of the CNCs (6 nm). The three-phase equilibrium static contact angle between CNC film, surfactant solution (concentration near CMC

in respective brine) and dodecane was measured using a sessile drop method in an Attension Theta optical tensiometer (NanoScience Instruments, Phoenix, AZ). Contact angles reported are the average of angles formed by both ends of the drop on the CNC film submerged in dodecane. At equilibrium, the phase contact angle is related to interfacial tension by the Young equation.[179]

$$cos\theta_{OW} = \frac{\gamma_{SO} - \gamma_{SW}}{\gamma_{OW}} \qquad (2)$$

In the above equation, γ_{SO} is interfacial tension between solid surface and oil phase, γ_{SW} is interfacial tension between solid surface and water and γ_{OW} is interfacial tension between oil and water.

2.8. Emulsion Preparation and Characterization

The aqueous phases of emulsions were prepared by adding surfactants to 200% brine; an equal volume part of 2 wt.% CNC suspension was then added to the surfactant solution while mixing to prevent gelation. The final concentration of surfactants in the aqueous phase corresponds to their ACC in brine. The pH of aqueous after addition of surfactants was close to neutral, except for CAA which was between pH 8 and 9. A total of 10 mL of n-dodecane and aqueous phase were added to a 20 mL screw-capped vial with volume ratios ranging from 90% to 10% aqueous phase. The samples were then homogenized using a high-shear homogenizer (IKA Ultra-Turrax T-25 Basic, Atkinson, NH) at 10000 rpm for 1 minute. Conductivity measurements using an Orion™ DuraProbe™ 4-Electrode Conductivity Cell having Pt/Pt electrode were used to characterize emulsions as oil in water (O/W) or water in oil (W/O) type (Appendix A Figure S1.4).

2.9. Emulsion stability

Emulsion stability was measured in terms of droplet coalescence and creaming. Droplet coalescence was studied by monitoring the change in emulsion droplet diameter over 24 hours. Droplet diameter was measured by image analysis of optical micrographs created by an optical microscope (AmScope 500MD). A small aliquot of the emulsion was transferred from its vial to a microscope slide by spatula. A uniform layer of the emulsion was formed by placing a glass coverslip over the top of the emulsion drop and droplets micrographs were analyzed using ImageJ to generate droplet size distribution. Emulsions' resistance to creaming was measured by monitoring the position of creaming front for 24 hours by analyzing pictures using ImageJ (U.S. NIH).

3. RESULTS AND DISCUSSION

3.1. Properties of CNC and surfactants in brine

Colloidal stability of CNC was diminished in the presence of electrolytes in solution. DLS measurements of 0.002 wt% CNC in DI water showed a hydrodynamic diameter of 164 nm, whereas in API and SSW it was near 10 μm, indicating aggregation of CNC in these brines. The addition of surfactants did not have a significant effect on the aggregation behavior of CNC in brines, with similar magnitude hydrodynamic diameters observed in the presence of surfactants. It should be pointed out that DLS measurements for aggregates above 1 μm only provide qualitative information. Visual examination of 1 wt% CNC suspensions in these brines showed that the particles do not precipitate within 26 hours and remain suspended as aggregates (or flocs). The CMC and ACC of the surfactants were measured in the presence and absence of CNC aggregates (Table 2-1). The CMC and ACC measurements provide important information about the behavior of surfactant adsorption at the air-brine interface in the presence of CNC. The results indicate that statistically, the CMC of surfactants did not change upon the addition of

CNC. The CMC of OGP is not reported as no clear minimum was observed up to the concentration of 10g/L.

Table 2-1: CMC for emulsifiers in SSW and API Brine in the presence and absence of 0.5wt% CNC

Brine	**CMC and ACC in API (g/L)**		**CMC and ACC in SSW (g/L)**	
Surfactant	w/CNC	w/o CNC	w/CNC	w/o CNC
OGP	--	--	--	--
CAA	0.07±0.06	0.01±0.02	0.01±0.03	0.01±0.04
DTAB	0.16±0.11	0.16±0.03	0.67±0.05	0.75±0.05

Errors represent standard errors

3.2. Adsorption of surfactants onto CNC

Adsorption of surfactants onto the CNC surface was expressed in terms of the mass of adsorbed surfactant per unit mass and unit area of CNC. The area calculation assumes flocs sufficiently exfoliated to expose the area of individual CNCs, in reality, the exposed area must be smaller. The calculation of adsorption per mass of CNC is unaffected by the aggregation state. The adsorption measurements were carried out at ambient temperature and pressure. Figure 2-1 indicates that in API brine all surfactants adsorb to a lesser extent compared to SSW. In API, all surfactants had a maximum adsorption ratio of nearly 0.22 g surfactant adsorbed per g surfactant in solution when the bulk concentration was 3 g/L. In SSW, however, the maximum adsorption ratios were 0.99 for CAA, 1.27 for DTAB, and 0.82 for OGP, when the equilibrium concentrations were 1.4 g/L, 0.88 g/L, and 1.10 g/L respectively. In the case of DTAB, higher adsorption in SSW could be due to the lower ionic strength compared to API brine, which makes the former a better environment for ionic interactions between CNCs and the positively charged

surfactant. Interestingly the same trend is observed between CAA and OGP even though they bear a neutral headgroup at the conditions tested; suggesting some other types of molecular interactions are also involved in the adsorption process. Furthermore, the isotherm of surfactant adsorption in SSW suggests a weak adsorption interaction at a lower concentration.

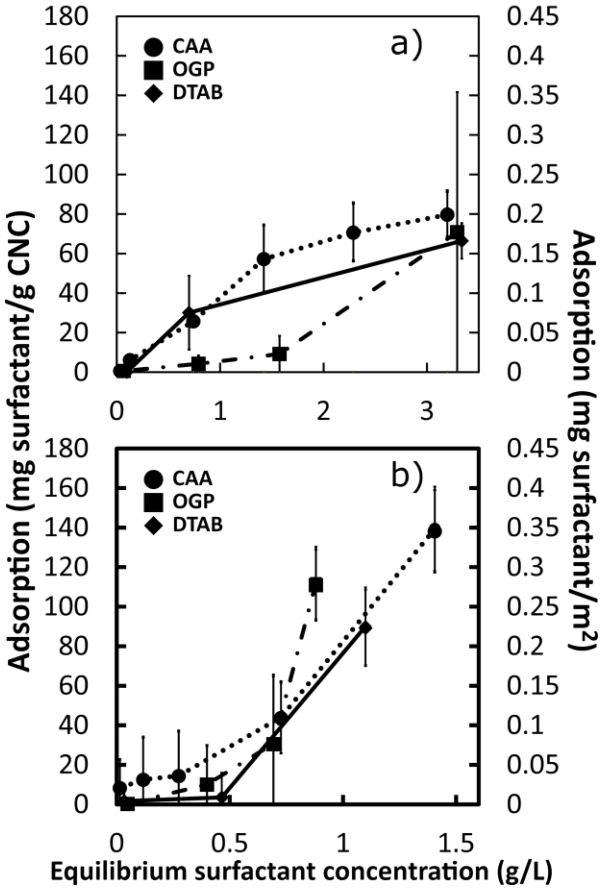

Figure 2-1: Adsorption isotherm of surfactants in a) API brine and b) SSW. The lines are to guide the eye.

Raman spectroscopy was used to elucidate other forms of intermolecular interactions between CNC and the surfactants. Since CAA and OGP can both hydrogen bond to CNC, special attention was placed on the -OH stretching signals (Figure 2-2). The addition of surfactants results in the formation of more structure in the OH stretching region of cellulose nanocrystals in SSW; the effect was less evident in API. The different peak sharpness,

broadening of the -OH signature peak, and definition suggest that –OH stretches are indeed sensitive probes to the CNC local environment. Such observations indicate the involvement of superficial hydroxyl groups of CNC in the adsorption process, providing evidence for the presence of H-bonding between CNC and surfactants in the complex mixtures.[188] However, the enhanced structure in the OH stretching region was also exhibited by DTAB which cannot receive or donate H-bonds; this may indicate an ion-dipole type interaction between the charged DTAB and the –OH groups on CNC. Interestingly, the Raman spectra observed after the addition of the surfactant strongly resembles that of CNC nanoparticles before the introduction to either SSW or API. This is shown in Appendix A Figure S1.5(a) to S1.5(d). This strongly suggests that the surfactants are counteracting the effects of interactions by CNC with species in the saltwater solutions.

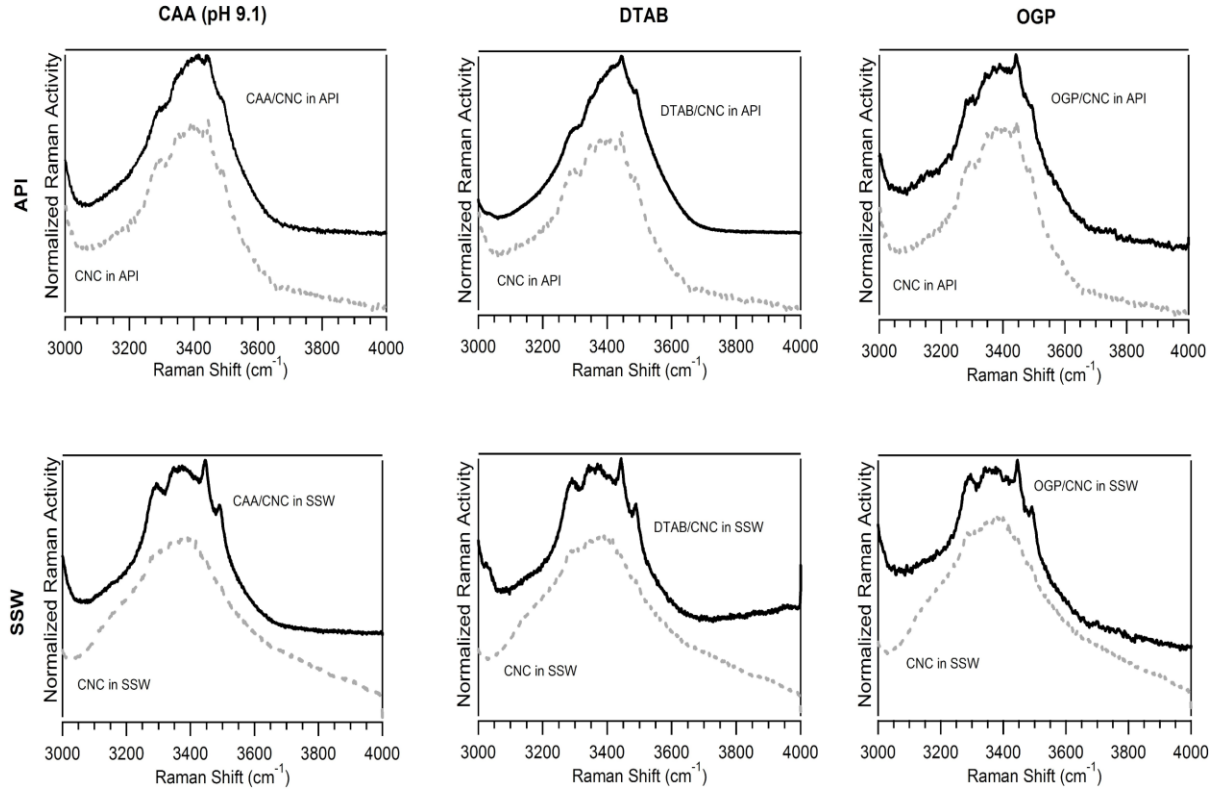

Figure 2-2: Raman spectra of CNC in API Brine (top) and SSW (bottom)

Raman spectra of CAA adsorbed onto CNC at different pHs in API brine was also measured. The structures in the -OH region was also affected by pH (Appendix A Figure S1.6). At pH 10, when the amine group of CAA is negatively charged (Appendix A Figure S1.7), a sharp peak was observed with small shoulders on the sides. At lower pH, where the amine group is protonated and positively charged, the –OH region was broader with less prominent peaks. The different peak patterns at variable pH suggest that in API brine, along with ion-dipole and H-bonding interactions, short electrostatic interactions may also be important in the adsorption of CAA onto the CNC surface.

3.3. Surface interactions and adsorption

The adsorption behavior of each surfactant and CNC was further studied through the dependence of surface tension (γ_{AW}) on emulsifier concentration. Surface tension vs surfactant concentration plots for each surfactant were generated in the presence and absence of CNC aggregates (Figure 2-3). Upon addition of 0.5wt.% CNC to a CAA-brine solution, the surface tension vs concentration plot shifts to the right; this effect is more prominent in API compared to SSW. Interestingly, despite adsorbing to the CNC surface, DTAB and OGP showed no significant curve shifting regardless of whether CNC aggregates were present in the dispersion or not. Such behavior suggests that in high ionic strength solutions, DTAB and OGP molecules preferentially migrate to the air-brine interface regardless of whether or not they adsorb onto CNC. CAA on the other hand, when adsorbed to the CNC surface does not migrate to the air/liquid interface and remain in the bulk. The observed trends thus suggest that the surfactant adsorption to nanoparticles may not affect of a surfactant solution. Thus surface tension study alone does not provide sufficient proof that the surfactant does not adsorb onto the nanoparticle.

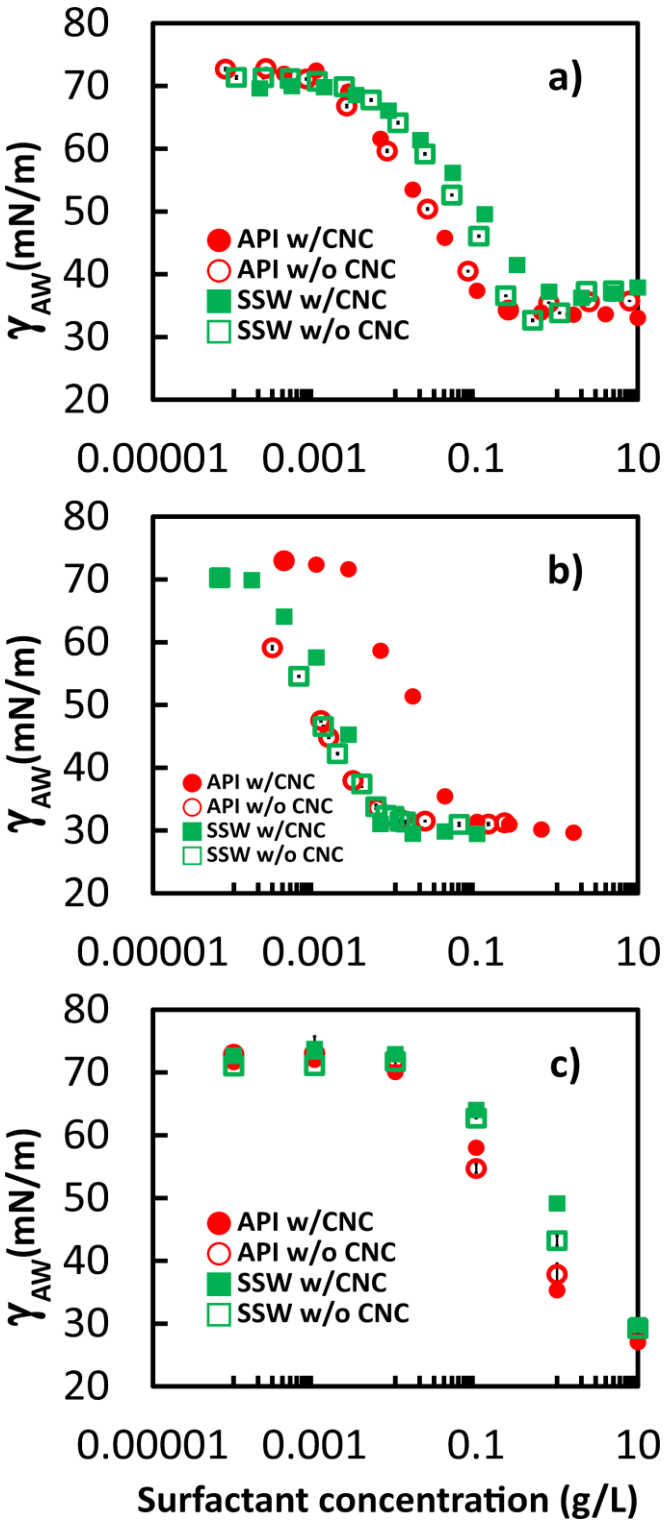

Figure 2-3: Surface tensions (γ_{AW}) a) DTAB, b) CAA and c) OGP as a function of surfactant concentration

Similar measurements carried out in DI water indicate the adsorption of surfactants onto well dispersed CNC is expected to be primarily driven by electrostatic attractive forces between the emulsifier's charged headgroup and the negative CNC surface. The plot for DTAB does shift to higher concentration in the presence of CNC when the experiment is done in DI water (Appendix A Figure S1.8); which is consistent with existing literature.[189,190] Similarly, if the surfactant and nanoparticle charges are similar, the surfactant might not adsorb to the particle's surface but instead competes to occupy the fluid/fluid interface.[191] In brine, however, the electric double layer collapses resulting in closer proximity between CNCs, and between CNC and the surfactants.[192],[77] Thus, in concentrated electrolytes solutions, the interaction between CNC and the emulsifiers is influenced by additional short-range intermolecular forces, which may include ion-dipole and H-bonding, in addition to electrostatic forces. This analysis is consistent with the vibrational Raman spectra, adsorption data, and surface tension measurements presented herein.

3.4. Interfacial behavior of CNC at the O/W interface

The effect of CNC concentration on brine's surface tension (γ_{AW}) and dodecane-brine interfacial tension (γ_{ow}) was studied in API and SSW (Figure 2-4). CNCs do not alter the surface and interfacial tensions in DI water[137]; however, in high salinity brine, CNC lowered both, as shown in Figure 2-4. The surface activity exhibited by CNC in brine occurs when they aggregate due to the collapse of the electrostatic double layer (EDL) stabilizing individual nanocrystals. The CNC aggregates then migrate towards a surface where they can adsorb and assemble, lowering the surface and interfacial tensions. It has been discussed by Kalashnikova et al. that CNCs orient themselves at the oil-water interface with the hydrophobic (2 0 0) edge inside the oil phase, further justifying their surface activity.[193]

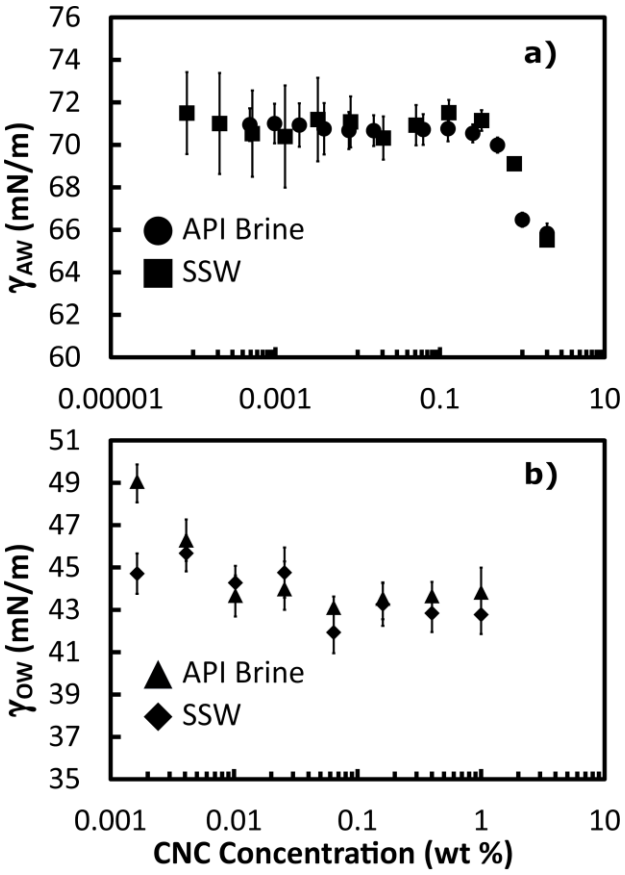

Figure 2-4: Surface tension a) and interfacial tension b) of dodecane/brine

3.5. CNC wettability and adsorption energy

Table 2-2 provides an overview of the contact angle (θ_{ow}) between the CNC film submerged in dodecane and surfactant solutions in brine, interfacial tension (γ_{ow}) between the two liquid phases, and the adsorption energy (ΔE_{rod}) of CNC onto the oil-water interface. The reported adsorption energies are calculated for individual rod-shaped CNCs ignoring CNC-CNC interactions. The contact angle measurements were taken after allowing the drop of surfactant solution to equilibrate with the CNC film for 100 s and are considered equilibrium static contact angle. The CNC film showed swelling when the surfactant solution was left for more than 5 minutes on top of it. The authors consider the measurements before swelling to be a closer representation of the contact angle between CNC, brine, and dodecane.

Table 2-2: Three-phase contact angle (θ_{ow}) interfacial tension (γ_{ow}) and CNC adsorption energy (ΔE) onto the oil/brine interface.

	API			SSW		
Surfactants	θ_{ow} (°)	γ_{ow} (mN/m)	ΔE_{rod} (kT)	θ_{ow} (°)	γ_{ow} (mN/m)	ΔE_{rod} (kT)
None	28.2±2.0	49.5±0.8	-413	33.4±3.0	46.7±0.8	-643
DTAB	37.7±1.3	12.8±1.3	-253	42.0±2.1	6.3±1.6	-167
CAA	24.3±4.2	14.9±0.5	-80.2	23.8±1.2	16.7±1.1	-86.2

Errors indicate standard error.

Table 2-2 indicates that the presence of CAA decreased the contact angle between brine and the CNC film, this was more prominent in SSW which has a lower ionic strength. DTAB, on the other hand, increases the contact angle, thus decreasing wettability. These results signal that the addition of CAA to a CNC dispersion in brine increases nanocrystal affinity towards the aqueous phase, while DTAB has the opposite effect.[194] Adsorption energies (ΔE_{rod}) were calculated for CNCs using Equation 3; which was derived based on Pawel Pieranski's approach (SI Derivation 1). It assumes individual CNCs of cylindrical shape (radius r and length L), lying flat on the oil-water interface.[195]

$$\Delta E_{rod} = 2rL\gamma_{OW}(\theta_{ow}\cos\theta_{ow} - \sin\theta_{ow}) + \gamma_{OW}r^2\cos\theta_{ow}\,[2\theta_{ow} - \sin(2\theta_{ow})] \quad (3)$$

In equation (3) the first term arises from the lateral sides of the nanoparticles and the second term represents the contact area from the particle ends. As shown in Table 2-2, DTAB has more negative adsorption energy compared to CAA in both brines; however, the magnitude is even larger for CNC without surfactants. Thus, CNCs alone have the highest tendency to stay at the oil/water interface. When comparing between DTAB and CAA, the former leads to preferential

adsorption to the interface. It must be pointed out that the CNCs in the aqueous is present as aggregates, thus the magnitudes of ΔE in Table 2-2 are likely underestimated.

In addition to adsorption energy; the free energy of drop formation (ΔG_{drop}) given by equation (4), is also expected to affect emulsion stability.[194,196]

$$\Delta G_{drop} = A_{OW}\gamma_{OW} + n_p(\Delta E_{ads} - T\Delta S_{ads}) \qquad (4)$$

The interfacial area is A_{ow} and the number of particles is n_p. The effect of the entropy term (ΔS_{ads}) in the equation is expected to be relatively small for large particles like the ones used in this study. It is expected that systems with very negative adsorption energy(ΔE_{ads}) are conducive to small values of ΔG_{drop} and are more stable. Similarly, the low interfacial tensions of CAA and, to a greater extent, DTAB are also expected to lower ΔG_{drop} and improve emulsion stability.

3.6. Emulsion stability

O/W emulsions were prepared using dodecane and 1 wt.% CNC suspensions in a brine/surfactant solution. Negatively charged, individual CNCs were not able to form stable emulsions in DI water and phase separation occurred within 1 min of mixing; however, in high ionic strength brine, where CNCs are aggregated, it was possible to prepare stable emulsions (Appendix A Figure S1.9). Thus, for CNC, decreasing colloidal stability by increasing salt concentration enables the formation of Pickering emulsion.

The position of the creaming front was monitored for 24 hours, by measuring the height of the aqueous phase eluted from the emulsion as indicated in Appendix A Figure S1.10 and Appendix A Figure S1.11. Emulsions in SSW were, in general, more stable to creaming compared to API. Emulsions prepared using CNC only were the most stable to creaming in most of the samples, the only exception being the emulsion prepared using DTAB+CNC in SSW with equal volume fractions of aqueous and organic phases (Appendix A Figure S1.11f). Emulsions

containing CAA were the least stable emulsions prepared; this is consistent with the very low contact angles, intermediate interfacial tension, and small adsorption energy observed for systems containing CAA in Table 2-2. According to Aveyard et al., colloidal particles with very large wettability are ineffective at stabilizing emulsions due to the particle remaining in the aqueous phase instead of adsorbing at the interface.[194] The combination of CNC and CAA appears to be detrimental to emulsion stability.

Emulsions containing 25% v/v aqueous phase formed highly stable emulsions as shown in Figure 2-5; remarkably, those inside the green box were stable to creaming for 21 months at the time of writing this article. On the contrary, the emulsions with 10% v/v aqueous phase separated quickly. At 25% v/v aqueous phase, the emulsions approach the phase inversion threshold, also evidenced by the low electric conductivity (Appendix A Figure S1.4). However since the CNC/surfactant mixtures are highly hydrophilic the emulsions do not invert phase, instead, a high organic phase emulsion gel is formed.[194] At water contents lower than 25% the highly hydrophilic particles cannot position themselves on the external side of the droplet and the emulsions cannot be stabilized.

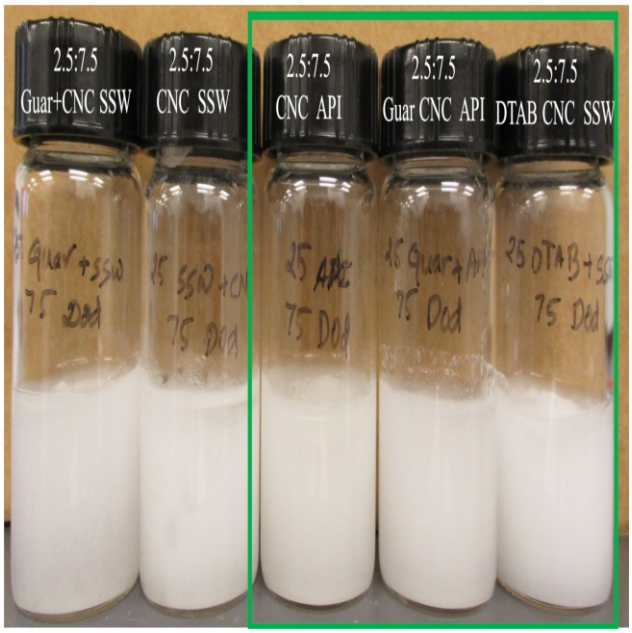

Figure 2-5: Stable emulsions after 6 months. Labels on vials indicate aqueous to oil phase volume ratio and components in the aqueous phase. Emulsions enclosed inside the green box were still stable after 21 months.

Figure 2-5 and Appendix A Figure S1.11 indicate that as the oil fraction increases, the addition of DTAB becomes beneficial for emulsion stability in SSW, but not in API brine. Interestingly the adsorption energy of CNC in DTAB is smaller than for CNC alone, which would indicate higher stability without the surfactant. However, in SSW, the interfacial tension γ_{ow} with DTAB is the smallest observed which according to equation 4 should improve emulsion stability. Ultimately, the balance of these competing effects leads to a positive synergistic effect between DTAB and CNC in SSW.

The stability of emulsions to coalescence was studied using optical micrographs of dodecane droplets over 24 hours (Figure 2-6). The coalescence results seem to follow a similar trend to creaming, with emulsions in SSW being more stable than those in API. Emulsions prepared using CNC in API (Figure 2-6a) showed broadening and shifting of the droplet

diameter peak, which was distinctly absent in emulsion prepared in SSW, indicating the latter are more stable to coalescence.

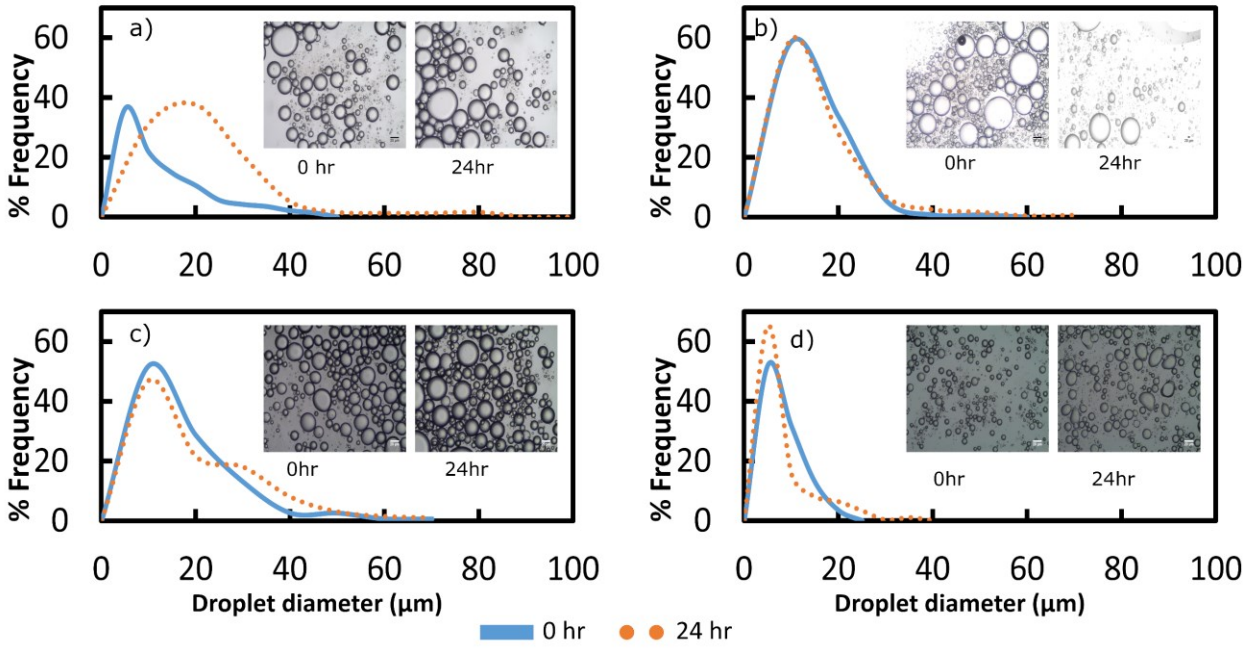

Figure 2-6: Droplet size distribution of a) CNC in API b) CNC + DTAB in API c) CNC in SSW and d) DTAB + CNC in SSW. The scale bar in the pictures represents 20μm.

3.7. CNC surface coverage and adsorption

The adsorption (Γ) of CNC onto the dodecane-brine interface was calculated for emulsions stabilized by CNC aggregates without surfactants according to equation 5.

$$\Gamma = \frac{m_P . d_{avg}}{6 . V_{oil}} \qquad (5)$$

The mass of CNC at the interface, m_p, was measured from the concentration change of CNC in the bulk aqueous phase eluted from the emulsions. The Sauter mean diameter, d_{avg}, was determined from the dodecane droplet size distribution. V_{oil} is the volume of the oil phase in the emulsion. Surface coverage (C) of emulsion droplets was estimated using equation 6.[53,110]

$$C = \frac{m_p d_{avg}}{6 h_p \rho_P V_{oil}} \qquad (6)$$

Where h_p is the height of CNC and ρ_p is the density of CNC equal to 1.64 g/cm^3. It should be noted that equation 6 assumes particles in the medium are dispersed without aggregation; hence any values calculated are an overestimation of the actual coverage. This equation, however, is used to compare with existing literature that uses the same method to quantify coverage.[54] Table 2-3 shows the adsorption (Γ) and estimated surface coverage of CNC at the brine/dodecane interface at different CNC concentrations in both API brine and SSW. The lowest surface coverage was 120±6% for dodecane/SSW with 25% aqueous phase. Coverage increased with decreasing oil content mainly due to the lower amount of interface available. It was determined that all the CNC in the system adsorbed at the oil-water interface in all cases. Cherhal et al. estimated a minimum of 84% cotton CNC coverage is required for the formation of Pickering emulsions stable for 1 month in a dilute 50 mM NaCl solution.[53] However, for the conditions tested here, surface coverage did not correlate to emulsion stability. The most stable emulsions were those with the lowest coverage; while the ones that creamed the most and broke fastest had 1800±93% coverage. Assuming a maximum packing density of 0.9[197], these adsorption amounts are equivalent to CNC crusts with minimum thicknesses of 12 nm for the most stable emulsion, and 135 nm for the least stable. Cherhal et al. studied the interfacial structure of CNC in oil-water interfaces at different CNC concentrations and ionic strengths up to 50 mM. They found, through small angle neutron scattering (SANS), that sulfated CNC in 50 mM solution formed interfacial layers with a thickness of 7±0.5 nm. However, unsulfated CNC, which aggregated in the aqueous medium, formed interfacial layers 19±0.5 nm thick. Furthermore, SANS and wide-angle X-ray scattering results indicated that CNC interacted with oil interfaces through the hydrophobic (2 0 0) plane with exposed CH groups.[53,193]

Table 2-3: Adsorption and surface coverage of CNC aggregates at the dodecane-brine interface

API			SSW		
Aq. v/v % in emulsion	Γ (g/m^2)	Coverage (%)	Aq. v/v % in emulsion	Γ (g/m^2)	Coverage (%)
90	0.58±0.03	5600±280	90	0.56±0.02	5400±300
75	0.20±0.01	1800±93	75	0.17±0.01	1670±90
50	0.060±0.004	580±30	50	0.059±0.004	570±30
25	0.018±0.001	170±10	25	0.012±0.001	120±6

Errors indicate standard error.

The fact that the most stable emulsions prepared in this study had intermediate coverage indicates that multiple competing effects influence emulsion stability. As the thickness of the cellulose crust covering the oil droplet increases, van der Waals attraction forces between droplets also grow, given that they are proportional to mass. In addition, a thicker CNC crust may increase the length and number of contact lines between oil, brine, and particles, leading to larger capillary forces. Both of these effects would reduce emulsion stability as more CNC is adsorbed onto the interface. On the other hand, the competing stabilizing effects of the CNC crust are expected to be steric repulsion between CNC aggregates on the surface and a large interfacial elasticity. The latter increases the drag force preventing droplets to approach each other by increasing the viscosity and elastic modulus of the interface.[72,198]

3.8. Interrelation between CNC and surfactants

The data presented herein suggest that CAA adsorption onto the CNC surface is detrimental to the stability of dodecane emulsions in a high ionic strength aqueous phases, while DTAB adsorption onto CNC only improves emulsion stability at or above 50% v/v dodecane in SSW. The findings reported herein suggest that regardless of whether small molecule emulsifiers adsorb onto the CNC or not; adsorption energy at the fluid/fluid interface and interfacial tension

are deterministic properties for Pickering emulsion stabilization. This is consistent with confocal microscopy observations by Hu et al, which indicate the HEC/CNC and MC/CNC particles adsorb at the fluid/fluid interface.[38]

Contact angle and surface tension measurements indicate that adsorption of CAA onto CNC increases their affinity towards brine, while DTAB adsorption has the opposite effect. Such observation suggests that CAA, a twice ethoxylated surfactant with a large headgroup, forms a bilayer assembly on the CNC surface with the hydrophilic side protruding towards the bulk aqueous phase (Figure 2-7c). Such assembly would make the surfactant coated CNC less hydrophobic, though they remain aggregated. DTAB, which has a small headgroup in high salinity solutions, adsorbs onto the CNC aggregates and diminishes their affinity toward the concentrated electrolyte solutions; thus, aiding their migration to the dodecane-brine interface (Figure 2-7b). CNC aggregates in brine without surfactants readily adsorb onto the dodecane-brine interface and are efficient emulsion stabilizers (Figure 2-7a).

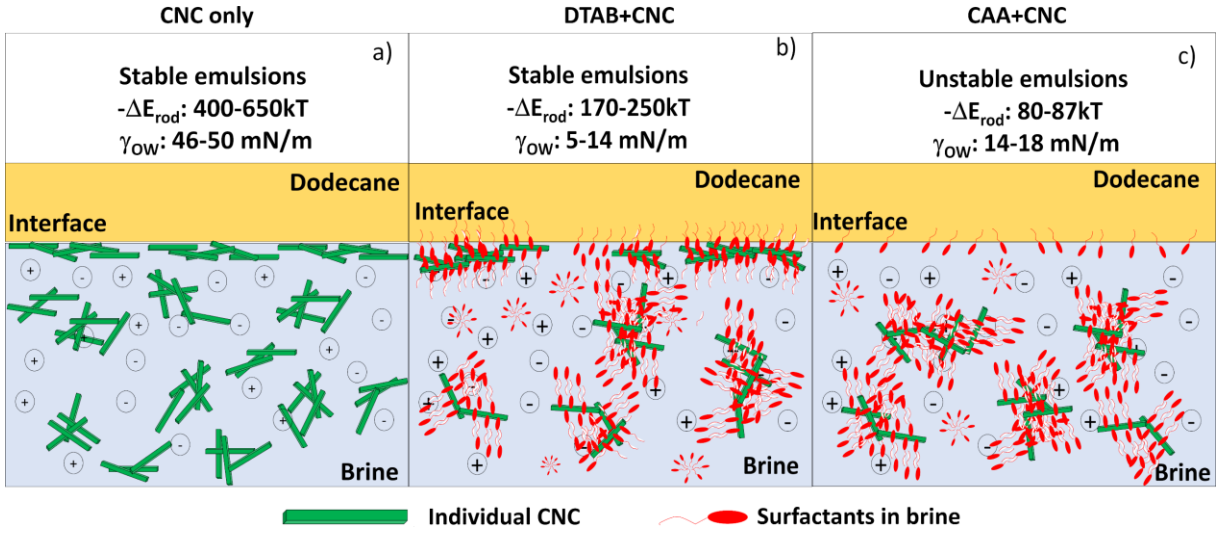

Figure 2-7: Schematics of a) assembly of CNC aggregates b) CNC + DTAB, and c) CAA assembly in the presence of CNC. Figure drawn not to scale.

4. CONCLUSIONS

Surface interactions and interfacial behavior of cellulose nanocrystals (CNC) aggregates and several surfactants were studied in two high ionic strength solutions, synthetic seawater (SSW: I = 0.65 M) and American Petroleum Institute (API: I = 1.9 M) brine, utilizing Raman spectroscopy and interfacial properties. All surfactants studied adsorbed to the CNC surface in both SSW and API brine; however, adsorption was smaller in API. Raman spectra indicated that hydroxyl groups on the CNC surface were involved in the adsorption of small molecule surfactants, providing evidence that H-bonding drives the adsorption of the non-ionic CAA and OGP onto CNC. Hydroxyl groups were also involved in the adsorption of DTAB, which cannot H-bond; suggesting other types of interaction, possibly ion-dipole, may drive their adsorption onto CNC. Addition of 0.5 wt% CNC to a CAA solution in API brine increased the surface tension by as much as 20 mN/m, while in SSW the increment was just a few mN/m. Surprisingly, for DTAB and OGP, the surface tension vs. concentration curves in SSW and API nearly overlapped with and without CNC, despite both surfactants adsorbing onto CNC. This observation, along with contact angle measurements, suggests that DTAB and OGP migrate to fluid-fluid interfaces irrespective of whether they are adsorbed to CNC or not. However, CAA, when adsorbed to CNC, preferentially remains in the bulk aqueous phase.

Emulsion stability measurements with added surfactants show that the effect of surfactants is highly dependent on the dodecane content, interfacial tension, and CNC adsorption energy. CAA significantly decreases the magnitude of the CNC adsorption energy onto the oil/brine interface and consistently reduced emulsion stability. DTAB decreases the adsorption energy to a lesser extent but also lowers interfacial tension to 6.3±1.6 mN/m in SSW and 12.8±1.3 mN/m in API. Thus, DTAB improves the emulsion stability of dodecane/SSW emulsions when the oil

content approaches the phase inversion composition. However, in API brine emulsions stabilized by CNC aggregates without surfactants were always the most stable. Emulsions stable for more than 21 months were prepared at 75% v/v dodecane content in SSW with added DTAB and in API brine without surfactants.

CHAPTER 3
Surface properties of cellulose nanocrystal stabilized crude oil emulsions and their effect on petroleum biodegradation

S. Parajuli, O. Alazzam, M. Wang, L.C. Mota, S. Adhikari, D. Wicks, E.E. Ureña-Benavides, Surface properties of cellulose nanocrystal stabilized crude oil emulsions and their effect on petroleum biodegradation, Colloids and Surfaces A: Physicochemical and Engineering Aspects. (2020) 124705. https://doi.org/10.1016/j.colsurfa.2020.124705.

ABSTRACT

The extent of biodegradation of C15-C20 aliphatic hydrocarbons in crude oil by *Serratia marcescens* after 5 days of incubation was improved from 1-12% to 6-19% by emulsifying crude oil using cellulose nanocrystals (CNC). Surface and physicochemical properties of prepared emulsions such as water salinity, presence of divalent ions and CNC concentration affect the extent of biodegradation due to their influence in emulsion stability. Stable oil in water (O/W) emulsions containing 5 v/v % crude oil and 95 v/v % brine was prepared with cellulose nanocrystals (CNC) at concentrations from 0.4 to 1.0 wt % in American Petroleum Institute (API) brine, synthetic seawater, and NaCl solutions. Creaming rate and droplet coalescence of emulsions were measured to study the impact of CNC concentration, divalent cations and ionic strength on emulsion stability. Results show a greater extent of droplet coalescence at CNC concentrations higher than 0.8 wt % for emulsions prepared in API. Coalescence was significant in API brine (ionic strength, I = 1.9 M); however, it was minimal in SSW (I = 0.65 M) and in NaCl solutions of the same ionic strength. Furthermore, no coalescence was observed in NaCl

solutions at ionic strengths of 0.32, 0.65, 0.95, and 1.9 M.

Keywords: Pickering emulsions, cellulose nanocrystals, biodegradation, adsorption, interfacial tension, crude oil

1. INTRODUCTION

Crude oil emulsions are an essential component of environmental protection services for cleanup of oil spills in seawater, produced water treatment and enhanced oil recovery. [199–201] Emulsions used for both marine oil-spill cleanup and oil/gas exploration are often stabilized using surfactants. However, in recent years polymers, nanoparticles (NPs) or their combination have gained interest in stabilizing these emulsions due to their lower toxicity, better thermal stability, and functionality. Bio-based NPs such as cellulose nanocrystals (CNCs) have additional advantages over conventional polymers and inorganic NPs such as silica, clay nanotubes, and gold as they are often more environmentally sustainable. CNCs are easily biodegradable and biocompatible in the marine environment making them an ideal candidate for applications in both oil field and oil-spill cleanup projects. [202–204] Currently available means of oil-spill cleanup methods in marine water include mechanical, chemical and biological treatment. Mechanical methods use oil booms and skimmers, while chemical treatments use dispersants; to break the oil sleek into finer droplets. Biological remediation of marine oil spill involves using microbial consortia that can either produce biosurfactants or microbes that can degrade hydrocarbons present in crude oil or the combination of both.[205–207]

In recent years, several studies have investigated the possibilities of using inorganic NPs such as alumina and polymer-coated iron-oxide for potential application as dispersant during the spill clean-up operation.[131,208–213] The NP concentration affects the stability of emulsions

and hence their ability to function as an oil-sleek dispersant. Frelichowska et al. used fumed hydrophobic silica NPs at a varying concentration to prepare emulsions containing 20 wt.% 2-ethylhexyl stearate and silicone oil in water. The authors found that increasing silica concentration decreased the size of the droplet giving more stable emulsions.[214] In a different study, the effect of monovalent and divalent ions on emulsion stability was investigated using canola oil/water emulsions stabilized using CNCs. CNCs were able to stabilize canola oil emulsions more effectively in the presence of Ca^{2+} ions <1mM, while in the presence of Na^{+} cations, 3mM electrolytes were needed to prepare stable emulsions. [111] These observations were attributed to the fact that electrolytes in aqueous medium screen charges on CNC surface thus promoting their migration and adsorption at the interface. Furthermore, a greater reduction in CNC zeta potential was observed with the addition of Ca^{2+} ions as compared to Na^{+} indicating more efficient charge screening by Ca^{2+} and thus diminished colloidal stability.[215,216] The stability of crude oil in water emulsions with aqueous volume fraction (ϕ_w) of 0.6 were prepared using different inorganic NPs (Fe_2O_3, Fe_3O_4, $Ca(OH)_2$, and clay). Their stability was studied in terms of water resolved upon centrifugation and electrical energy requirement for emulsion breaking. The results indicated that decreasing individual particle size and increasing particle concentration improved the stability of crude oil emulsion.[217]

Chitosan in conjunction with petroleum degrading bacteria was used to prepare stable emulsions of n-tetradecane. The emulsions containing bacteria and chitosan improved the rate and extent of biodegradation of tetradecane as compared to bacteria alone.[218] In a similar study, carbonized kaolinite NPs were used to stabilize hexadecane emulsions in the presence of model hydrocarbon-degrading bacteria (*Alcanivorax borkumensis*). The results indicated that 90% of the hexadecane were degraded by the bacteria, however, the addition of clay NPs did not

improve either the rate or the extent of degradation. The results indicated that despite a five-fold increase in surface area of the oil, the authors hypothesized that biodegradation occurs through the consumption of hydrocarbons solubilized in the bulk solution that is close to the interface or within biosurfactant micelles.[219]

Chemical dispersants are commonly used to increase the concentration of oil in the water column by emulsifying the oil to form tiny droplets. These dispersants, however, several studies have shown that they can have a toxic effect on the aquatic and marine ecosystems. It was found LC50 and EC50 concentration of that Corexit 9527 and 9500 towards amphipods and a marine sand snail were significantly lower than crude oil, [220] suggesting the addition of these chemicals were more harmful to those species than crude oil. In a separate study, coral larvae were exposed to source crude oil Deepwater Horizon spill and dispersant (Corexit 9500). The study found that settlement and survival corals decreased significantly following exposure to increased concentrations of crude oil and Corexit. [221] Toxicity of heavy crude oil and 3 different dispersants on marine fish was studied, the resulted showed that 24 hour LC50 of individual dispersants and oil was at least 1500 ppm and 325 mg/L respectively, however, a combination of oil and dispersants at lower concentration was more lethal to marine fish.[222]

The existing literature indicates that currently existing technologies for chemical remediation of oil-spills are either toxic to the marine environment as in the case of dispersants or are not significantly effective in improving the rate of biodegradation. This study highlights a potential application of the use of non-toxic and biodegradable CNC as dispersants for oil-spill remediation. We study parameters such as CNC concentration, aqueous phase ionic strength, and electrolyte type on the stability of crude oil/brine Pickering emulsions. Emulsion stability is described in terms of creaming rates and droplet coalescence. This study intends to characterize

emulsions prepared at high ionic strength aqueous phases, determine a range of conditions in which the emulsions are stable for potential biodegradation and how emulsification affects the biodegradability of crude oil. The effect of droplet surface area on crude oil biodegradation was studied by tracking the concentration of C15 to C20 alkanes via gas chromatography.

2. MATERIALS AND METHODS

2.1. Materials

Cellulose nanocrystals (11.5 wt.%), prepared from Pinus strobus (Northern pine) wood pulp, made by the USDA Forest Products Laboratory were purchased from the University of Maine and used as received. Calcium chloride ($CaCl_2$), 99.8 % purity, sodium chloride (NaCl), synthetic seawater (SSW), and reagent grade toluene were all purchased from Fisher Scientific and used as received. *Serratia marcescens* strain was obtained from Dr. Patrick Curtis' collection at the University of Mississippi Department of Biology. American Petroleum Institute (API) brine was prepared with a concentration of 8 wt.% NaCl and 2 wt.% $CaCl_2$ in DI water. DI water was obtained from a MilliporeSigma (Danvers, MA) Direct-Q 3 water purification system and had an electrical resistivity of 18.2 MΩ·cm at 25°C. Crude oil was kindly provided by Valero Refinery, Memphis TN and was used as received. The alkane standards C15-C20 were purchased from Sigma-Aldrich (Saint Louis, MO, USA).

2.2. Methods

2.2.1. Characterization of CNC

AFM measurements were carried out using a Nanoscope IIIA multimode scanning probe microscope from Bruker (Billerica, MA). Unmodified CNCs were dispersed in DI water at a concentration of 0.0001 wt% CNC and placed on top of freshly cleaved mica surface. The prepared sample was then allowed to dry overnight in a desiccator prior to taking AFM images. Topographic images of CNC were generated in tapping mode and processed using Gwyddion

2.51 to measure the length and height of cellulose nanocrystals. At least 150 individual particles were counted to generate length and height distributions of the particles used for the study.

Sulfur content on the CNC surface was measured via conductometric titration using a method explained elsewhere.[185,223] The concentration of sulfur (S) present on the surface of CNC was expressed in terms of %S using equation 1.

$$\%S = \left(\frac{V_{NaOH}C_{NaOH}MW_{sulfur}}{m_{susp}C_{susp}}\right) \times 100 \qquad (1)$$

In equation 1, V_{NaOH} and C_{NaOH} are the volume and concentration of NaOH used to neutralize the sulfonate groups on the CNC surface, MW_{sulfur} is the molecular weight of sulfur, $m_{susp,}$ and c_{susp} are mass and concentration of CNC suspension respectively.

2.2.2. Emulsion preparation, characterization and stability

The aqueous phases of emulsions were prepared by adding equal volume parts of 1.6 wt.% DI water-CNC suspension in 2x concentrated brine while mixing to prevent gelation. Crude oil and CNC/brine dispersions were added into 20 mL screw-capped vial to prepare 10 mL emulsions with volume fractions of oil to aqueous phase ranging from 0.05 to 0.95. The samples were then emulsified at 10000 rpm for 1 minute using a high-shear homogenizer (IKA Ultra-Turrax T-25 Basic, Atkinson, NH). Prepared emulsions were then characterized as either oil in water (O/W) or water in oil (W/O) type through conductivity measurements with an Orion™ DuraProbe™ 4-Electrode Conductivity Cell having Pt/Pt electrode.

The stability of emulsions was measured in terms of resistance to creaming and coalescence. Creaming was quantified by measuring the height fraction of aqueous phase eluted from the emulsion in the vial with respect to time over 24 hours. The digital photos of emulsions were taken over time and analyzed using the software ImageJ (U.S. National Institutes of Health). Droplet sizes were measured by image analysis of optical micrographs created by a

compound optical microscope (AmScope 500MD) and processed using ImageJ. Emulsion stability was also studied by generating droplet size distributions of at least 500 droplets from emulsion micrographs at different times to measure coalescence.

2.2.3. Interfacial tension

The pendant drop method was used to perform axisymmetric drop shape analysis of a captive crude oil drop formed in a U-shaped needle in the presence of excess CNC/brine dispersion after equilibrating for 60 mins. The interfacial tension was measured using an optical tensiometer (NanoScience Instruments, Phoenix, AZ). Contours of the oil droplet's shape were fitted to the Young-Laplace equation to calculate interfacial tension using equation 2.[187]

$$\Delta p = \rho g h - \gamma \left(\frac{1}{R_1} + \frac{1}{R_2}\right) \qquad (2)$$

Where Δp is the pressure difference across the interface, γ is surface/ interfacial tension, R_1 and R_2 are principal radii of curvature and the term ρgh is the hydrostatic pressure.

2.2.4. Biodegradation of crude oil

Preliminary experiments were performed to test if *S. marcescens* would grow in various brine solutions. API brine, synthetic seawater, Luria-Bertani (LB) broth, and crude oil were autoclaved at 121ºC for 20 mins. The stock culture of *Serratia marcescens* was inoculated in 5 mL LB broth and incubated at 37ºC overnight. A solution of 5 mL of SSW, API brine, and LB were inoculated respectively, with 0.5 mL bacteria solution previously mentioned, and incubated at 32ºC at 120 rpm for 24 hr. Bacterial growth was assessed by measuring absorbance at 600 nm using a spectrophotometer (Genesys 20, Thermo Scientific). The *Serratia marcescens* bacteria strain tested in this study did not grow in API brine (A_{600}= 0.04), hence biodegradation was only attempted in SSW (A_{600}=0.64). Samples tested for biodegradation were prepared by making crude oil emulsion in SSW in the presence/absence of CNC using the method explained in the

earlier section. The crude oil emulsion (10 ml), with and without CNC, was carefully transferred to a petri dish and 0.5 ml of the bacterial culture grown overnight in LB broth was added to the sample. In order to minimize salt dilution, 0.5 ml of autoclaved SSW was also added to the petri dish. Samples containing crude oil emulsions and bacteria were then incubated in a shaking incubator (120 rpm) at 32ºC, the extent of biodegradation was studied after 5 days of incubation.

After 5 days the Petri dishes were removed from the incubator and washed with excess toluene to recover the remaining crude oil. The samples collected were then centrifuged at 4980g for 20 mins, followed by careful recovery of the supernatant containing dissolved crude oil in toluene. These samples were then analyzed for the concentration of aliphatic hydrocarbons (C15-C20) using GC/Q-ToF to examine the extent of biodegradation. The analysis was carried out on an Agilent Technologies 7250 accurate-mass Q-ToF GC/MS systems equipped with an Agilent J&W HP-5MS UI (30 m x 0.25 mm ID, 0.25 µm film thickness) capillary column. The GC separation was carried out using the program described as follows: 1 µL of the sample was injected into the column with the initial oven temperature set at 45ºC (held for 2 mins), the temperature was then increased sequentially in steps from 45 to 150ºC at a rate of 2ºC min^{-1}, and 150 to 280ºC at a rate of 5ºC min^{-1}, then held isothermally for 10 mins at 280ºC. Helium was used as carrier gas at a flow rate of 1.0 ml/min. Both the inlet and transfer line were set to 280ºC. Split injection mode was used with a split ratio of 25:1. The Q-ToF spectra were recorded at a scan mode with the EI voltage set to 70 eV. The calibration curves for the used reference standards of C15-C20 were realized by plotting peak area versus analytes concentration (1.9, 5.7, 9.5, 19.0, 28.6 and 38.1 µg/mL). The extent of biodegradation was expressed as a percentage of C15-C20 hydrocarbons consumed by the bacteria according to equation 3.

$$\%\, Degradation_i = \frac{(C_{i.0} - C_{i,t})}{C_{i,0}} * 100 \qquad (3)$$

Where, $C_{i,0}$ and $C_{i,t}$ are the concentration of hydrocarbon having chain length (i).

3. RESULTS AND DISCUSSIONS

3.1. Characterization of crystalline nanocellulose

Figure 3-1 shows an AFM image of the typical CNC used during the project. The results showed the average length of the CNC used was 130.3±41.5 nm while the average height was 6.3±1.8nm giving particle aspect ratio (length: height) of 20.6. Previous studies have indicated that the CNC derived from wood pulp has the lengths ranging from 100-300nm, height ranging from 3-7nm resulting in aspect ratio ranging from 20-100.[224,225] CNCs prepared using sulfuric acid hydrolysis results in the addition of $-OSO_3^-$ on their surface, thus giving them a negative charge. Conductometric titration of CNC with 0.1M NaOH was carried out at room temperature using the method explained elsewhere[185,223] and the degree of sulfation or charge was expressed as the percentage of sulfur (S) present at the surface determined from equation 1. The sulfur content on the surface of CNC is affected by factors including reaction time, the concentration of sulfuric acid and reaction temperature.[226] Results showed (Appendix B Figure S2.1) that the average sulfur content on the CNC used on the project was 0.4% g-sulfur/g- CNC. The degree of sulfation affects the ability of CNC to interact with divalent cations such as Ca^{2+} and Mg^{2+} present in aqueous media. Divalent cations may replace the proton counterion and form ionic bridges between sulfate half-esters on adjacent CNCs leading to aggregation [227], which is expected to affect emulsions stability.[40]

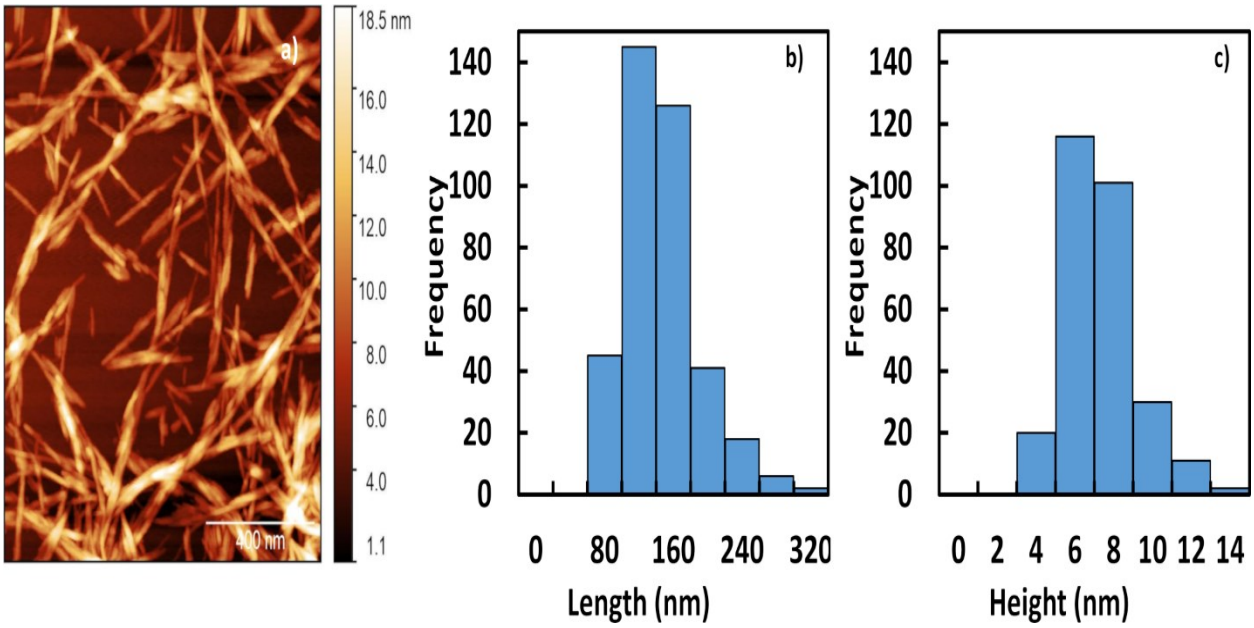

Figure 3-1. (a) Topographic image of wood-pulp derived CNC using AFM along with (b) length distribution and (c) the height distribution.

3.2. Emulsion characteristics and stability

3.2.1. Emulsion type

Emulsions prepared using crude oil and various brine solutions were characterized as either oil in water (O/W) or water in oil (W/O). The electrical conductivity of emulsions prepared was measured and plotted as the function of aqueous phase volume fraction (ϕ_w). The conductivity plot was used to distinguish the emulsions as either O/W or W/O (Appendix B Figure S2.2). The results indicate that all emulsions prepared in this study were O/W type. CNCs prepared using sulfuric acid possess negative surface charge and are colloidally stable in DI water. In the presence of electrolytes, however, the electrostatic double layer (EDL) responsible for colloidal stability of the CNC suspension collapses due to screening of the surface charges by the charges in the bulk and results in the aggregation of CNC suspension.[77] The induced colloidal instability drives the migration of CNC aggregates to the oil-brine interface where they orient themselves such that their hydrophobic edges are oriented towards the oil phase.[32] The hydrophilic nature of the CNC implies that they are wetted by the aqueous phase and have

contact angle less than 90° resulting in the formation of O/W type emulsions.[69]

3.2.2. Creaming

Emulsion stability was measured in terms of two stability parameters; first the resistance of emulsion to creaming over 24 hours and second, quantifying droplet size distribution to study droplet coalescence. Both stability parameters were examined under a set of different physicochemical conditions. Figure 3-2 shows the creaming profile of emulsions (ϕ_w=0.95) in different aqueous phases. The effect of CNC concentration on emulsions prepared in 100% API is shown in Figure 3-2a; at concentrations below 0.4 wt.% no emulsions were stable and as the concentration of CNC increased the emulsions became more resistant to creaming. After 24 hours at 0.4 wt% CNC, approximately 38% of the aqueous phase was resolved from the emulsion phase compared to about 18% resolved aqueous phase when 1wt% CNC was used. Similar results were observed when using silica NPs to stabilize emulsions, it was found that decreasing the NP concentration decreased the stability of emulsions to creaming. [214,228] The addition of a higher concentration of NPs results in the formation of a network of aggregates leading to gelation and subsequent increase in viscosity of the aqueous phase thus slowing down creaming as described by Stokes equation (equation 4). [194]

$$\nu = \frac{d^2 g(\rho_1 - \rho_2)}{\eta} \qquad (4)$$

Where ν is the sedimentation velocity, d is the average diameter of the droplets, g is the acceleration due to gravity, ρ_1 and ρ_2 are the density of the different fluid components and η is the viscosity of the continuous phase. Interestingly, the eluted aqueous phase is virtually free of CNC, as is evident from the clear liquid at the bottom of the vials in Figure 3-2e and by UV-vis spectroscopy measurements. This indicates the CNC mainly remains adsorbed at the oil/brine interface. The creaming profiles of the samples appear to show initial dead time before the

creaming process starts. This initial lag could be related to the time required for the reorganization of NPs at the oil-water interface.

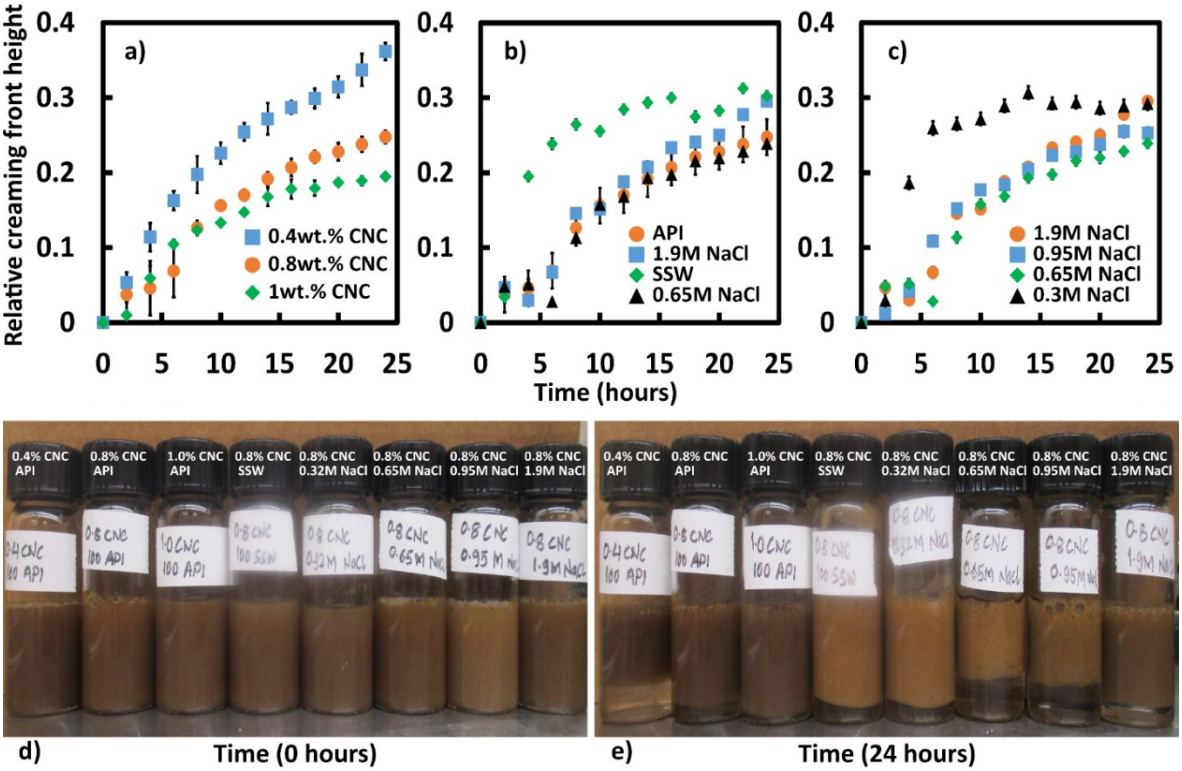

Figure 3-2. Emulsion creaming: a) Effect of CNC concentration, (b) Effect of divalent cations at and (c) Effect of ionic strength. Pictures (d) and (e) are representative emulsions immediately after emulsification and after 24 hours.

Varanasi et al. found that the addition of Ca^{2+} to an aqueous suspension of CNC lowered the concentration of CNC required to stabilize crude oil emulsion.[111] In this study, the presence of divalent cations did not have a significant effect on creaming behavior at the ionic strength of API brine. However, in SSW (Figure 3-2b) the initial rate of creaming was higher than the emulsions with the same ionic strength of NaCl, although the amount of aqueous phase-resolved after 24 hours was similar (approximately 30%) in both cases.

The effect of ionic strength of electrolytes on emulsion resistance to creaming was also studied (Figure 3-2c). The results indicate that at lower ionic strength (0.3M NaCl) the rate of emulsion creaming is faster compared to emulsions prepared in higher ionic strength solutions (0.65M, 0.95M, and 1.9M). However, after 24 hours the total resolved fraction for all ionic strengths studied was similar. The reasons for the faster initial rate of creaming at 0.3 M are uncertain; however, it could be due to the lower viscosity of the continuous phase at lower ionic strengths. It is also possible that adsorption of the CNC onto the interface occurs faster at low ionic strength.[111,194]

3.2.3. Coalescence

Emulsion stability was also measured in terms of droplet coalescence by tracking the droplet size distribution of emulsion droplets for 24 hours using optical micrographs. The micrographs were generated immediately after emulsification and after resting the emulsion at countertop for 24 hours and room temperature. Ostwald ripening is not expected to be significant in this system due to the low curvature of the interface and low crude oil solubility. The Sauter mean droplet diameters D[3,2] are between 29 and 39 μm in all cases (Appendix B Table S2.1), while the solubility limit of crude oil in distilled water is close to 40 ppm or less, and an even lower solubility is expected at the high ionic strengths studied herein.[229]

3.2.3.1. Effect of CNC concentration

Crude oil emulsions (ϕ_w= 0.95) containing a varying concentration of CNC in the aqeous phase were prepared in API brine to study the effect of CNC concentration in droplet coalescence. Figure 3-3 shows the effect of CNC concentration on the stability of emulsions to coalescence. Results indicate that at the concentration of 0.4wt% CNC (Figure 3-3a) there was no significant change in the droplet size distribution of the crude oil emulsions. Interestingly, as the concentration of CNC increases to 0.8 wt% CNC (Figure 3-3b) and 1 wt% CNC (Figure 3-

3c) the distribution curve broadens and/or shift to the higher droplet diameter over a 24 h period indicating coalescence of emulsion droplets. The difference between the populations' means was verified by a hypothesis test with 95% confidence as indicated in Supporting Information Table S1. This result is in contradiction to other findings in the literature where the increase in the concentration of NPs reduced coalescence.[194,230,231] AlYousef et al. observed that increasing NP flocculation and concentration helps improve the stability of Pickering foams; however, they suggest too many flocs at high NP concentration can be detrimental by lowering maximum capillary pressure.[57] Thin-film integrity is crucial for the stability of Pickering emulsions and foams; the maximum capillary pressure (P_c^{max}) beyond which the film collapses and promotes coalescence is governed by equation 5.[57,85]

$$P_c^{max} = p\frac{2\sigma_{ow}}{R}(\cos\theta + z) \qquad (5)$$

Where p is packing parameter, R is a radius of the NPs, σ_{ow} is interfacial tension between oil and water phase, θ is contact angle and z is a parameter related to the arrangement of particles in the thin aqueous film. The contact angle of brine on CNC could not be measured due to swelling of CNC film submerged in brine and the lack of optical transparency when the film was submerged in crude oil; however, its value is independent of CNC concentration, as is the interfacial tension. The parameters p is related to the coverage of the interfacial area, while z is related to the assembly of the second layer of NPs. The value of parameters p and z of the CNC crust around the droplets is not expected to vary significantly within the concentration range studied herein. The presence of electrolytes in aqueous medium induces aggregation of CNCs which in turn affects their packing at the interface, typically resulting in enhanced stability of Pickering emulsion. However, at a high enough concentration CNC can form excessively large aggregates increasing the effective radius. This would lower the maximum capillary pressure (P_c^{max}), in

accordance with Eqn. 5, thereby decreasing the stability of the emulsion.[57,85]

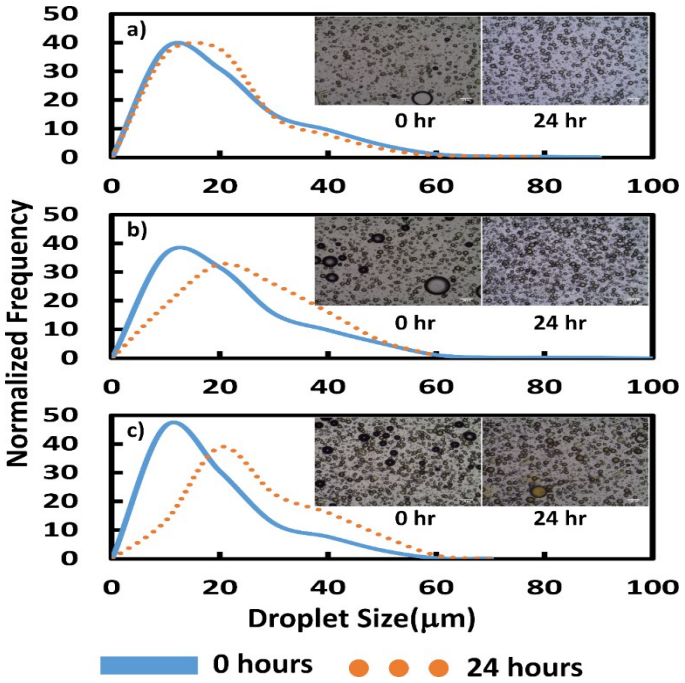

Figure 3-3. Droplet size distribution of emulsions prepared in API brine and CNC concentration a) 0.4 wt.%, b) 0.8 wt.%, and c) 1 wt.%

3.2.3.2. Effect of divalent ions

Crude oil emulsions (ϕ_w= 0.95) containing 0.8 wt.% CNC in aqueous phase were prepared in salt solutions with I = 1.9 M (API brine and 1.9 M NaCl) and I = 0.65 M (SSW and 0.65 M NaCl). The effect of the presence of divalent ions on droplet coalescence was studied by observing the droplet size distribution (Figure 3-4) of crude oil droplets for 24 hours. Results indicate that the presence of divalent ions in SSW (Figure 3-4c) did not affect droplet coalescence when compared to 0.65 M NaCl (Figure 3-4d). In both cases, the emulsions showed no coalescence for 24 h as indicated in Appendix B Table S2.1. The initial D[3,2] was 32.8 μm (s=11.0 μm) for SSW and 39.0 μm (s=12.7 μm) for 0.65M NaCl. After 24 hours no significant change in D[3,2] was seen on either SSW (D[3,2]=33.15 μm, s=11.2 μm) or 0.65 M (D[3,2]=37.9 μm s=12.9 μm) emulsions.

Interestingly, in API coalescence was observed as indicated by the shift in droplet size distribution to higher droplet diameter (Figure 3-4a) and by a hypothesis test comparing both means (Appendix B Table S2.1). Interestingly, the D[3,2] of emulsion droplets remained unchanged over a 24 h period, with initial and final values of 34.5 μm (s=12.3 μm) and 32.6 μm (s=11.5 μm), respectively. This behavior is due to the presence of a long tail (larger droplets) in the initial distribution which is absent in the droplet distribution after 24 hours. The largest droplets either coalesced into a separate oil phase or creamed to the top of the emulsion phase and were not sampled. When the emulsions were prepared in 1.9M NaCl, D[3,2] decreased from an initial value of 38.2 μm (s=13.8 μm) to 30.2 μm (s=9.8 μm), however, statistical analysis did not show enough evidence to conclude that the changes in the mean were statistically significant at 95% confidence. Further study is needed to understand why such behavior was observed however, it can be hypothesized that larger droplets cream faster than the smaller ones based on Stoke's law (equation 4). Closer proximity between larger droplets would lead to faster coalescence, possibly due to an increased length and number of CNC/oil/brine contact lines resulting in a decrease in D[3,2] values.[176,40]

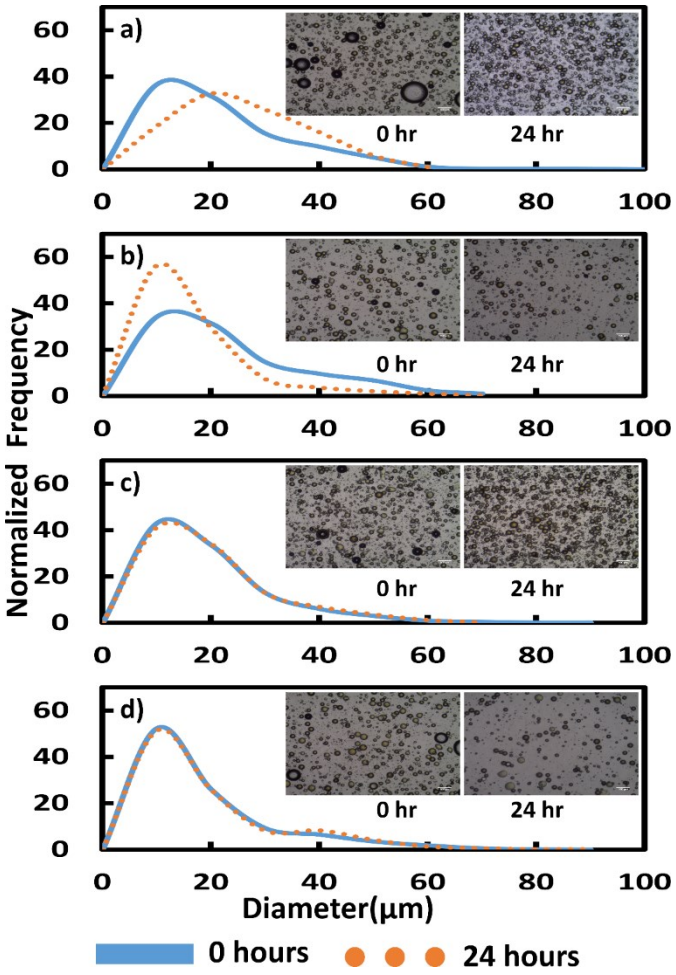

Figure 3-4. Effect of the presence of divalent ions on the coalescence of crude oil emulsion droplets prepared in a) API brine, b) 1.9 M NaCl, c) SSW and d) 0.65 M NaCl.

3.2.3.3. Effect of ionic strength

The effects of ionic strength (*I*) of the aqueous medium on emulsion stability was studied by preparing crude oil emulsions (ϕ_w= 0.95) containing 0.8 wt.% CNC in the aqueous phase and NaCl solutions at 4 different ionic strengths: 1.9M, 0.95M, 0.65M, and 0.3M (Figure 3-5a-3-5d respectively). Figure 3-5 indicates that the ionic strength of the solution did not have a significant effect on the extent of droplet coalescence for 24 hours. The behavior of emulsion droplets in 0.65 M NaCl was similar to that of emulsions prepared 1.9M NaCl, with an apparent decrease in D[3,2] for 24 hours however statistical analysis showed that the mean diameters remained

unchanged in both cases at 95% confidence. For lower ionic strengths, the D[3,2] did not change significantly over the same time. The addition of salt to CNC dispersions has been shown to improve emulsions stability.[131,213] However, most studies are limited to low ionic strengths of 5% NaCl or less. Herein we note that the increased ionic strength of the monovalent ion did not have a significant effect on droplet coalescence.

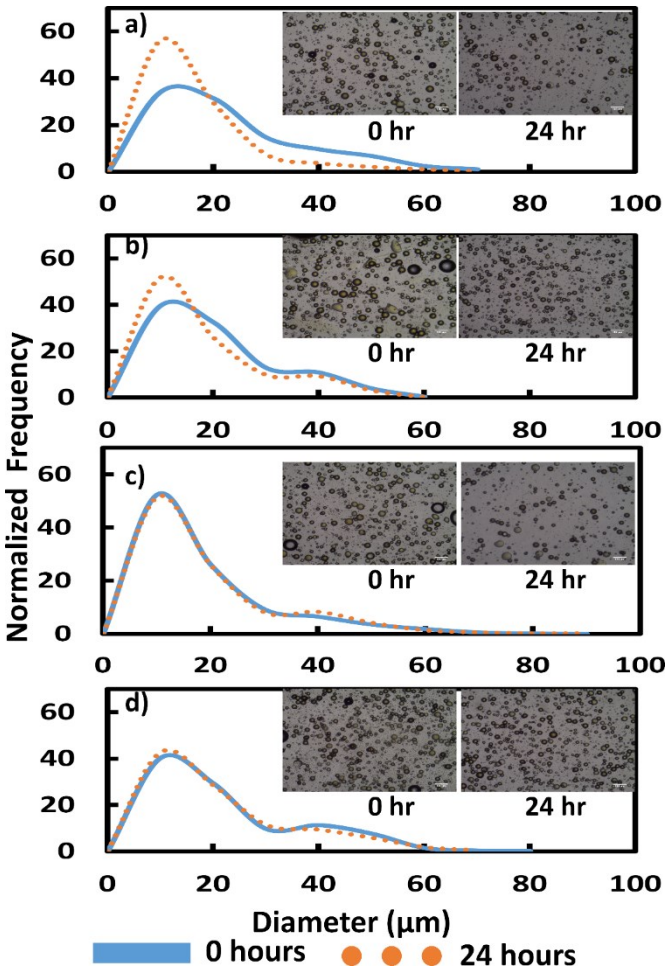

Figure 3-5: Effect of ionic strength of NaCl a)1.9M b) 0.95M c) 0.65M and d) 0.32M on the droplet size distribution of emulsions.

3.3. Interfacial tension

The effect of CNC concentration on interfacial tension (IFT) between crude-oil and various aqueous phases was measured using a pendant drop method with a rising oil drop in a U-

shaped needle suspended in the excess aqueous phase. The system was allowed to equilibrate for 60 minutes before taking the measurements. Figure 3-6 represents the change in interfacial tension as the function of CNC concentration. It can be seen from the figure that for all aqueous phases, the interfacial tension measured was in the range between 5.5-7.0 mN/m. Such low interfacial tensions favor the formation of droplets due to low free energy of drop formation.[40] The results indicate that over the concentration range studied, the IFT between various aqueous phases and crude oil did not change significantly with the increase in CNC concentration. In the absence of CNC, the IFTs of crude oil with API brine, 1.9 M NaCl, SSW, and 0.65 M NaCl were 5.7±0.3, 6.9±0.3, 5.5±0.3 and 6.7±0.3 mN/m respectively. The addition of up to 0.064 wt% CNC onto the aqueous phase did not change the interfacial tension between brines and crude-oil, which is typical of NP stabilized systems. Larger concentrations could not be studied since the dispersion becomes turbid, preventing adequate imaging of the suspended drop. The enhanced stability of Pickering emulsions as a consequence of NP addition has often been attributed to an increased maximum capillary pressure, the viscosity of the continuous phase, and the energy of desorption. [40,57]

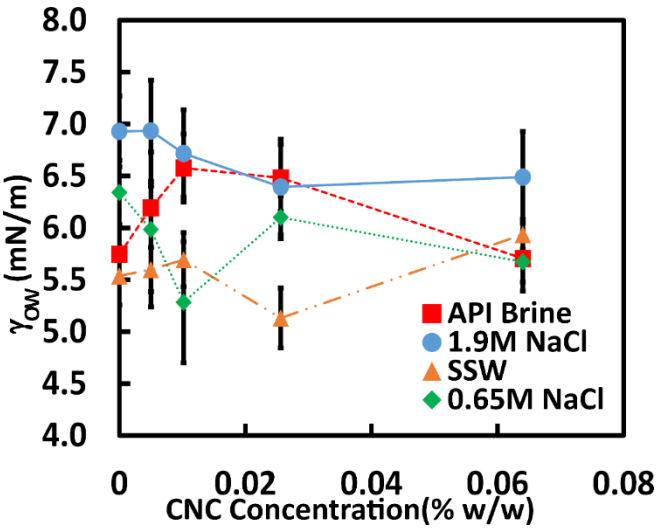

Figure 3-6: Interfacial tension between different brines and crude oil at different CNC concentration

3.4. Adsorption/Surface coverage of CNC at oil/water interface

Adsorption (Γ) of CNC aggregates onto the oil/water interface can be estimated based on the Sauter mean diameter D[3,2] of emulsion droplets, the volume of oil added to the emulsion (V_{oil}), and mass of CNC (m_p) at the interface using equation 6.

$$\Gamma = \frac{m_p D[3,2]}{6V_{oil}} \qquad (6)$$

The volume per area (V^S) of adsorbed CNC aggregates can be estimated from the adsorption.

$$V^S = \frac{\Gamma}{\rho_p} \qquad (7)$$

In equation 7, ρ_p is the density of CNC (1.6 g/ml)[232]. The volume per area of CNC can be interpreted as the minimum possible thickness (δ) the CNC layer would have if it had no porosity; the actual δ would necessarily be larger. Table 3-1 summarizes the adsorption and volume per surface area of CNC at the crude oil-brine interface. The results indicate that CNC adsorption does not necessarily correlate to resistance to coalescence and emulsion stability. Rather interestingly, when the concentration of CNC was increased, the adsorption increased by the factor of 2.5, however, with increasing concentration, the emulsion stability decreased. This

is the opposite trend observed in other studies where a higher amount of CNC at the surface improved stability.[53,110] Contrary to the work presented herein, CNC adsorption was very small in those studies, less than one monolayer. The data in Table 1 indicate a thick crust of CNC exists around the crude oil droplets. At the high concentrations studied herein, excess CNC appears to be detrimental to stability. A balance between competing effects appears to exist. Increasing the CNC concentration would raise the viscosity of the liquid film between droplets, which would slow down the drainage and improve stability. Moreover, a repulsive force is expected to arise due to steric effects. On the contrary, van der Waal's attractive forces, which are proportional to the mass of the droplets and the crust would increase leading to lower stability. Furthermore, capillary forces may lead to the breakage of the thin film between droplets, which is determined by the maximum capillary pressure described in equation 5. As suggested by AlYousef et al., it is possible that excessively large CNC aggregates may lower the maximum capillary pressure. [57]

Table 3-1: Mass adsorption and volume of CNC per interfacial area.

Samples	Γ adsorption (g/m^2)	V^S (μm)	Coalescence over 24 hours
0.4% API CNC	0.42±0.15	0.26±0.14	No
0.8% API CNC	0.85±0.30	0.52±0.29	Yes
1% API CNC	1.08±0.37	0.66±0.36	Yes
0.8% CNC SSW CNC	0.86±0.29	0.53±0.28	No
0.8% CNC 1.9M NaCl	0.79±0.25	0.48±0.25	No
0.8% CNC 0.98M NaCl	0.78±0.29	0.48±0.28	No
0.8% CNC 0.65 M NaCl	0.99±0.33	0.60±0.32	No
0.8% CNC 0.32M NaCl	0.92±0.33	0.56±0.32	No

3.5. Quantification of biodegradation of crude oil

Biodegradation of crude oil by *Serratia marcescens was* measured by quantifying the concentration of C15-C20 aliphatic hydrocarbons using GC/Q-ToF. Figure 3-7 shows the chromatograms of hydrocarbon standards (Figure 3-7a) along with the crude oil (Figure 3-7b). The results of the biodegradation study were expressed as the percentage (error bars represent standard errors) of hydrocarbons degraded (Figure 3-7c) by the bacteria after 5 days of incubation in the presence and absence of CNCs. It was found that after 5 days of incubation, the presence of CNC in crude oil to emulsify them resulted in improved degradation of hydrocarbons in the crude oil. For C15 hydrocarbons the extent of degradation improved from 1.3±1.1% without CNC to 6.2±3.3% in the presence of CNC. Similarly, after 5 days of incubation, the average degradation tended to increase from 8.3±2.5 to 9.0±6.5, 11.8±0.1 to 15.1±6.1, 6.9±4.7 to 11.8±6.2, 11.5±3.4 to 19.2±5.2, and 6.8±5.2 to 13.6±4.4 % in the presence of CNC for C16, C17, C18, C19, and C20 respectively. Unfortunately, the magnitude of errors prevents conclusive evidence that the biodegradation increased for the emulsified oil. This observation suggests that a larger surface area of the oil drops due to emulsification by CNC may lead to increased biodegradation of linear alkanes by bacteria. The formation of stable oil droplets increases the surface area of the oil available for the microbes to colonize, it also promotes the diffusion of microbes to the oil-brine interface and provides an aquatic environment for microbial growth and biodegradation of oil.[233,234] It has been suggested that the biological degradation observed in could primarily be due to the consumption of hydrocarbons close to the oil-water interface, further highlighting the importance of an increase in oil surface area to promote biodegradation.[219]

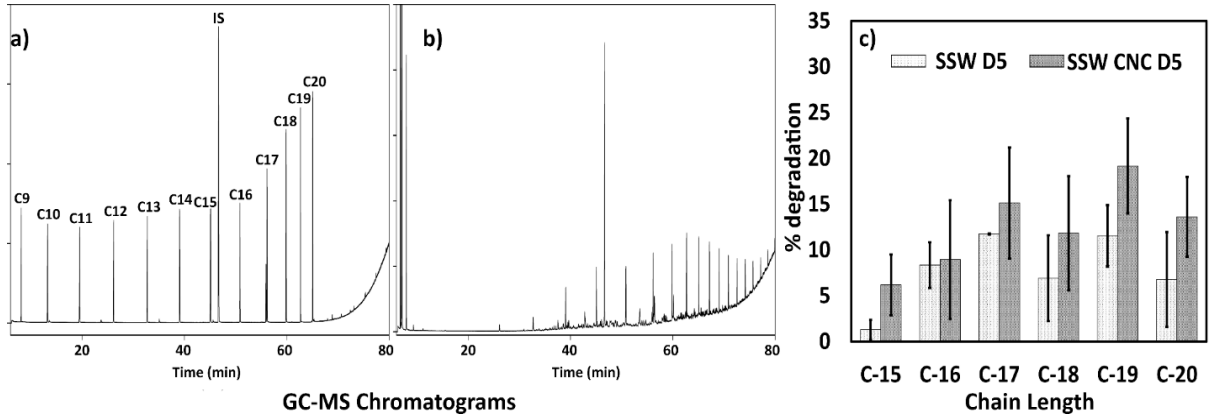

Figure 3-7: a) a GC chromatogram of hydrocarbon standards (C15-C20) with internal standard b) GC chromatogram of crude oil control after 5 days of incubation c) Biodegradation of crude oil hydrocarbons by *Serratia marcescens* in the presence and absence of CNC.

It should be noted, however, that samples containing no CNC degraded more after 10 days of incubation and CNC either decreased or did not significantly improve the degradation of crude oil linear alkanes. Under the incubation conditions (32^{o}C and shaking at 120 rpm), the emulsions broke within 5 days. It is not clear at the moment as to what could cause the degradation to cease but it could be because the breaking of emulsions would result in limited surface area of oil which in turn would limit the degradation of hydrocarbons. High emulsion viscosity would possibly result in limited motility of the microorganisms keeping them away from the interfacial region. It has been reported that small increment in viscosity (0.8 to 5 mPa.s) increases the swimming velocities of flagellated bacteria, however, beyond 10 mPa.s, further increase in viscosity severely reduced the motility of bacteria.[235] Overall, the results suggest that emulsification by CNC could be effective at increasing rates of crude oil biodegradation, as long as emulsion conditions such as viscosity and superficial affinity are adjusted to provide a better environment for the microorganism.

The effectiveness of common emulsifiers on improving the biodegradation of hydrocarbons using different *Pseudomonas* and *Bacillus* strains was tested in a study. The results showed that the presence of emulsifiers does not necessarily translate into improved

biodegradation.[236] For instance, the presence of emulsifier AT7, Tween 80, L-10, and Lutensol GD did not improve the biodegradation of hydrocarbons by *Pseudomonas aeruginosa* and in some instance adversely affected the ability of the bacteria to degrade hydrocarbons. In the absence of emulsifiers, however, the bacterial strain degraded a higher percentage (30-50%) of the hydrocarbon than the bacteria used in this study (1-12%). It is further argued that the synergistic interactions between bacterial strain and emulsifiers are very important for improved efficiency of biodegradation.

The outer surface of *Serratia marcescens,* a gram-negative bacterium, is negatively charged due to the presence of different lipopolysaccharides (LPS). These LPS molecules bind to each other in the presence of electrolytes and screen the negative surface charge.[237] A similar phenomenon is the screening of superficial negative charge on CNC surface results in the aggregation of CNCs as well. Thus under conditions tested herein where the electrolyte concentration is very high in the aqueous medium, the electrostatic repulsion between CNC and the bacterial cell wall is limited to a range of few Angstroms (Å) and the electrostatic potential between two surfaces can essentially be considered close to 0 mV.[77] This creates a favorable environment for adsorption of bacteria to the surface of CNC stabilized oil-droplets which in turn could potentially improve the biodegradation of hydrocarbons.

4. CONCLUSIONS

The biodegradation of petroleum hydrocarbons by *Serratia marcescens* appears to have increased from 1-12% to 6-19% over a 5 days incubation period in the presence of non-toxic and environmentally benign CNCs but could not be determined conclusively due to overlapping margin of errors. Such improvement in hydrocarbons degradations without any use of chemical dispersants could imply that CNC can be potentially be used as an alternative to chemical

dispersants in events of oil-spills. The ability of the bacteria to effectively decompose alkanes in crude oil was governed by the stability of crude oil emulsion in brine prepared using CNC. Stable O/W emulsions of crude oil were prepared using CNC suspension in different brine solutions. The stability of emulsions (ϕ_w=0.95) prepared using 0.8 wt% CNC was studied in terms of their resistance to creaming and droplet coalescence. It was shown that increasing the CNC concentration decreased the rate of emulsion creaming, however, as the CNC concentration increased the extent of droplet coalescence also increased. Higher CNC concentrations likely increased the viscosity of the continuous phase resulting in reduced creaming. At the same time, it is proposed that a thick CNC crust and larger aggregates would increase van der Waals' attraction forces and lower the resistance to capillary forces of the thin film between droplets. Coalescence was only evident in API brine (I = 1.9 M) after 24 h. For emulsions prepared in 1.9 M NaCl, the proportion of larger droplets and D[3,2] decreased after 24 hours, however, a hypothesis test indicated no change on the mean diameters. The presence of divalent cations only had an effect on coalescence for ionic strengths of 1.9 M. No significant change in droplet size distribution was observed over 24 h for emulsions prepared at lower ionic strengths, including in synthetic seawater.

CHAPTER 4

Stabilization of CO_2 emulsions and foams stabilized by a combination of cellulose nanocrystals and cationic surfactant in high ionic-strength brine at elevated temperature and pressure

ABSTRACT

Stable supercritical CO_2 ($scCO_2$) emulsions and foams with the CO_2 volume fraction of 0.75 were prepared at 25°C and 70°C respectively using CNC suspensions in API brine in the presence and absence of DTAB. The results indicate CNC can be used as an emulsion/foam stabilizer for potential underground CO_2 storage and EOR applications. The results showed that CNC suspension can stabilize $scCO_2$ emulsions and foams that were resistant to creaming and macroscopic coalescence over 24 hours. DTAB containing emulsions and foams showed creaming at 25ºC and macroscopic bubble coarsening at 70ºC. The Kamlet Taft parameter for polarizability (π^*) for heptane (π^*=-0.07) and PFO (π^*=-0.41) at ambient conditions is identical to π^* for CO_2 at 60 °C at the pressures of 4930 psi and 1300 psi respectively. Emulsion stability studies of heptane and perfluorooctane (PFO), as model compounds, at 25 and 70ºC showed heptane formed stable emulsions at both temperatures and PFO did not form stable emulsions with either CNC or CNC+DTAB conjugates present in brine. The result suggests the polarity of the oil phase is an important factor governing the stability of emulsions. CNC suspensions lowered γ_{ow} between heptane and brine from 50.6±0.2 mN/m to 37.6±0.5 mN/m, however, the presence of CNC did not alter γ_{ow} between PFO and brine suggesting CNCs preferentially adsorb

onto the heptane-brine interface. However, when DTAB is present, CNC increased γ_{ow} between heptane and the DTAB/brine solution suggesting the adsorption of DTAB onto CNC surface.Excess stress of heptane CNC stabilized emulsions was higher at that of CNC+DTAB stabilized at a lower shear rate, whereas, the trend was reversed at a higher shear rate. Heptane emulsions prepared using CNC only produced larger droplets but showed no droplet coalescence over 24 hours, whereas, CNC+DTAB stabilized emulsions produced finer droplets but showed droplets coalescence.

Keywords: $scCO_2$ emulsions, Cellulose nanocrystals, Foams, Viscosity, Excess stress, Interfacial tension, Surfactants

1. INTRODUCTION

Emulsions and foams form a range of consumer and industrial products that are used regularly. These heterogeneous mixtures of fluids (liquid-liquid or liquid-gas) find applications in consumer products such as food cosmetics and pharmaceuticals.[238–241] They are also frequently used for enhanced oil recovery (EOR) and oil spill cleanup.[242–244] Nanoparticles (NPs) can produce a more stable fluid-fluid interface due to the high energy of desorption associated with these particles adsorbed at the fluid-fluid interface. Surfactants polymers and nanoparticles have all been used with varying degrees of success to stabilize emulsions and foams. Surfactants favor droplet/bubble formation by lowering the surface/interfacial tension between the fluids, thus lowering Gibbs free energy of droplet formation. Nanoparticles, on the other hand, form a rigid barrier around droplets and foams and prevent their coalescence.[69,175,177] At elevated temperatures surfactant stabilized emulsions and foam can coalesce due to the desorption of surfactants from the interface while particle-stabilized

Pickering emulsions and foams are more likely to be resistant to coalescence due to their irreversible adsorption at the interface.[64,178]

A combination of nanoparticles and surfactants have been used in recent years to improve the stability of Pickering emulsions and foams. Inorganic nanoparticles such as silica CuO and clay have been used in conjunction with polymers (polyacrylamide) and surfactant (sodium dodecyl sulfate) to produces O/W Pickering emulsions containing 25% v/v lubricant oil that was stable up to the temperature of 98ºC and ambient pressure. The results indicated the addition of nanoparticles improved the thermal stability of emulsions in comparison to emulsions stabilized using only polymer and surfactant. [245] Furthermore it was found that at identical surfactant and polymer concentration clay nanoparticles generated thermally stable emulsions at a lower concentration.[245] The stability of D-limonene emulsions in water stabilized by 0.2wt. % cellulose nanocrystals (CNCs) to creaming at different temperatures was examined by placing the prepared emulsion in a water bath at temperatures ranging from 20ºC to 70ºC. It was found that an increase in temperature resulted in a decrease in the creaming of the emulsions. The authors speculated that the adsorption of CNC to the oil-water interface formed a 2D network at the interface which upon increasing the temperature resulted in a decrease in the interparticle distance which in turn enhanced attractive force among the particles.[246]

Stable CO_2 emulsions and foams can be used extensively for EOR processes for the displacement of oil during CO_2 flooding. However CO_2 emulsions and foams that are stable at elevated temperatures and pressures that mimic geological underground conditions can also be used to efficiently store CO_2 underground thus contributing to mitigate global warming.[247,248] Traditionally these CO_2 emulsions and foams are stabilized by polymers and surfactants. In recent years however silica NPs have been successfully used to prepare supercritical CO_2

emulsions at temperature and pressures up to 95°C and 4000 psi, respectively.[249–251] CO_2 emulsions with volume fractions as high as 0.95 were stabilized [252]; it was found that the addition of surfactants resulted in their adsorption to the surface of hydrophilic silica and an increase in the carbon dioxide/water/nanoparticle contact angle contributing to the stabilization of the CO_2-water interface. The interfacial tension between CO_2 and water was also decreased due to the adsorption of surfactants to the fluid-fluid interface which facilitates the formation of emulsion droplets.[64]

Inorganic nanoparticles possess significant advantages over traditional surfactants but in recent years biobased anisotropic nanoparticles such as cellulose nanocrystals (CNC) and chitosans have attracted research interest as anisotropic nanoparticles are more efficient than their identical isotropic spherical counterparts in stabilizing these emulsions and foam.[127,141,253,254] Furthermore, these biobased NPs have other desirable properties such as biocompatibility, lower toxicity, surface reactivity, and bioavailability, making them attractive candidates for preparing CO_2 emulsions and foams at elevated temperatures and pressures. Chitosan (0.1% w/v) stabilized emulsions containing 20% v/v medium-chain triglycerides (MCTs) were placed in a water bath and the temperature was increased to 90^{o}C. The emulsion stability was measured in terms of creaming and coalescence, it was reported that the emulsions were stable for up to 50^{o}C with no change in D[4,3] or creaming index reported. Beyond 50^{o}C the emulsion broke as indicated by an increase in both the creaming index and D[4,3] of the emulsion droplets.[255]

In this study, we report for the first time the preparation of CO_2 emulsions at high temperature and pressure using CNC and determine the effect of CNC and DTAB addition on the interfacial tension between CO_2 and brine. We also report the effect of organic phase

polarity, temperature and pressure on stability and surface properties of CNC stabilized emulsions and foams in the presence of the cationic surfactant DTAB. Emulsions were prepared using heptane and perfluorooctane (PFO) to mimic the polarity of CO_2 at different conditions of temperature and pressure. The stability of these emulsions at elevated temperatures was examined in terms of creaming and coalescence in high salinity brine, whereas PFO did not emulsify at all, while heptane formed stable emulsions with brine.

2. EXPERIMENTAL SECTION

2.1. Materials

Cellulose nanocrystals (11.5 wt.%) prepared from Pinus strobus (Northern pine) wood pulp made by the USDA Forest Products Laboratory and distributed by The University of Maine was used as received. The dimensions (length = 130.3±41.5 nm, height = 6.3±1.8 nm)and characteristics of the nanocrystals used are detailed in our earlier publication.[9] Reagent grade heptane (99.8%) Perfluorooctane (99.9%) was purchased from Sigma Aldrich (St. Louis MO) and was used as received. Dodecyltrimethylammonium bromide (DTAB) ≥ 90%, calcium chloride dihydrate ($CaCl_2 \cdot 2H_2O$) and sodium chloride (NaCl) were all purchased from Sigma Aldrich and used as received. Supercritical fluid grade carbon dioxide $scCO_2$ (<50 ppm moisture) was purchased from Airgas USA LLC (Tupelo MS) and was used as received. API brine (100%) was prepared using 2 wt.% $CaCl_2$ and 8 wt.% NaCl.

2.2. Preparation of aqueous phase

The aqueous phase used in the study was 1.5 wt. % CNC suspensions in 100% API brine with and without 0.45 g/L DTAB. Briefly, surfactant in brine solution was first prepared by adding 0.9 g/L DTAB to 200% API brine; an equal volume parts of 3 wt.% CNC in DI water was then added to the surfactant solution while mixing to prevent gelation to make the aqueous phase with final CNC concentration of 1.5 wt. % and DTAB concentration of 0.45 g/L in the

aqueous phase. For the measurement of interfacial tensions between the aqueous and organic phases, 0.5 wt.% CNC suspensions were used to avoid particle sedimentation and blockage of capillary tubes and needles utilized during the measurements. The pH of all aqueous phases used in the study was adjusted to approximately 3.0 using 0.1 M HCl. This is the equilibrium pH for a CO_2/API brine mixture at 70°C and 2940 psi. The aqueous phases in the study thus consist of flocculated CNC dispersed in solutions of DTAB in API brine.

2.3. Interfacial tension measurements

The interfacial tensions between the aqueous phases and oil or CO_2 were measured at 25ºC and 50ºC. The organic phase consisted of heptane or perfluorooctane, in addition, CO_2 in its liquid and supercritical state was also used for interfacial tension measurements between aqueous phases and CO_2. Interfacial tension (γ_{ow}) measurements between solutions that did not have CNC were carried out using the DuNuoy's ring method after allowing the fluids to equilibrate for 10 mins in a Sigma 701 force tensiometer (Nanoscience Instruments Phoenix Arizona). The γ_{ow} of samples that contained 0.5 wt.% CNC dispersion was measured using axisymmetric drop shape analysis of a pendant aqueous phase drop in the presence of excess oil in an Attention theta optical tensiometer (NanoScience Instruments Phoenix AZ).[187] It should be noted that when perfluorooctane was used as an organic phase a U-shaped needle was used to keep the aqueous droplet in place due to the higher density of the organic phase. Contours of the resulting droplet's shape were fitted to the Young-Laplace equation [176] to calculate interfacial tension between oil and brine.

$$\Delta p = \rho g h - \gamma \left(\frac{1}{R_1} + \frac{1}{R_2}\right) \qquad (1)$$

Where Δp is the pressure difference across the interface, γ is surface or interfacial tension, R_1 and R_2 are principal radii of curvature, and the term ρgh is hydrostatic pressure.

The interfacial tension between $scCO_2$ and the aqueous phases at 25°C and 70°C were measured at different pressures using the same optical tensiometer but with slight modifications. An in-house built pressure view cell (Figure 4-1), with temperature control, was used to measure the interfacial tension. Briefly, the high-pressure view cell was pressurized using an ISCO pump upto the desired pressure and then separated from the pump at valve (V6') the temperature inside the view cell was controlled using a heating tape connected to a PID controller. The view cell was then placed carefully on top of the tensiometer stage and its windows aligned with the camera (Appendix C Figure S3.1). The aqueous phase containing CNC suspension and surfactants in brine was pressurized to a pressure slightly higher than that inside the view cell, using a manual hand pump. A drop of the aqueous phase was formed at the end of the needle placed inside the view cell by allowing the aqueous phase to flow into the view cell by opening a valve (V3'). The interfacial tension was then measured using equation 1.

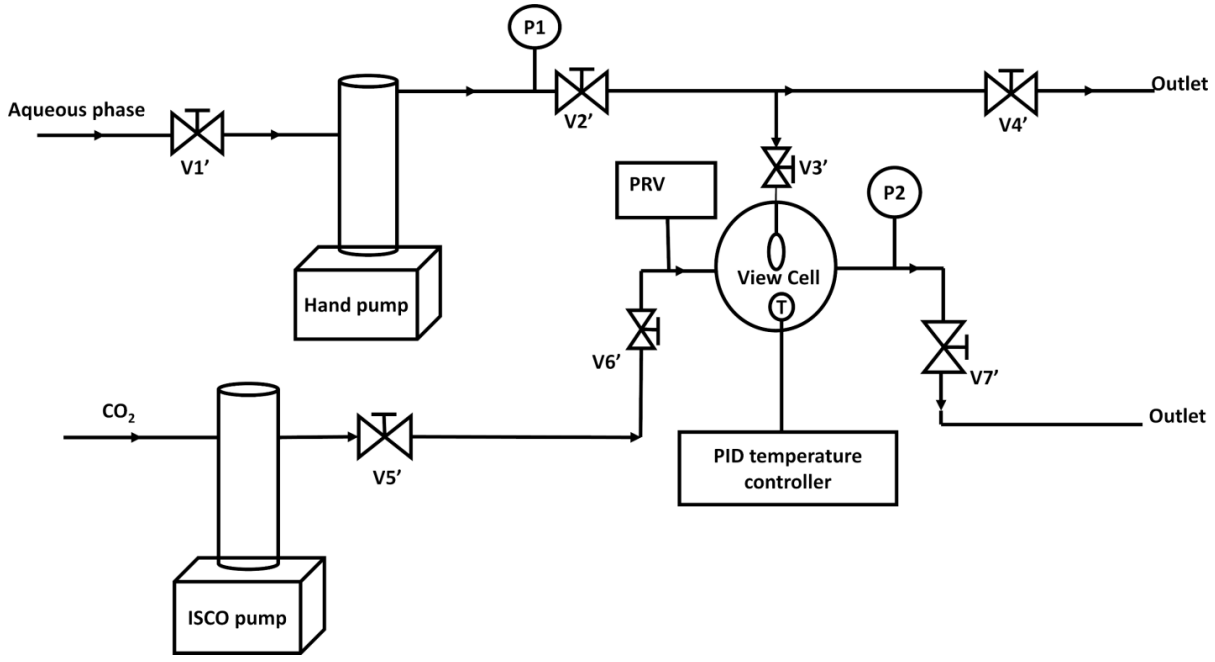

Figure 4-1: Schematic diagram of the apparatus used to measure the interfacial tension between CO_2 and CNC in brine

2.4. Emulsion Preparation and Characterization

The emulsions were prepared using heptane and PFO as model dispersed phases with similar polarity as supercritical CO_2. The Kamlet Taft parameter dipolarity/polarizability parameter (π^*) is used to quantify the polarity of solvents; supercritical CO_2 at 60 °C and 90 bar have a π^* of - 0.47, while at the same temperature and 340 bar, it is - 0.04. At ambient conditions, perfluorooctane has a value of -0.41 and heptane - 0.07.[256–258] The solvents used do have some limitations in mimicking properties of supercritical CO_2 one being the density difference between these organic solvents and supercritical CO_2, however, these fluids can be used to narrow down and identify optimal conditions for generation of CO_2 emulsions and foams. Mixtures containing aqueous phase volume fractions (ϕ_w) of 0.1, 0.2 and 0.25, and organic solvents (heptane or perfluorooctance) volume fractions (ϕ_o) of 0.9, 0.8 and 0.75, were added to a 20 mL screw-capped vial to make the final liquid volume 10 ml. The samples were then homogenized using a high-shear mixer IKA Ultra-Turrax T-25 Basic (Atkinson NH) at

8000 rpm for 1 minute. In order to prepare emulsions at a high temperature the organic and aqueous phases were added to Aceglass high-pressure tubes and mixed using the high shear mixer. The resulting emulsions were then placed in an oil bath such that the temperature of emulsions inside the tube was 70^{o}C.

2.5. Emulsion stability

Emulsion stability was measured in terms of droplet coalescence and creaming. Droplet coalescence at room temperature was studied by monitoring the change in emulsion droplet diameter over 24 hours by image analysis of optical micrographs created by an optical microscope (AmScope 500MD). A small aliquot of the emulsion was transferred to a microscope slide by spatula and a uniform layer of the emulsion was formed by gently placing a glass coverslip over the top of the emulsion drop; droplets micrographs were analyzed using ImageJ software (U.S. NIH) to generate droplet size distribution. The stability of emulsions to increase in temperature was thus measured in terms of change in average droplet diameter at 25^{o}C and 70^{o}C. Emulsions' resistance to creaming was measured by monitoring the position of creaming front over 24 hours by analyzing pictures using ImageJ (U.S. NIH).

2.6. Emulsion rheology and excess stress

The viscosity of aqueous phases and emulsions (ϕ_w=0.75) were measured as a function of shear rate at room temperature using Bohlin Visco 88 viscometer (Malvern Panalytical UK) fitted with cup and bob probe. Furthermore, for incompressible fluids, the excess stress (σ_{excess}) of the emulsions having an oil volume fraction (ϕ_o) was calculated using equations 2 and 3. [259]

$$\sigma = -P\boldsymbol{I} + (1-\phi_o)\tau_m + \phi_o\tau_d - \Gamma\mathbf{q} \qquad (2)$$

Where σ is total stress P is hydrostatic pressure, $\boldsymbol{I}$ is unit tensor, τ_m is stress acting on the continuous phase, τ_d is the stress on discrete phase, Γ is the interfacial tension between the

continuous and discrete phase, and **q** is specific anisotropy tensor. The final term of equation 2 relates interfacial tension to bulk stress and is referred to as excess stress (σ_{excess}). Thus ignoring the hydrostatic pressure (first term in equation 2) in all samples and considering only stress in the flow direction transferred perpendicular to it, equation 2 can be reduced to equation 3. [259]

$$\sigma_{excess} = \sigma - (1 - \phi_o)\tau_m + \phi_o\tau_d \qquad (3)$$

2.7. CO_2/brine emulsions/foam generation and apparent viscosity measurement

A schematic diagram of the apparatus used to generate CO_2/brine foams is shown in Figure 4-2. CO_2 and CNC dispersions in brine were pumped into the apparatus using ISCO Pumps controlled by D-series controllers. CO_2 foams and emulsions were generated at 25°C and 70°C. The total volumetric flow rate of the fluids into the apparatus was set at 1.5 ml/min with the volumetric ratio of CO_2: aqueous phase set at either 0.75:0.25 or 0.8:0.2. During the experimentation at 70°C volumetric thermal expansion of CO_2 was take in into account to ensure that the total flow rate and volume ratios were maintained inside the glass bead pack. The porosity of the bead pack was calculated to be 0.39 with the pore volume (PV) of 0.41 ml (ID: 0.16 cm length: 29.74 cm). The permeability (k) of the beadpack at the flow rate of 1.5 ml/min was calculated to be 45.5 darcy, the superficial velocity of the fluid inside the beadpack was 0.32 cm/s and the residence time inside the beadpack was 16.45 s. The shear rate experienced by the fluids in the capillary coil was calculated to be 497.4s^{-1}. The temperature inside the apparatus was maintained at 70°C using a thermostat connected immersion heater and the pressure was maintained at 3000 psig using a backpressure regulator (Swagelok AL) with a control range of 0-4000 psig. Before starting the experiment, the beadpack was conditioned by pumping 25 PV (10 ml) of CNC dispersion through it. The experiments were typically conducted for 140–150 beadpack PVs of total flow. The apparent(μ_{app}) and bulk viscosity (μ_{bulk}) of the foams flowing at

the volumetric flow rate (Q) through a packed bed and capillary were calculated using Darcy's (equation 4) and Hagen-Poisueille equations (equation 5), [260] respectively assuming the foam as single-phase system. The pressure drops (ΔP_1) and (ΔP_2) were measured across the packed bed and capillary coil (R: 0.08 cm L: 210 cm) respectively.

$$Q = \frac{kA\Delta P_1}{\mu_{app} L_1} \qquad (4)$$

In equation 4, k is the permeability of the packed bed, A is the cross-sectional area of the bed and L1 is the length of the bed across which the pressure drop is measured. [261]

$$Q = \frac{\pi R^4 \Delta P_2}{8\mu_{bulk} L_2} \qquad (5)$$

In equation 5, R is the internal radius and L_2 is the length of the capillary coil. The effect of temperature on the apparent and bulk viscosities of CO_2 emulsions and foams were measured at 25°C and 70°C.

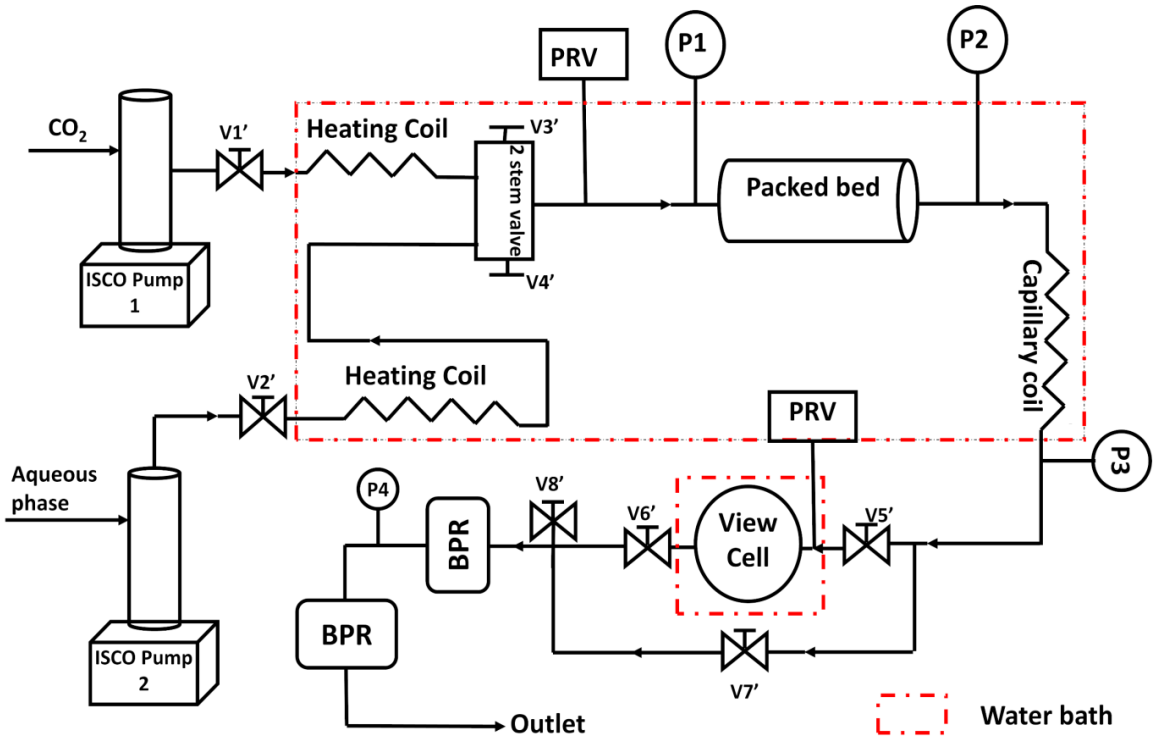

Figure 4-2: Schematic diagram of the CO2-brine emulsion/foam generating apparatus

Finally, the stability of foam/emulsion generated was examined by allowing the foams to flow into the high-pressure view-cell immersed in a water bath maintained at the desired temperature. The emulsions/foams were then isolated inside the view-cell by closing the inlet and outlet to the view-cell. The digital photographs of the foams/emulsions were then taken through a sapphire glass window located on the cross-section of the view cell for 24 hours to study their stability to coalescence and creaming.

3. RESULTS AND DISCUSSIONS

3.1. Brine-oil interfacial tension and interactions

The interfacial tensions between brine and oils were measured at 25°C and 50°C in the presence of 0.5 wt.% CNC, 0.45 g/L DTAB and with a combination of both, the results are summarized in Table 4-1. The interfacial tensions between API brine and heptane were lowered

to 37.6±0.5 mN/m and 6.2±0.1 mN/m in the presence of CNC and DTAB respectively. The observation suggests that the CNC flocs migrate to the heptane-water interface where they are most likely to orient themselves such that the hydrophobic (2 0 0) edges are aligned in heptane.[32] The addition of CNC to the DTAB solution in brine increased the γ_{ow} to 13.3±1.8 mN/m, suggesting adsorption of DTAB onto the surface of CNC. Such occurrence is likely to result in a decreased surface concentration of DTAB molecules causing the γ_{ow} to increase.[40,180,262] Our earlier study indicates that short-range electrostatic and ion-dipole interactions between negatively charged CNC and cationic DTAB could act as a driving force for the adsorption of DTAB molecules onto the surface of CNC.[40] PFO-brine interfacial tension, however, was unaffected by the presence of CNC but DTAB lowered γ_{ow} to 13.1±0.1 mN/m, suggesting that due to its lower polarity, CNCs do not adsorb to the PFO-brine interface. Upon addition of CNC to DTAB-brine solution, an increase in γ_{ow} was observed in the heptane-brine interface, however, no change in γ_{ow} was observed between PFO and the DTAB-brine solution. Further study is needed to fully comprehend the migration of DTAB and CNC to the oil-brine interface. It is could be possible that due to the lower polarity of PFO in comparison to heptane, free DTAB, CNC, and the DTAB+CNC conjugate, can all partition to the heptane-brine interface. PFO, on the other hand, is comparatively non-polar which could result in preferential partitioning of CNC and CNC+DTAB conjugates to the aqueous phase. In such a case any changes in γ_{ow} would only be attributed to DTAB molecules hence no clear effect in γ_{ow} in the presence of CNC.

The increase in temperature slightly lowered the interfacial tension between API brine and heptane regardless of the presence of additives in the solution, although the effect was more

prominent in heptane. The changes observed in γ_{ow} with temperature were not statistically significant in case of the PFO-brine interface.

Table 4-1: Measured γ_{ow} between API brine and heptane or PFO at 25°C and 50°C in the presence of either DTAB CNC or their combination. DTAB concentration: 0.45g/L, CNC concentration: 0.5 wt.%.

	Heptane				Perfluorooctane			
Stabilizer	25°C		50°C		25°C		50°C	
	γ_{ow} (mN/m)	Std.dev (mN/m)	γ_{ow} (mN/m)	Std.dev (mN/m)	γ_{ow} (mN/m)	Std.dev (mN/m)	γ_{ow} (mN/m)	Std.dev (mN/m)
None	50.6	0.2	49.1	0.2	50.7	0.6	50.8	0.9
DTAB	6.2	0.1	5.8	0.2	13.1	0.1	13.3	0.8
CNC	37.6	0.5	31.8	0.7	50.9	0.9	--	--
CNC+DTAB	13.3	1.8	13.2	0.2	14.2	0.7	--	--

3.2. Stability of emulsions prepared using heptane and perfluorooctane

A total of 10 ml emulsion was prepared using heptane and PFO at ϕ_w of 0.9, 0.8 and 0.75 as oil phase and 1.5 wt. % CNC, 0.45g/L DTAB, or 1.5 wt.% CNC+ 0.45g/L DTAB as aqueous phase. Figure 4-3 shows the creaming behavior of emulsions prepared using CNC suspension in brine as the aqueous phase and heptane as the organic phase at 25°C (Figure 4-3a) and 70°C (Figure 4-3b-3d). It was found that at 25°C, emulsions prepared using only 0.45g/L DTAB creamed very fast and separated into individual phases within one hour of emulsification. CNC and CNC+ DTAB produced significantly more stable emulsions for all ϕ_w tested that were resistant to creaming for at least 24 hours. The emulsions prepared using CNCs and CNC+DTAB were stable to creaming for at least 4 months. CNC and CNC+DTAB conjugates in high ionic strength brine (I=1.9M) have their surface charge screened due to the collapse of the electric double layer causing the aggregation of individual particles and conjugates. This results in the formation of the CNC and CNC+DTAB networks contributing to an increase of the aqueous phase and thereby forming gel-like emulsions.[121,127,128] The adsorption of DTAB

onto the surface CNC aggregates in brine that increases the hydrophobicity of the CNC aggregates and thus facilitates the migration of CNC onto the oil-water interface.[40,42] Emulsions prepared using PFO, on the other hand, were not stabilized by either DTAB, CNC or their combination, at 25°C. This observation coupled with the interfacial tension measurement further indicates that due to the low polarity of PFO, CNC and CNC+DTAB conjugates, do not migrate to nor stabilize the PFO-brine interface, and preferentially partition to the aqueous phase.

The heptane emulsions stored at 70°C prepared using DTAB only (Figure 4-3b) broke within 1 hour, whereas CNC or CNC+DTAB stabilized emulsions (Figure 4-3c-3d) with ϕ_w of 0.25 and 0.2, were stable at the elevated temperature. Emulsions in PFO, however, could not be stabilized at 70°C either (Figure 4-4). The higher density difference between the PFO and aqueous phase along with the lower polarity of PFO possibly contributes to the low stability of the PFO-brine interface. It has been reported that as the polarity of the oil decreases, the oil-water interfacial tension increases which can increase the energy required for the drop formation resulting in unstable emulsions. [263] The observation further supports claims that the adsorption of particles at the interface can be essentially considered irreversible due to the high adsorption energy (E_{ads}) at the interface. [264]

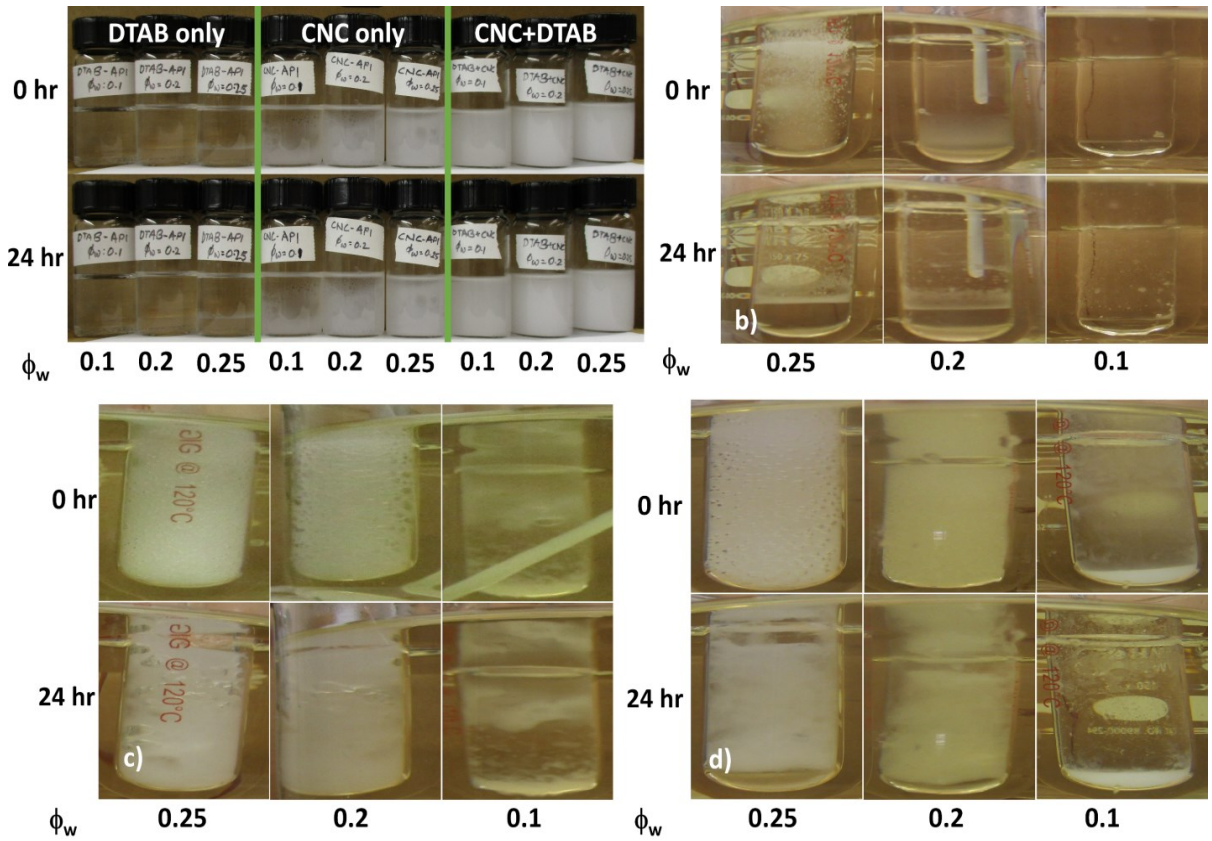

Figure 4-3: Heptane emulsions prepared at a) 25ºC using the combination of CNC and surfactants. Emulsions at 70ºC using b) DTAB only c) CNC only and d) CNC+DTAB; ϕ_w represents the volume fraction of the aqueous phase in the emulsions.

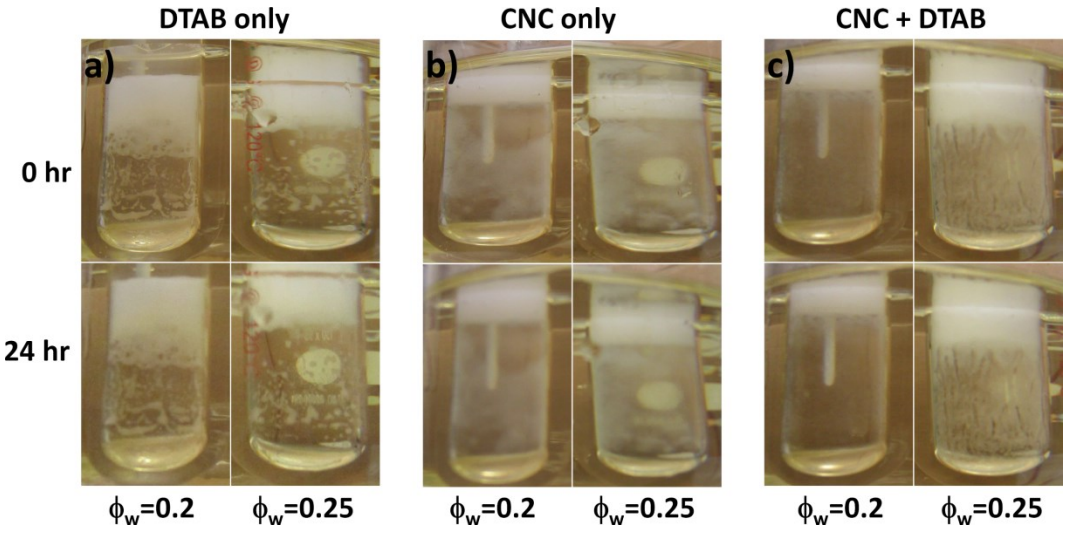

Figure 4-4: PFO emulsions at 70ºC prepared using a) DTAB only b) CNC only and c) combination of CNC and DTAB

The emulsions prepared using CNC only generated larger droplets (Appendix C Table S3.1) but showed no signs of droplet coalescence over 24 hours period (Figure 4-5a-5c). Interestingly the presence of DTAB in the aqueous phase resulted in the formation of smaller initial emulsion droplets (Appendix C Table S3.1), however, emulsions prepared using DTAB only completely coalesced within 1 hour of emulsification. Emulsions prepared using CNC+DTAB showed an increase in droplet diameters (Appendix C Table S3.1) over 24 hours and a slight broadening of size distribution peak (Figure 4-5d-5f) after 24 hours. It is not clear at this moment as to why the CNC+DTAB stabilized emulsions initially produced finer droplets and showed coalescence. One possible explanation could be that in emulsions stabilized by CNC+DTAB, the proportion of DTAB, CNC, and CNC+DTAB conjugates at the surface of droplets are likely to differ from one droplet to another. In such conditions, it is plausible to expect the droplets stabilized by a relatively higher proportion of DTAB to coalesce to a bigger droplet until CNC or CNC+DTAB account for surface coverage of droplets that arrests the droplet growth.

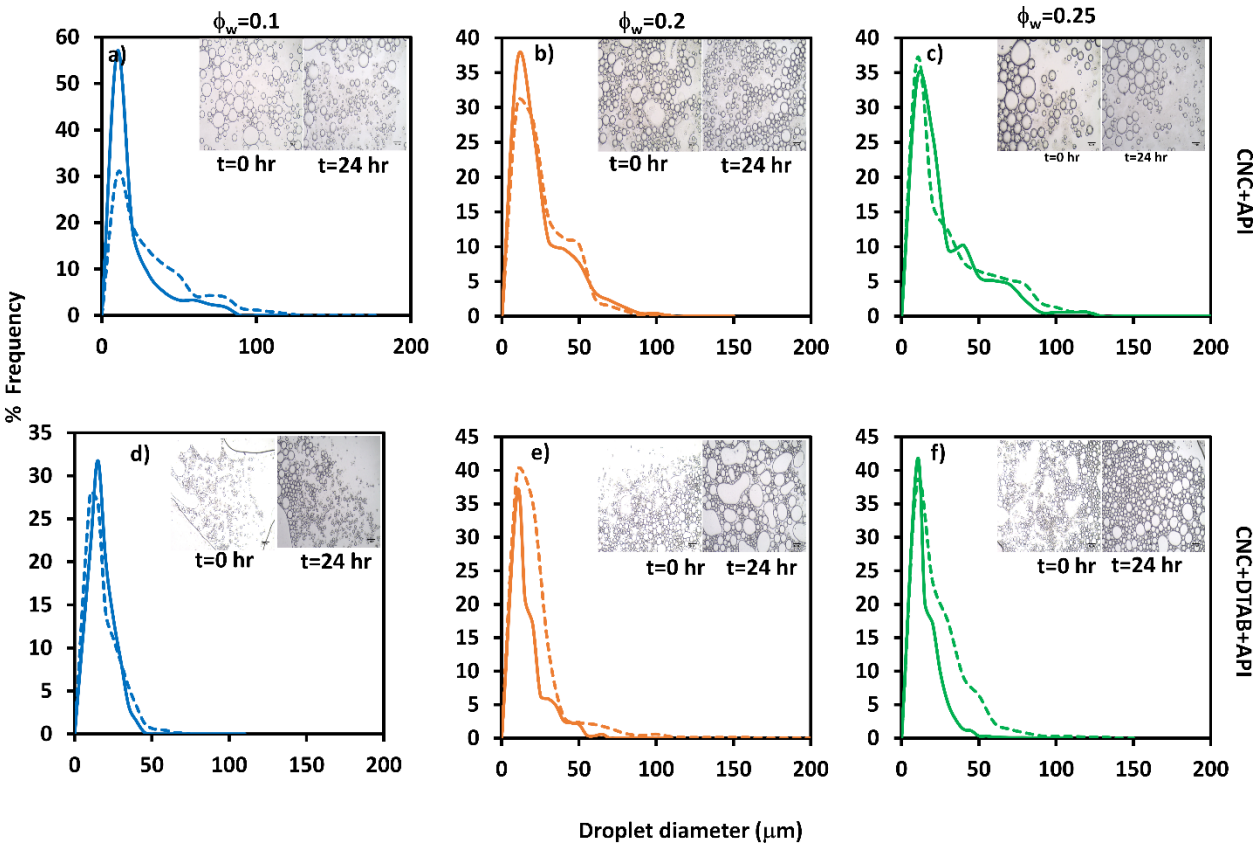

Figure 4-5: Droplet size distribution of heptane emulsions at room temperature using CNC only with the aqueous phase volume fraction of a) ϕ_w=0.1 b) ϕ_w=0.2 and c)ϕ_w=0.25 and using a combination of CNC+DTAB with the aqueous phase volume fraction of d) ϕ_w=0.1 e) ϕ_w=0.2 and f) ϕ_w=0.25. Solid Line=0 hour, Dashed line=24 hours

3.3. Heptane-emulsion viscosity and excess stress

The viscosity of heptane emulsions and the aqueous phases used (CNC and CNC+DTAB) to prepare them were measured using the Bohlin Visco-88 rheometer. The viscosity of the samples plotted as the function of the shear rate is presented in Appendix C Figure S3.3. The addition of CNCs to the brine solution resulted in the formation of a non-Newtonian suspension and increased its viscosity from approximately 1 mPa.s to 250 mPa.s at the lowest shear rate studied (14.9 s^{-1}). It has been established that polymers and nanoparticles increase the viscosity of the continuous phase in O/W emulsions and thereby retard the movement of droplets, increase the maximum droplet concentration, and decrease the rate of

creaming and coalescence.[265] The results indicate that the presence of DTAB did not significantly affect the viscosity of the aqueous phase. The viscosities of aqueous phases were approximately 250 mPa.s which increased to approximately 1200 mPa.s for the emulsions (ϕ_w=0.25) at 14.9 s^{-1}. The σ_{excess} in mixtures of incompressible fluids measures the direct contribution of interfacial tension to bulk stress. [259] It was calculated using equation 3 and plotted as the function of the shear rate in Figure 4-6. The result appears to indicate that σ_{excess} of CNC+DTAB stabilized emulsions were higher than the excess stress of emulsions stabilized using CNC only however there is no conclusive evidence for this observation due to overlapping of the margin of error. This indicates the contribution of the interface to the overall stress transfer appears to be greater for CNC+DTAB conjugates. It is possible that at lower shear rates, the CNC stabilized emulsions also lead to a greater interfacial contribution, but it was not possible to accurately measure viscosities at lower shear rates.

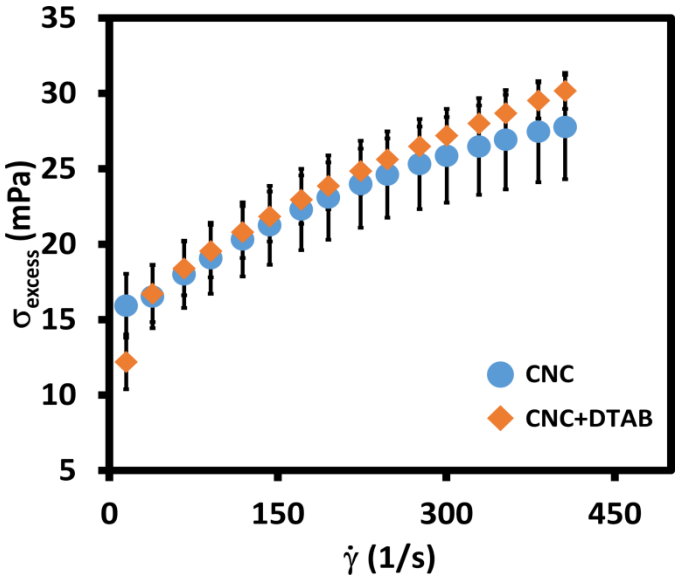

Figure 4-6: Excess stress plotted as a function of shear rate for heptane-brine interface stabilized by CNC and CNC+DTAB

3.4. $scCO_2$ emulsions and foams

CO_2 emulsions and foams were prepared at 25ºC and 70ºC, and a pressure of 3000 psig using CNC and CNC+DTAB. The stability of the prepared emulsions and foams was measured in terms of change in foam volume. Figure 4-7 shows the macroscopic structure of the emulsions and foams over the 24 hours. The CO_2 emulsions with CNC only were stable for 24 hours with no significant signs of creaming, whereas the emulsions prepared using CNC+DTAB conjugates showed the creaming of the emulsions. Image analysis of the emulsions indicated that the volume of the CNC+DTAB stabilized CO_2 emulsions dropped by 22.0±0.6 % over 24 hours, there were no visual signs of droplet coarsening at 25°C in either sample. At 70°C, $scCO_2$ foams stabilized by CNC+DTAB conjugates showed a volume decrease (21.3±0.3%) as well as bubble coarsening that was visible macroscopically. CNC stabilized foams at 70°C also showed slight creaming, but no macroscopic signs of coalescence were observed. The enhanced stability of the foams and emulsions prepared using CNC is likely attributed to the large desorption energy requirement for particles from the interface compared to surfactants. In a previous study, we determined adsorption energy of CNC in a dodecane/API brine interface of -413 kT, while the addition of DTAB lowered its magnitude to -253 kT.[40] Additional work is still required to provide similar measurements in $scCO_2$. It should be noted that emulsions and foams with lower ϕ_w (Appendix C Figure S3.4) could not be stabilized by the aqueous phase consisting of CNC only or CNC+DTAB.

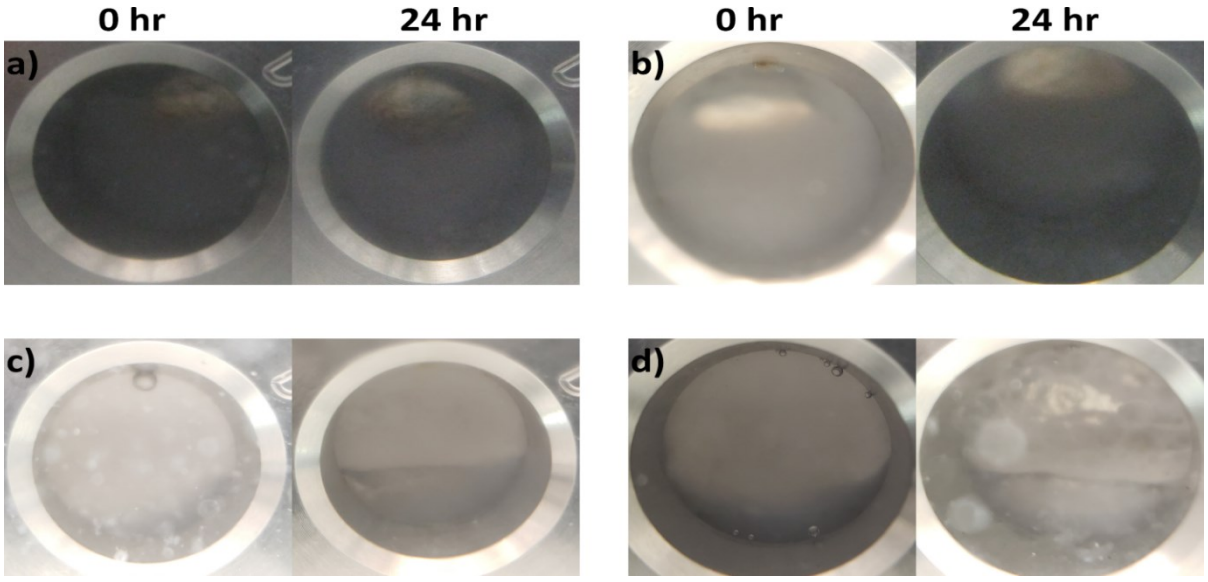

Figure 4-7: Images of CO_2 emulsions and foams prepared using CNC only at a) 25ºC and b) 70ºC and conjugates of CNC+DTAB at c) 25ºC and d)70ºC. Pressure = 3000±50 psi

At the conditions tested in this study (high pressure and temperature) the solubility of CO_2 increases,[266] this increased solubility is likely to contribute to the process of Ostwald ripening resulting in the diffusion of CO_2 from the smaller droplets (or bubbles) into larger ones, resulting in droplet coarsening. The maximum capillary pressure (P_c^{max}) a film stabilized by particles of radius (R) can withstand before it ruptures and is given by equation 7.[57,85,86]

$$P_c^{max} = p^* \frac{2\sigma}{R}(\cos\theta + z) \qquad (7)$$

In equation 6, p* is a positive dimensionless parameter that is a function of interface coverage and packing parameter of the particles at the interface. σ is the interfacial tension between fluids, θ is the contact angle between particle and fluids and z is a constant dependent on the arrangement of fluids in the film. In cases of high internal phase emulsions and foams, the capillary pressure increases with an increase in the volume fraction of the internal phase [252]

pushing it closer to P_c^{max} and thus increasing the likelihood of film rupture and droplet coalescence.

The apparent viscosity of emulsions and foams in the bed pack and the bulk viscosity was measured using darcy's equation and the Hagen–Poiseuille equation respectively. It should be noted that the Hagen–Poiseuille equation approximates the emulsions (or foam) as a single component system consisting of a Newtonian incompressible fluid. These assumptions are not valid for the system tested in this study; however, it provides a meaningful tool for qualitative comparisons between different systems. As such, the Hagen-Poiseuille equation has been extensively used in literature to provide rough estimates of steady shear viscosities.[64,252,267] The calculated viscosities of the emulsions, foams and aqueous phases are listed in Table 4-2. The results indicate that viscosities of CNC stabilized emulsions (or foams) were not significantly different than the viscosities of aqueous phase alone. The viscosities of CNC+DTAB stabilized emulsions, however, showed an increase in viscosities compared to the aqueous phase consisting of CNC+DTAB conjugates. It should be noted, however, that the emulsions (and foams) in Table 4-2 only have 20% v/v aqueous phase and the CO_2 has a nearly negligible viscosity compared to the aqueous phase. The fact that the viscosity of the emulsion (and foam) is similar to that of the aqueous phase indicate a significant contribution of the interface. Interestingly, despite the increased viscosity, more creaming was observed in CNC+DTAB stabilized emulsions and foams and in general produced less stable emulsions, compared to CNC stabilized systems. This result suggests that the rheology of emulsions and foams alone cannot predict the stability of emulsions and foams.

Table 4-2: Apparent and bulk viscosities of $scCO_2$ emulsions and foams stabilized by CNC and CNC+DTAB conjugates. $\phi_w = 0.25$.

Temperature		*Emulsions/Foam*				*Aq. Phase*			
		CNC API		CNC+ DTAB		CNC API		CNC+ DTAB	
		Average	Std. dev	Average	Std. dev	Average	Std. dev	Average	Std. dev
25°C	μ_a (mPa.s)	5.0	2.4	26.8	5.2	4.5	0.5	9.9	4.7
	μ_{bulk} (mPa.s)	2.7	0.6	27.5	3.6	2.6	1.2	2.6	0.9
70°C	μ_a (mPa.s)	9.9	1.0	31.4	3.7	7.4	2.0	6.9	1.3
	μ_{bulk} (mPa.s)	2.1	0.8	22.5	2.7	2.0	0.6	4.6	2.1

4. CONCLUSIONS

Stable $scCO_2$ emulsions and foams with the CO_2 volume fraction of 0.75 were prepared for the first time at 25°C and 70°C respectively using CNC as a stabilizer in API brine in the presence and absence of DTAB. The results highlight that CNC in conjunction with DTAB can be used to generate high internal phase $scCO_2$ emulsions and foams in brine that can be used for underground CO_2 storage or EOR applications. The results showed that CNC suspension can stabilize $scCO_2$ emulsions and foams that were resistant to creaming and macroscopic coalescence over 24 hours. In the presence of DTAB, the emulsions (and foams) volume decreased by 22.0±0.6 % at 25°C and 21.3±0.3 % at 70°C after 24 hours. At 70°C, CNC+DTAB stabilized emulsions showed bubble coarsening that was visible macroscopically. The stability of heptane and PFO emulsions at 25 and 70°C were studied. Emulsions were also prepared using heptane and PFO as organic phases to examine the effect of oil polarity on emulsion stability. The results show that comparatively polar heptane ($\pi^* = -0.07$) formed stable emulsions at both 25°C and 70°C. Interfaces of the non-polar PFO ($\pi^* = -0.41$) and brine were not stabilized by either CNC or CNC+DTAB conjugates at either temperature tested. The examination of optical micrographs of heptane-brine emulsions prepared at 25°C suggested CNC+DTAB conjugates produced finer initial droplets, but significant droplet coalescence occurred; whereas in

emulsions stabilized using only CNC no coalescence was observed over 24 hours. CNC suspensions lowered γ_{ow} between heptane and brine from 50.6±0.2 mN/m to 37.6±0.5 mN/m, however, the presence of CNC did not alter γ_{ow} between PFO and brine, suggesting CNCs can adsorb onto the heptane/brine interface, but not onto PFO/brine interfaces. Furthermore, the presence of CNC increased γ_{ow} between heptane and DTAB solutions in brine, but had no effect when PFO was used instead. Excess stress measurements of heptane emulsions showed that interfaces stabilized by CNC contributed more to the stress transferred compared to DTAB+CNC at 14.9 s^{-1}, the opposite was true at higher shear rates.

CHAPTER 5

General Conclusions and Future Recommendations

The goal of this study was to understand the fundamental mechanisms, interfacial interactions, and physicochemical properties of oil and aqueous phases that control the adsorption of cellulose nanocrystals (CNC) to liquid-liquid and gas-liquid interfaces in brine in the presence/absence of various surfactants. The key idea behind studying these complex phenomena was to understand key parameters that can be controlled while using CNC as an emulsion/foam stabilizer for multiple applications such as underground storage of supercritical CO_2, enhanced oil recovery applications, and enhancing the rate and extent of petroleum biodegradation. This section highlights the major conclusions of each chapter discussed in this dissertation.

Objective 1: Understand the interfacial interactions between CNC and surfactants in brine at the oil-brine interface.

The study in Chapter 2 successfully identified CNC can be used to stabilize dodecane-brine emulsions of water phase volume fraction ranging from 0.25-0.9. It elucidated that at high ionic strength (I=1.9M and 0.65M) intermolecular interactions such as H-bonding, ion-dipole interactions, and short-range electrostatic interactions were involved in adsorption of surfactants onto CNC surface. The study also highlighted that the wettability of CNC by brine and oil content in emulsions are more critical to emulsion stability that surfactant adsorption.

Future Recommendations 1:

Surface modifications of CNC to increase the hydrophobicity of CNC could enhance the ability of these nanoparticles to stabilize emulsions more efficiently and is one research area that could be explored. Furthermore, such modifications could allow for stabilization of emulsions at lower ionic strength aqueous solutions as well, these modifications would enable researching possibilities of using CNCs as food-grade emulsifiers.

Objective 2: Understand surface and physicochemical properties that controls emulsion stability and biodegradation of crude oil

The study in Chapter 3 relates to the emulsification of crude oil by CNC in brine solutions without using any surfactants to enhance the microbial degradation of crude oil. The findings of the study indicate that the emulsification of crude oil by CNC enhances the biodegradation of aliphatic hydrocarbons possibly due to the increase in surface area of the oil available for bacteria to adsorb and degrade. It was also found that physicochemical parameters such as ionic strength of aqueous phase, presence of divalent cations, and CNC concentration affect the emulsion stability which in turn affects the extent of biodegradation.

Future Recommendations 2:

The use of microbial consortia commonly found in oil wells that are better adapted to degrade crude oil instead of a one bacteria could improve the extent of biodegradation of crude oil and could provide a significant step towards examining the potential use of CNCs for large scale oil-spill cleanup operations in a marine environment. To that end, for large scale operations, the efficiency of degradation needs to be comparable or better than currently available chemical dispersants thus comparing the performance of CNC with chemical dispersants would be an important research step.

Objective 3: Apply understandings of interactions and mechanisms from earlier studies to prepare stable emulsions and foams of $scCO_2$ using CNC at 70°C and 3000psig

In this study, we concluded that the polarity of the oil phase is critical to the stabilization of emulsions and foams using CNC. It was found that CNC and CNC+DTAB could stabilize $scCO_2$ emulsions upto the CO_2 volume fraction of 0.75. An emulsion stability study on model fluids heptane and perfluorooctane suggested that polarity of the oil phase is a crucial factor in determining emulsion stability. Comparatively, polar heptane produced stable emulsions at both room temperature and 70°C whereas, non-polar perfluorooctane did not produce emulsions at either temperature.

Future Recommendations 3:

Future research should be designed to produce stable $scCO_2$ emulsions and foams with a higher volume fraction of CO_2. Surface modification of CNCs with hydrophobic thermostable polymers could potentially be used to increase the water contact angle of the CNC that could potentially increase the volume fraction of CO_2 that can be entrapped as emulsion/foam.

LIST OF REFERENCES

LIST OF REFERENCES

[1] H. Thomas, Cellulose: Structure and Properties, in: Cellulose Chemistry and Properties: Fibers, Nanocelluloses and Advanced Materials, Springer International Publishing, 2016. //www.springer.com/us/book/9783319260136 (accessed August 29, 2018).

[2] R.J. Moon, A. Martini, J. Nairn, J. Simonsen, J. Youngblood, Cellulose nanomaterials review: structure, properties and nanocomposites, Chemical Society Reviews. 40 (2011) 3941. https://doi.org/10.1039/c0cs00108b.

[3] D. Klemm, B. Heublein, H.-P. Fink, A. Bohn, Cellulose: Fascinating Biopolymer and Sustainable Raw Material, Angewandte Chemie International Edition. 44 (2005) 3358–3393. https://doi.org/10.1002/anie.200460587.

[4] Y. Habibi, L.A. Lucia, O.J. Rojas, Cellulose Nanocrystals: Chemistry, Self-Assembly, and Applications, Chemical Reviews. 110 (2010) 3479–3500. https://doi.org/10.1021/cr900339w.

[5] B.G. Rånby, Fibrous macromolecular systems. Cellulose and muscle. The colloidal properties of cellulose micelles, Discuss. Faraday Soc. 11 (1951) 158–164. https://doi.org/10.1039/DF9511100158.

[6] E. Abraham, D. Kam, Y. Nevo, R. Slattegard, A. Rivkin, S. Lapidot, O. Shoseyov, Highly Modified Cellulose Nanocrystals and Formation of Epoxy-Nanocrystalline Cellulose (CNC) Nanocomposites, ACS Appl. Mater. Interfaces. 8 (2016) 28086–28095. https://doi.org/10.1021/acsami.6b09852.

[7] P. Grey, S.N. Fernandes, D. Gaspar, J. Deuermeier, R. Martins, E. Fortunato, M.H. Godinho, L. Pereira, Ionically Modified Cellulose Nanocrystal Self-Assembled Films with a Mesoporous Twisted Superstructure: Polarizability and Application in Ion-Gated Transistors, ACS Appl. Electron. Mater. 2 (2020) 426–436. https://doi.org/10.1021/acsaelm.9b00652.

[8] I. Kalashnikova, H. Bizot, P. Bertoncini, B. Cathala, I. Capron, Cellulosic nanorods of various aspect ratios for oil in water Pickering emulsions, Soft Matter. 9 (2013) 952–959. https://doi.org/10.1039/C2SM26472B.

[9] S. Parajuli, O. Alazzam, M. Wang, L.C. Mota, S. Adhikari, D. Wicks, E.E. Ureña-Benavides, Surface properties of cellulose nanocrystal stabilized crude oil emulsions and their effect on petroleum biodegradation, Colloids and Surfaces A: Physicochemical and Engineering Aspects. (2020) 124705. https://doi.org/10.1016/j.colsurfa.2020.124705.

[10] J.O. Zoppe, R.A. Venditti, O.J. Rojas, Pickering emulsions stabilized by cellulose nanocrystals grafted with thermo-responsive polymer brushes, Journal of Colloid and Interface Science. 369 (2012) 202–209. https://doi.org/10.1016/j.jcis.2011.12.011.

[11] S. Hiranphinyophat, Y. Asaumi, S. Fujii, Y. Iwasaki, Surface Grafting Polyphosphoesters on Cellulose Nanocrystals To Improve the Emulsification Efficacy, Langmuir. 35 (2019) 11443–11451. https://doi.org/10.1021/acs.langmuir.9b01584.
[12] P. Bertsch, M. Diener, J. Adamcik, N. Scheuble, T. Geue, R. Mezzenga, P. Fischer, Adsorption and Interfacial Layer Structure of Unmodified Nanocrystalline Cellulose at Air/Water Interfaces, Langmuir. 34 (2018) 15195–15202. https://doi.org/10.1021/acs.langmuir.8b03056.
[13] A.G. Cunha, J.-B. Mougel, B. Cathala, L.A. Berglund, I. Capron, Preparation of Double Pickering Emulsions Stabilized by Chemically Tailored Nanocelluloses, Langmuir. 30 (2014) 9327–9335. https://doi.org/10.1021/la5017577.
[14] I. Capron, O.J. Rojas, R. Bordes, Behavior of nanocelluloses at interfaces, Current Opinion in Colloid & Interface Science. 29 (2017) 83–95. https://doi.org/10.1016/j.cocis.2017.04.001.
[15] Y. Matsuda, K. Kowsaka, K. Okajima, K. Kamide, Structural change of cellulose contained in immature cotton boll during its growth, Polymer International. 27 (1992) 347–351. https://doi.org/10.1002/pi.4990270410.
[16] A.C. O'Sullivan, Cellulose: the structure slowly unravels, Cellulose. 4 (1997) 173–207.
[17] B.G. Rånby, Fibrous macromolecular systems. Cellulose and muscle. The colloidal properties of cellulose micelles, Discuss. Faraday Soc. 11 (1951) 158–164. https://doi.org/10.1039/DF9511100158.
[18] D. Bondeson, A. Mathew, K. Oksman, Optimization of the isolation of nanocrystals from microcrystalline cellulose by acid hydrolysis, Cellulose. 13 (2006) 171–180. https://doi.org/10.1007/s10570-006-9061-4.
[19] X. Xu, F. Liu, L. Jiang, J.Y. Zhu, D. Haagenson, D.P. Wiesenborn, Cellulose nanocrystals vs. Cellulose nanofibrils: A comparative study on their microstructures and effects as polymer reinforcing agents, ACS Applied Materials and Interfaces. 5 (2013) 2999–3009. https://doi.org/10.1021/am302624t.
[20] M.R.K. Sofla, R.J. Brown, T. Tsuzuki, T.J. Rainey, A comparison of cellulose nanocrystals and cellulose nanofibres extracted from bagasse using acid and ball milling methods, Advances in Natural Sciences: Nanoscience and Nanotechnology. 7 (2016) 035004. https://doi.org/10.1088/2043-6262/7/3/035004.
[21] J.A. Ávila Ramírez, E. Fortunati, J.M. Kenny, L. Torre, M.L. Foresti, Simple citric acid-catalyzed surface esterification of cellulose nanocrystals, Carbohydrate Polymers. 157 (2017) 1358–1364. https://doi.org/10.1016/j.carbpol.2016.11.008.
[22] S.A. Kedzior, H.S. Marway, E.D. Cranston, Tailoring Cellulose Nanocrystal and Surfactant Behavior in Miniemulsion Polymerization, Macromolecules. 50 (2017) 2645–2655. https://doi.org/10.1021/acs.macromol.7b00516.
[23] T. Zhang, W. Wang, D. Zhang, X. Zhang, Y. Ma, Y. Zhou, L. Qi, Biotemplated Synthesis of Gold Nanoparticle–Bacteria Cellulose Nanofiber Nanocomposites and Their

Application in Biosensing, Advanced Functional Materials. 20 (2010) 1152–1160. https://doi.org/10.1002/adfm.200902104.
[24] M. Nogi, H. Yano, Transparent Nanocomposites Based on Cellulose Produced by Bacteria Offer Potential Innovation in the Electronics Device Industry, Advanced Materials. 20 (2008) 1849–1852. https://doi.org/10.1002/adma.200702559.
[25] S.Y. Ooi, I. Ahmad, Mohd.C.I.M. Amin, Cellulose nanocrystals extracted from rice husks as a reinforcing material in gelatin hydrogels for use in controlled drug delivery systems, Industrial Crops and Products. 93 (2016) 227–234. https://doi.org/10.1016/j.indcrop.2015.11.082.
[26] S.P. Akhlaghi, R.C. Berry, K.C. Tam, Surface modification of cellulose nanocrystal with chitosan oligosaccharide for drug delivery applications, Cellulose. 20 (2013) 1747–1764. https://doi.org/10.1007/s10570-013-9954-y.
[27] S. Salmieri, F. Islam, R.A. Khan, F.M. Hossain, H.M.M. Ibrahim, C. Miao, W.Y. Hamad, M. Lacroix, Antimicrobial nanocomposite films made of poly(lactic acid)-cellulose nanocrystals (PLA-CNC) in food applications: part A—effect of nisin release on the inactivation of Listeria monocytogenes in ham, Cellulose. 21 (2014) 1837–1850. https://doi.org/10.1007/s10570-014-0230-6.
[28] S. Fujisawa, E. Togawa, K. Kuroda, Nanocellulose-stabilized Pickering emulsions and their applications, Sci Technol Adv Mater. 18 (2017) 959–971. https://doi.org/10.1080/14686996.2017.1401423.
[29] C. Salas, T. Nypelö, C. Rodriguez-Abreu, C. Carrillo, O.J. Rojas, Nanocellulose properties and applications in colloids and interfaces, Current Opinion in Colloid & Interface Science. 19 (2014) 383–396. https://doi.org/10.1016/j.cocis.2014.10.003.
[30] Y. Nishiyama, P. Langan, H. Chanzy, Crystal Structure and Hydrogen-Bonding System in Cellulose Iβ from Synchrotron X-ray and Neutron Fiber Diffraction, Journal of the American Chemical Society. 124 (2002) 9074–9082. https://doi.org/10.1021/ja0257319.
[31] W. Helbert, Y. Nishiyama, T. Okano, J. Sugiyama, Molecular Imaging ofHalocynthia papillosaCellulose, Journal of Structural Biology. 124 (1998) 42–50. https://doi.org/10.1006/jsbi.1998.4045.
[32] I. Kalashnikova, H. Bizot, B. Cathala, I. Capron, Modulation of Cellulose Nanocrystals Amphiphilic Properties to Stabilize Oil/Water Interface, Biomacromolecules. 13 (2012) 267–275. https://doi.org/10.1021/bm201599j.
[33] S. Liu, M. Jin, Y. Chen, H. Gao, X. Shi, W. Cheng, L. Ren, Y. Wang, High internal phase emulsions stabilised by supramolecular cellulose nanocrystals and their application as cell-adhesive macroporous hydrogel monoliths, Journal of Materials Chemistry B. 5 (2017) 2671–2678. https://doi.org/10.1039/C7TB00145B.
[34] H. Valo, S. Arola, P. Laaksonen, M. Torkkeli, L. Peltonen, M.B. Linder, R. Serimaa, S. Kuga, J. Hirvonen, T. Laaksonen, Drug release from nanoparticles embedded in four different nanofibrillar cellulose aerogels, European Journal of Pharmaceutical Sciences. 50 (2013) 69–77. https://doi.org/10.1016/j.ejps.2013.02.023.

[35] B.L. Tardy, S. Yokota, M. Ago, W. Xiang, T. Kondo, R. Bordes, O.J. Rojas, Nanocellulose–surfactant interactions, Current Opinion in Colloid & Interface Science. 29 (2017) 57–67. https://doi.org/10.1016/j.cocis.2017.02.004.
[36] Y. Chevalier, M.-A. Bolzinger, Emulsions stabilized with solid nanoparticles: Pickering emulsions, Colloids and Surfaces A: Physicochemical and Engineering Aspects. 439 (2013) 23–34. https://doi.org/10.1016/j.colsurfa.2013.02.054.
[37] J.O. Zoppe, R.A. Venditti, O.J. Rojas, Pickering emulsions stabilized by cellulose nanocrystals grafted with thermo-responsive polymer brushes, Journal of Colloid and Interface Science. 369 (2012) 202–209. https://doi.org/10.1016/j.jcis.2011.12.011.
[38] A. Schröder, J. Sprakel, K. Schroën, J.N. Spaen, C.C. Berton-Carabin, Coalescence stability of Pickering emulsions produced with lipid particles: A microfluidic study, Journal of Food Engineering. 234 (2018) 63–72. https://doi.org/10.1016/j.jfoodeng.2018.04.007.
[39] S. Tsuji, H. Kawaguchi, Thermosensitive Pickering Emulsion Stabilized by Poly(N-isopropylacrylamide)-Carrying Particles, Langmuir. 24 (2008) 3300–3305. https://doi.org/10.1021/la701780g.
[40] S. Parajuli, A.L. Dorris, C. Middleton, A. Rodriguez, M.O. Haver, N.I. Hammer, E. Ureña-Benavides, Surface and Interfacial Interactions in Dodecane/Brine Pickering Emulsions Stabilized by the Combination of Cellulose Nanocrystals and Emulsifiers, Langmuir. 35 (2019) 12061–12070. https://doi.org/10.1021/acs.langmuir.9b01218.
[41] P. Bertsch, A. Thoma, J. Bergfreund, T. Geue, P. Fischer, Transient measurement and structure analysis of protein–polysaccharide multilayers at fluid interfaces, Soft Matter. 15 (2019) 6362–6368. https://doi.org/10.1039/C9SM01112A.
[42] A.J. Worthen, L.M. Foster, J. Dong, J.A. Bollinger, A.H. Peterman, L.E. Pastora, S.L. Bryant, T.M. Truskett, C.W. Bielawski, K.P. Johnston, Synergistic Formation and Stabilization of Oil-in-Water Emulsions by a Weakly Interacting Mixture of Zwitterionic Surfactant and Silica Nanoparticles, Langmuir. 30 (2014) 984–994. https://doi.org/10.1021/la404132p.
[43] E. Vignati, R. Piazza, T.P. Lockhart, Pickering Emulsions: Interfacial Tension, Colloidal Layer Morphology, and Trapped-Particle Motion, Langmuir. 19 (2003) 6650–6656. https://doi.org/10.1021/la034264l.
[44] J. Pelipenko, J. Kristl, R. Rošic, S. Baumgartner, P. Kocbek, Interfacial rheology: An overview of measuring techniques and its role in dispersions and electrospinning, Acta Pharmaceutica. 62 (2012) 123–140. https://doi.org/10.2478/v10007-012-0018-x.
[45] N.T. Cervin, E. Johansson, J.-W. Benjamins, L. Wågberg, Mechanisms Behind the Stabilizing Action of Cellulose Nanofibrils in Wet-Stable Cellulose Foams, Biomacromolecules. 16 (2015) 822–831. https://doi.org/10.1021/bm5017173.
[46] F. Ravera, G. Loglio, V.I. Kovalchuk, Interfacial dilational rheology by oscillating bubble/drop methods, Current Opinion in Colloid & Interface Science. 15 (2010) 217–228. https://doi.org/10.1016/j.cocis.2010.04.001.

[47] H.W. Yarranton, P. Urrutia, D.M. Sztukowski, Effect of interfacial rheology on model emulsion coalescence: II. Emulsion coalescence, Journal of Colloid and Interface Science. 310 (2007) 253–259. https://doi.org/10.1016/j.jcis.2007.01.098.
[48] C. Monteux, G.G. Fuller, V. Bergeron, Shear and Dilational Surface Rheology of Oppositely Charged Polyelectrolyte/Surfactant Microgels Adsorbed at the Air−Water Interface. Influence on Foam Stability, J. Phys. Chem. B. 108 (2004) 16473–16482. https://doi.org/10.1021/jp047462+.
[49] R. Myrvold, F.K. Hansen, Surface Elasticity and Viscosity from Oscillating Bubbles Measured by Automatic Axisymmetric Drop Shape Analysis, Journal of Colloid and Interface Science. 207 (1998) 97–105. https://doi.org/10.1006/jcis.1998.5745.
[50] S. Arditty, V. Schmitt, F. Lequeux, F. Leal-Calderon, Interfacial properties in solid-stabilized emulsions, The European Physical Journal B. 44 (2005) 381–393. https://doi.org/10.1140/epjb/e2005-00137-0.
[51] Y. Fan, S. Simon, J. Sjöblom, Interfacial shear rheology of asphaltenes at oil–water interface and its relation to emulsion stability: Influence of concentration, solvent aromaticity and nonionic surfactant, Colloids and Surfaces A: Physicochemical and Engineering Aspects. 366 (2010) 120–128. https://doi.org/10.1016/j.colsurfa.2010.05.034.
[52] B. Madivala, S. Vandebril, J. Fransaer, J. Vermant, Exploiting particle shape in solid stabilized emulsions, Soft Matter. 5 (2009) 1717–1727. https://doi.org/10.1039/B816680C.
[53] F. Cherhal, F. Cousin, I. Capron, Structural Description of the Interface of Pickering Emulsions Stabilized by Cellulose Nanocrystals, Biomacromolecules. 17 (2016) 496–502. https://doi.org/10.1021/acs.biomac.5b01413.
[54] I. Kalashnikova, H. Bizot, B. Cathala, I. Capron, New Pickering Emulsions Stabilized by Bacterial Cellulose Nanocrystals, Langmuir. 27 (2011) 7471–7479. https://doi.org/10.1021/la200971f.
[55] C. Whitby, E. Wanless, Controlling Pickering Emulsion Destabilisation: A Route to Fabricating New Materials by Phase Inversion, Materials. 9 (2016) 626. https://doi.org/10.3390/ma9080626.
[56] S. Arditty, C.P. Whitby, B.P. Binks, V. Schmitt, F. Leal-Calderon, Some general features of limited coalescence in solid-stabilized emulsions, Eur. Phys. J. E. 11 (2003) 273–281. https://doi.org/10.1140/epje/i2003-10018-6.
[57] Z.A. AlYousef, M.A. Almobarky, D.S. Schechter, The effect of nanoparticle aggregation on surfactant foam stability, Journal of Colloid and Interface Science. 511 (2018) 365–373. https://doi.org/10.1016/j.jcis.2017.09.051.
[58] D. Langevin, Influence of interfacial rheology on foam and emulsion properties, Advances in Colloid and Interface Science. 88 (2000) 209–222. https://doi.org/10.1016/S0001-8686(00)00045-2.

[59] N. Saleh, T. Sarbu, K. Sirk, G.V. Lowry, K. Matyjaszewski, R.D. Tilton, Oil-in-Water Emulsions Stabilized by Highly Charged Polyelectrolyte-Grafted Silica Nanoparticles †, Langmuir. 21 (2005) 9873–9878. https://doi.org/10.1021/la050654r.

[60] D. Demircioglu, Surface Active Silica Sols: Effect of PEG-Silica Interactions, CHALMERS UNIVERSITY OF TECHNOLOGY, 2011. http://publications.lib.chalmers.se/records/fulltext/147781.pdf (accessed November 4, 2018).

[61] J. Tang, R.M. Berry, K.C. Tam, Stimuli-Responsive Cellulose Nanocrystals for Surfactant-Free Oil Harvesting, Biomacromolecules. 17 (2016) 1748–1756. https://doi.org/10.1021/acs.biomac.6b00144.

[62] C. Tang, S. Spinney, Z. Shi, J. Tang, B. Peng, J. Luo, K.C. Tam, Amphiphilic Cellulose Nanocrystals for Enhanced Pickering Emulsion Stabilization, Langmuir. 34 (2018) 12897–12905. https://doi.org/10.1021/acs.langmuir.8b02437.

[63] T.S. Horozov, B.P. Binks, Particle-Stabilized Emulsions: A Bilayer or a Bridging Monolayer?, Angewandte Chemie International Edition. 45 (2006) 773–776. https://doi.org/10.1002/anie.200503131.

[64] A.J. Worthen, S.L. Bryant, C. Huh, K.P. Johnston, Carbon dioxide-in-water foams stabilized with nanoparticles and surfactant acting in synergy, AIChE Journal. 59 (2013) 3490–3501. https://doi.org/10.1002/aic.14124.

[65] S. Simovic, C.A. Prestidge, Nanoparticles of Varying Hydrophobicity at the Emulsion Droplet−Water Interface: Adsorption and Coalescence Stability, Langmuir. 20 (2004) 8357–8365. https://doi.org/10.1021/la0491807.

[66] S. Roohinejad, R. Greiner, I. Oey, J. Wen, Emulsion-Based Systems for Delivery of Food Active Compounds: Formation, Application, Health and Safety, John Wiley & Sons, Incorporated, Newark, UNITED KINGDOM, 2018. http://ebookcentral.proquest.com/lib/olemiss/detail.action?docID=5341519 (accessed November 27, 2018).

[67] Y. Yuan, T.R. Lee, Contact Angle and Wetting Properties, in: G. Bracco, B. Holst (Eds.), Surface Science Techniques, Springer Berlin Heidelberg, Berlin, Heidelberg, 2013: pp. 3–34. https://doi.org/10.1007/978-3-642-34243-1_1.

[68] Y. Sakazaki, V. Schmitt, U. Olsson, Particles with tunable wettability for solid-stabilized emulsions, Journal of Dispersion Science and Technology. 0 (2018) 1–12. https://doi.org/10.1080/01932691.2018.1467772.

[69] B.P. Binks, Colloidal Particles at a Range of Fluid–Fluid Interfaces, Langmuir. 33 (2017) 6947–6963. https://doi.org/10.1021/acs.langmuir.7b00860.

[70] P. Finkle, H.D. Draper, J.H. Hildebrand, THE THEORY OF EMULSIFICATION, J. Am. Chem. Soc. 45 (1923) 2780–2788. https://doi.org/10.1021/ja01665a002.

[71] J.N. Israelachvili, 1 - Historical Perspective, in: J.N. Israelachvili (Ed.), Intermolecular and Surface Forces (Third Edition), Academic Press, San Diego, 2011: pp. 3–22. https://doi.org/10.1016/B978-0-12-375182-9.10001-6.

[72] H.-J. Butt, M. Kappl, Surface and Interfacial Forces, 1 edition, Wiley-VCH, Weinheim, 2010.
[73] H.N.W. Lekkerkerker, R. Tuinier, Colloids and the Depletion Interaction, Springer Netherlands, 2011. //www.springer.com/us/book/9789400712225 (accessed January 24, 2019).
[74] A.D. McLachlan, Van der Waals forces between an atom and a surface, Molecular Physics. 7 (1964) 381–388. https://doi.org/10.1080/00268976300101141.
[75] J. Lyklema, Fundamentals of Interface and Colloid Science, 1 edition, Academic Press, London, 1991.
[76] I. Gentle, G. Barnes, Interfacial Science: An Introduction, 2005.
[77] P.C. Hiemenz, R. Rajagopalan, Principles of colloids and Surface Chemistry, 3rd ed., Marcel Dekker Inc, New York, 1997.
[78] J.N. Israelachvili, Chapter 14 - Electrostatic Forces between Surfaces in Liquids, in: J.N. Israelachvili (Ed.), Intermolecular and Surface Forces (Third Edition), Academic Press, San Diego, 2011: pp. 291–340. https://doi.org/10.1016/B978-0-12-375182-9.10014-4.
[79] J.N. Israelachvili, 15 - Solvation, Structural, and Hydration Forces, in: J.N. Israelachvili (Ed.), Intermolecular and Surface Forces (Third Edition), Academic Press, San Diego, 2011: pp. 341–380. https://doi.org/10.1016/B978-0-12-375182-9.10015-6.
[80] W.A. Ducker, Z. Xu, D.R. Clarke, J.N. Israelachvili, Forces between Alumina Surfaces in Salt Solutions: Non-DLVO Forces and the Implications for Colloidal Processing, Journal of the American Ceramic Society. 77 (1994) 437–443. https://doi.org/10.1111/j.1151-2916.1994.tb07012.x.
[81] S. Asakura, F. Oosawa, Interaction between particles suspended in solutions of macromolecules, Journal of Polymer Science. 33 (1958) 183–192. https://doi.org/10.1002/pol.1958.1203312618.
[82] S. Ji, J.Y. Walz, Depletion forces and flocculation with surfactants, polymers and particles — Synergistic effects, Current Opinion in Colloid & Interface Science. 20 (2015) 39–45. https://doi.org/10.1016/j.cocis.2014.11.006.
[83] Y. Mao, M.E. Cates, H.N.W. Lekkerkerker, Depletion force in colloidal systems, Physica A: Statistical Mechanics and Its Applications. 222 (1995) 10–24. https://doi.org/10.1016/0378-4371(95)00206-5.
[84] D. Marenduzzo, K. Finan, P.R. Cook, The depletion attraction: an underappreciated force driving cellular organization, J Cell Biol. 175 (2006) 681–686. https://doi.org/10.1083/jcb.200609066.
[85] G. Kaptay, On the equation of the maximum capillary pressure induced by solid particles to stabilize emulsions and foams and on the emulsion stability diagrams, Colloids and Surfaces A: Physicochemical and Engineering Aspects. 282–283 (2006) 387–401. https://doi.org/10.1016/j.colsurfa.2005.12.021.

[86] N.D. Denkov, I.B. Ivanov, P.A. Kralchevsky, D.T. Wasan, A possible mechanism of stabilization of emulsions by solid particles, Journal of Colloid and Interface Science. 150 (1992) 589–593. https://doi.org/10.1016/0021-9797(92)90228-E.
[87] G. Kaptay, Interfacial criteria for stabilization of liquid foams by solid particles, Colloids and Surfaces A: Physicochemical and Engineering Aspects. 230 (2003) 67–80. https://doi.org/10.1016/j.colsurfa.2003.09.016.
[88] P.M. Kruglyakov, S.I. Elaneva, N.G. Vilkova, About mechanism of foam stabilization by solid particles, Advances in Colloid and Interface Science. 165 (2011) 108–116. https://doi.org/10.1016/j.cis.2011.02.003.
[89] L. Wang, R.-H. Yoon, Hydrophobic forces in thin aqueous films and their role in film thinning, Colloids and Surfaces A: Physicochemical and Engineering Aspects. 263 (2005) 267–274. https://doi.org/10.1016/j.colsurfa.2004.12.045.
[90] Y. Li, X. Liu, Z. Zhang, S. Zhao, G. Tian, J. Zheng, D. Wang, S. Shi, T.P. Russell, Adaptive Structured Pickering Emulsions and Porous Materials Based on Cellulose Nanocrystal Surfactants, Angewandte Chemie. 130 (2018) 13748–13752. https://doi.org/10.1002/ange.201808888.
[91] L.E. Low, B.T. Tey, B.H. Ong, E.S. Chan, S.Y. Tang, Palm olein-in-water Pickering emulsion stabilized by Fe3O4-cellulose nanocrystal nanocomposites and their responses to pH, Carbohydrate Polymers. 155 (2017) 391–399. https://doi.org/10.1016/j.carbpol.2016.08.091.
[92] Z. Hu, H.S. Marway, H. Kasem, R. Pelton, E.D. Cranston, Dried and Redispersible Cellulose Nanocrystal Pickering Emulsions, ACS Macro Lett. 5 (2016) 185–189. https://doi.org/10.1021/acsmacrolett.5b00919.
[93] A. Madadlou, E. Rakhshi, A. Abbaspourrad, Engineered emulsions for obesity treatment, Trends in Food Science & Technology. 52 (2016) 90–97. https://doi.org/10.1016/j.tifs.2016.04.009.
[94] A.G. Cunha, J.-B. Mougel, B. Cathala, L.A. Berglund, I. Capron, Preparation of Double Pickering Emulsions Stabilized by Chemically Tailored Nanocelluloses, Langmuir. 30 (2014) 9327–9335. https://doi.org/10.1021/la5017577.
[95] A.J. Svagan, A. Musyanovych, M. Kappl, M. Bernhardt, G. Glasser, C. Wohnhaas, L.A. Berglund, J. Risbo, K. Landfester, Cellulose Nanofiber/Nanocrystal Reinforced Capsules: A Fast and Facile Approach Toward Assembly of Liquid-Core Capsules with High Mechanical Stability, Biomacromolecules. 15 (2014) 1852–1859. https://doi.org/10.1021/bm500232h.
[96] A.G. Cunha, J.-B. Mougel, B. Cathala, L.A. Berglund, I. Capron, Preparation of Double Pickering Emulsions Stabilized by Chemically Tailored Nanocelluloses, Langmuir. 30 (2014) 9327–9335. https://doi.org/10.1021/la5017577.
[97] K.-Y. Lee, J.J. Blaker, R. Murakami, J.Y.Y. Heng, A. Bismarck, Phase Behavior of Medium and High Internal Phase Water-in-Oil Emulsions Stabilized Solely by

Hydrophobized Bacterial Cellulose Nanofibrils, Langmuir. 30 (2014) 452–460. https://doi.org/10.1021/la4032514.
[98] S.S. Vadodaria, A.J. Onyianta, D. Sun, High-shear rate rheometry of micro-nanofibrillated cellulose (CMF/CNF) suspensions using rotational rheometer, Cellulose. 25 (2018) 5535–5552. https://doi.org/10.1007/s10570-018-1963-4.
[99] T. Moberg, K. Sahlin, K. Yao, S. Geng, G. Westman, Q. Zhou, K. Oksman, M. Rigdahl, Rheological properties of nanocellulose suspensions: effects of fibril/particle dimensions and surface characteristics, Cellulose. 24 (2017) 2499–2510. https://doi.org/10.1007/s10570-017-1283-0.
[100] X. Sun, Q. Wu, S. Lee, Y. Qing, Y. Wu, Cellulose Nanofibers as a Modifier for Rheology, Curing and Mechanical Performance of Oil Well Cement, Scientific Reports. 6 (2016) 1–9. https://doi.org/10.1038/srep31654.
[101] K. Dimic-Misic, P.A.C. Gane, J. Paltakari, Micro- and Nanofibrillated Cellulose as a Rheology Modifier Additive in CMC-Containing Pigment-Coating Formulations, Ind. Eng. Chem. Res. 52 (2013) 16066–16083. https://doi.org/10.1021/ie4028878.
[102] K. Dimic-Misic, A. Puisto, P. Gane, K. Nieminen, M. Alava, J. Paltakari, T. Maloney, The role of MFC/NFC swelling in the rheological behavior and dewatering of high consistency furnishes, Cellulose. 20 (2013) 2847–2861. https://doi.org/10.1007/s10570-013-0076-3.
[103] Y. Lu, X. Qian, W. Xie, W. Zhang, J. Huang, D. Wu, Rheology of the sesame oil-in-water emulsions stabilized by cellulose nanofibers, Food Hydrocolloids. 94 (2019) 114–127. https://doi.org/10.1016/j.foodhyd.2019.03.001.
[104] C. Jiménez Saelices, I. Capron, Design of Pickering Micro- and Nanoemulsions Based on the Structural Characteristics of Nanocelluloses, Biomacromolecules. 19 (2018) 460–469. https://doi.org/10.1021/acs.biomac.7b01564.
[105] Y. Lu, X. Qian, W. Xie, W. Zhang, J. Huang, D. Wu, Rheology of the sesame oil-in-water emulsions stabilized by cellulose nanofibers, Food Hydrocolloids. 94 (2019) 114–127. https://doi.org/10.1016/j.foodhyd.2019.03.001.
[106] M. Gestranius, P. Stenius, E. Kontturi, J. Sjöblom, T. Tammelin, Phase behaviour and droplet size of oil-in-water Pickering emulsions stabilised with plant-derived nanocellulosic materials, Colloids and Surfaces A: Physicochemical and Engineering Aspects. 519 (2017) 60–70. https://doi.org/10.1016/j.colsurfa.2016.04.025.
[107] B. Madivala, S. Vandebril, J. Fransaer, J. Vermant, Exploiting particle shape in solid stabilized emulsions, Soft Matter. 5 (2009) 1717–1727. https://doi.org/10.1039/B816680C.
[108] X.-C. Luu, J. Yu, A. Striolo, Ellipsoidal Janus Nanoparticles Adsorbed at the Water–Oil Interface: Some Evidence of Emergent Behavior, J. Phys. Chem. B. 117 (2013) 13922–13929. https://doi.org/10.1021/jp407495z.
[109] F. Cherhal, F. Cousin, I. Capron, Influence of Charge Density and Ionic Strength on the Aggregation Process of Cellulose Nanocrystals in Aqueous Suspension, as Revealed by

Small-Angle Neutron Scattering, Langmuir. 31 (2015) 5596–5602. https://doi.org/10.1021/acs.langmuir.5b00851.
[110] I. Kalashnikova, H. Bizot, P. Bertoncini, B. Cathala, I. Capron, Cellulosic nanorods of various aspect ratios for oil in water Pickering emulsions, Soft Matter. 9 (2013) 952–959. https://doi.org/10.1039/C2SM26472B.
[111] S. Varanasi, L. Henzel, L. Mendoza, R. Prathapan, W. Batchelor, R. Tabor, G. Garnier, Pickering Emulsions Electrostatically Stabilized by Cellulose Nanocrystals, Front. Chem. 6 (2018). https://doi.org/10.3389/fchem.2018.00409.
[112] L. Bai, S. Huan, W. Xiang, O.J. Rojas, Pickering emulsions by combining cellulose nanofibrils and nanocrystals: phase behavior and depletion stabilization, Green Chem. 20 (2018) 1571–1582. https://doi.org/10.1039/C8GC00134K.
[113] J.O. Zoppe, R.A. Venditti, O.J. Rojas, Pickering emulsions stabilized by cellulose nanocrystals grafted with thermo-responsive polymer brushes, Journal of Colloid and Interface Science. 369 (2012) 202–209. https://doi.org/10.1016/j.jcis.2011.12.011.
[114] M. Salajková, L. A. Berglund, Q. Zhou, Hydrophobic cellulose nanocrystals modified with quaternary ammonium salts, Journal of Materials Chemistry. 22 (2012) 19798–19805. https://doi.org/10.1039/C2JM34355J.
[115] L. Wei, U.P. Agarwal, K.C. Hirth, L.M. Matuana, R.C. Sabo, N.M. Stark, Chemical modification of nanocellulose with canola oil fatty acid methyl ester, Carbohydrate Polymers. 169 (2017) 108–116. https://doi.org/10.1016/j.carbpol.2017.04.008.
[116] N. Nikfarjam, N. Taheri Qazvini, Y. Deng, Surfactant free Pickering emulsion polymerization of styrene in w/o/w system using cellulose nanofibrils, European Polymer Journal. 64 (2015) 179–188. https://doi.org/10.1016/j.eurpolymj.2015.01.007.
[117] S. Varanasi, L. Henzel, L. Mendoza, R. Prathapan, W. Batchelor, R. Tabor, G. Garnier, Pickering Emulsions Electrostatically Stabilized by Cellulose Nanocrystals, Front Chem. 6 (2018). https://doi.org/10.3389/fchem.2018.00409.
[118] T.A. Dankovich, D.G. Gray, Contact Angle Measurements on Smooth Nanocrystalline Cellulose (I) Thin Films, Journal of Adhesion Science and Technology. 25 (2011) 699–708. https://doi.org/10.1163/016942410X525885.
[119] J. Dong, A.J. Worthen, L.M. Foster, Y. Chen, K.A. Cornell, S.L. Bryant, T.M. Truskett, C.W. Bielawski, K.P. Johnston, Modified Montmorillonite Clay Microparticles for Stable Oil-in-Seawater Emulsions, ACS Appl. Mater. Interfaces. 6 (2014) 11502–11513. https://doi.org/10.1021/am502187t.
[120] H.A. Son, K.Y. Yoon, G.J. Lee, J.W. Cho, S.K. Choi, J.W. Kim, K.C. Im, H.T. Kim, K.S. Lee, W.M. Sung, The potential applications in oil recovery with silica nanoparticle and polyvinyl alcohol stabilized emulsion, Journal of Petroleum Science and Engineering. 126 (2015) 152–161. https://doi.org/10.1016/j.petrol.2014.11.001.
[121] A.E. Way, L. Hsu, K. Shanmuganathan, C. Weder, S.J. Rowan, pH-Responsive Cellulose Nanocrystal Gels and Nanocomposites, ACS Macro Lett. 1 (2012) 1001–1006. https://doi.org/10.1021/mz3003006.

[122] L.E. Low, B.T. Tey, B.H. Ong, E.S. Chan, S.Y. Tang, Palm olein-in-water Pickering emulsion stabilized by Fe3O4-cellulose nanocrystal nanocomposites and their responses to pH, Carbohydrate Polymers. 155 (2017) 391–399. https://doi.org/10.1016/j.carbpol.2016.08.091.
[123] Q.-H. Chen, J. Zheng, Y.-T. Xu, S.-W. Yin, F. Liu, C.-H. Tang, Surface modification improves fabrication of pickering high internal phase emulsions stabilized by cellulose nanocrystals, Food Hydrocolloids. 75 (2018) 125–130. https://doi.org/10.1016/j.foodhyd.2017.09.005.
[124] A. Pandey, M. Derakhshandeh, S.A. Kedzior, B. Pilapil, N. Shomrat, T. Segal-Peretz, S.L. Bryant, M. Trifkovic, Role of interparticle interactions on microstructural and rheological properties of cellulose nanocrystal stabilized emulsions, Journal of Colloid and Interface Science. 532 (2018) 808–818. https://doi.org/10.1016/j.jcis.2018.08.044.
[125] F. Liu, J. Zheng, C.-H. Huang, C.-H. Tang, S.-Y. Ou, Pickering high internal phase emulsions stabilized by protein-covered cellulose nanocrystals, Food Hydrocolloids. 82 (2018) 96–105. https://doi.org/10.1016/j.foodhyd.2018.03.047.
[126] R. Aaen, F.W. Brodin, S. Simon, E.B. Heggset, K. Syverud, Oil-in-Water Emulsions Stabilized by Cellulose Nanofibrils—The Effects of Ionic Strength and pH, Nanomaterials. 9 (2019) 259. https://doi.org/10.3390/nano9020259.
[127] A. Pandey, M. Derakhshandeh, S.A. Kedzior, B. Pilapil, N. Shomrat, T. Segal-Peretz, S.L. Bryant, M. Trifkovic, Role of interparticle interactions on microstructural and rheological properties of cellulose nanocrystal stabilized emulsions, Journal of Colloid and Interface Science. 532 (2018) 808–818. https://doi.org/10.1016/j.jcis.2018.08.044.
[128] Q.-H. Chen, J. Zheng, Y.-T. Xu, S.-W. Yin, F. Liu, C.-H. Tang, Surface modification improves fabrication of pickering high internal phase emulsions stabilized by cellulose nanocrystals, Food Hydrocolloids. 75 (2018) 125–130. https://doi.org/10.1016/j.foodhyd.2017.09.005.
[129] S.S. Datta, D.D. Gerrard, T.S. Rhodes, T.G. Mason, D.A. Weitz, Rheology of attractive emulsions, Phys. Rev. E. 84 (2011) 041404. https://doi.org/10.1103/PhysRevE.84.041404.
[130] M. Hermes, P.S. Clegg, Yielding and flow of concentrated Pickering emulsions, Soft Matter. 9 (2013) 7568–7575. https://doi.org/10.1039/c3sm50889g.
[131] J. Ojala, J.A. Sirviö, H. Liimatainen, Nanoparticle emulsifiers based on bifunctionalized cellulose nanocrystals as marine diesel oil–water emulsion stabilizers, Chemical Engineering Journal. 288 (2016) 312–320. https://doi.org/10.1016/j.cej.2015.10.113.
[132] J. Tang, M.F.X. Lee, W. Zhang, B. Zhao, R.M. Berry, K.C. Tam, Dual Responsive Pickering Emulsion Stabilized by Poly[2-(dimethylamino)ethyl methacrylate] Grafted Cellulose Nanocrystals, Biomacromolecules. 15 (2014) 3052–3060. https://doi.org/10.1021/bm500663w.
[133] E. Abraham, D. Kam, Y. Nevo, R. Slattegard, A. Rivkin, S. Lapidot, O. Shoseyov, Highly Modified Cellulose Nanocrystals and Formation of Epoxy-Nanocrystalline Cellulose

(CNC) Nanocomposites, ACS Appl. Mater. Interfaces. 8 (2016) 28086–28095. https://doi.org/10.1021/acsami.6b09852.
[134] N. Wang, E. Ding, R. Cheng, Surface modification of cellulose nanocrystals, Front. Chem. Eng. China. 1 (2007) 228–232. https://doi.org/10.1007/s11705-007-0041-5.
[135] C. Tang, S. Spinney, Z. Shi, J. Tang, B. Peng, J. Luo, K.C. Tam, Amphiphilic Cellulose Nanocrystals for Enhanced Pickering Emulsion Stabilization, Langmuir. 34 (2018) 12897–12905. https://doi.org/10.1021/acs.langmuir.8b02437.
[136] Z. Hu, T. Patten, R. Pelton, E.D. Cranston, Synergistic Stabilization of Emulsions and Emulsion Gels with Water-Soluble Polymers and Cellulose Nanocrystals, ACS Sustainable Chem. Eng. 3 (2015) 1023–1031. https://doi.org/10.1021/acssuschemeng.5b00194.
[137] Z. Hu, S. Ballinger, R. Pelton, E.D. Cranston, Surfactant-enhanced cellulose nanocrystal Pickering emulsions, Journal of Colloid and Interface Science. 439 (2015) 139–148. https://doi.org/10.1016/j.jcis.2014.10.034.
[138] J. Ojala, M. Visanko, O. Laitinen, M. Österberg, J.A. Sirviö, H. Liimatainen, Emulsion Stabilization with Functionalized Cellulose Nanoparticles Fabricated Using Deep Eutectic Solvents, Molecules. 23 (2018). https://doi.org/10.3390/molecules23112765.
[139] Z. Hu, S. Ballinger, R. Pelton, E.D. Cranston, Surfactant-enhanced cellulose nanocrystal Pickering emulsions, Journal of Colloid and Interface Science. 439 (2015) 139–148. https://doi.org/10.1016/j.jcis.2014.10.034.
[140] S.L. Kadam, P. Yadav, S. Bhutkar, V.D. Patil, P.G. Shukla, K. Shanmuganathan, Sustained release insect repellent microcapsules using modified cellulose nanofibers (mCNF) as pickering emulsifier, Colloids and Surfaces A: Physicochemical and Engineering Aspects. 582 (2019) 123883. https://doi.org/10.1016/j.colsurfa.2019.123883.
[141] L. Bai, S. Huan, W. Xiang, O.J. Rojas, Pickering emulsions by combining cellulose nanofibrils and nanocrystals: phase behavior and depletion stabilization, Green Chemistry. 20 (2018) 1571–1582. https://doi.org/10.1039/C8GC00134K.
[142] R.J. Pugh, The stability/instability of bubbles and foams, Bubble and Foam Chemistry. (2016). https://doi.org/10.1017/CBO9781316106938.008.
[143] A.J. de Vries, Foam stability: Part. II. Gas diffusion in foams, Recueil Des Travaux Chimiques Des Pays-Bas. 77 (1958) 209–223. https://doi.org/10.1002/recl.19580770302.
[144] S.S. Borkotoky, P. Dhar, V. Katiyar, Biodegradable poly (lactic acid)/Cellulose nanocrystals (CNCs) composite microcellular foam: Effect of nanofillers on foam cellular morphology, thermal and wettability behavior, International Journal of Biological Macromolecules. 106 (2018) 433–446. https://doi.org/10.1016/j.ijbiomac.2017.08.036.
[145] T. Song, S. Tanpichai, K. Oksman, Cross-linked polyvinyl alcohol (PVA) foams reinforced with cellulose nanocrystals (CNCs), Cellulose. 23 (2016) 1925–1938. https://doi.org/10.1007/s10570-016-0925-y.

[146] N. Lavoine, L. Bergström, Nanocellulose-based foams and aerogels: processing, properties, and applications, J. Mater. Chem. A. 5 (2017) 16105–16117. https://doi.org/10.1039/C7TA02807E.
[147] P. Bertsch, M. Arcari, T. Geue, R. Mezzenga, G. Nyström, P. Fischer, Designing Cellulose Nanofibrils for Stabilization of Fluid Interfaces, Biomacromolecules. 20 (2019) 4574–4580. https://doi.org/10.1021/acs.biomac.9b01384.
[148] P. Bertsch, P. Fischer, Interfacial Rheology of Charged Anisotropic Cellulose Nanocrystals at the Air–Water Interface, Langmuir. 35 (2019) 7937–7943. https://doi.org/10.1021/acs.langmuir.9b00699.
[149] A. Stocco, E. Rio, B.P. Binks, D. Langevin, Aqueous foams stabilized solely by particles, Soft Matter. 7 (2011) 1260–1267. https://doi.org/10.1039/C0SM01290D.
[150] N.T. Cervin, E. Johansson, J.-W. Benjamins, L. Wågberg, Mechanisms Behind the Stabilizing Action of Cellulose Nanofibrils in Wet-Stable Cellulose Foams, Biomacromolecules. 16 (2015) 822–831. https://doi.org/10.1021/bm5017173.
[151] P. Bertsch, P. Fischer, Adsorption and interfacial structure of nanocelluloses at fluid interfaces, Advances in Colloid and Interface Science. (2019) 102089. https://doi.org/10.1016/j.cis.2019.102089.
[152] X. Li, J. Li, J. Gong, Y. Kuang, L. Mo, T. Song, Cellulose nanocrystals (CNCs) with different crystalline allomorph for oil in water Pickering emulsions, Carbohydrate Polymers. 183 (2018) 303–310. https://doi.org/10.1016/j.carbpol.2017.12.085.
[153] A.J. Svagan, A. Müllertz, K. Löbmann, Floating solid cellulose nanofibre nanofoams for sustained release of the poorly soluble model drug furosemide, Journal of Pharmacy and Pharmacology. 69 (2017) 1477–1484. https://doi.org/10.1111/jphp.12793.
[154] Z. Hu, R. Xu, E.D. Cranston, R.H. Pelton, Stable Aqueous Foams from Cellulose Nanocrystals and Methyl Cellulose, Biomacromolecules. 17 (2016) 4095–4099. https://doi.org/10.1021/acs.biomac.6b01641.
[155] N. Scheuble, T. Geue, S. Kuster, J. Adamcik, R. Mezzenga, E.J. Windhab, P. Fischer, Mechanically Enhanced Liquid Interfaces at Human Body Temperature Using Thermosensitive Methylated Nanocrystalline Cellulose, Langmuir. 32 (2016) 1396–1404. https://doi.org/10.1021/acs.langmuir.5b04231.
[156] N. Scheuble, T. Geue, E.J. Windhab, P. Fischer, Tailored Interfacial Rheology for Gastric Stable Adsorption Layers, Biomacromolecules. 15 (2014) 3139–3145. https://doi.org/10.1021/bm500767c.
[157] N.T. Cervin, L. Andersson, J.B.S. Ng, P. Olin, L. Bergström, L. Waìšgberg, Lightweight and strong cellulose materials made from aqueous foams stabilized by nanofibrillated cellulose, Biomacromolecules. 14 (2013) 503–511. https://doi.org/10.1021/bm301755u.
[158] W. Xiang, N. Preisig, A. Ketola, B.L. Tardy, L. Bai, J.A. Ketoja, C. Stubenrauch, O.J. Rojas, How Cellulose Nanofibrils Affect Bulk, Surface, and Foam Properties of Anionic Surfactant Solutions, Biomacromolecules. 20 (2019) 4361–4369. https://doi.org/10.1021/acs.biomac.9b01037.

[159] N.T. Cervin, E. Johansson, P.A. Larsson, L. Wågberg, Strong, Water-Durable, and Wet-Resilient Cellulose Nanofibril-Stabilized Foams from Oven Drying, ACS Appl. Mater. Interfaces. 8 (2016) 11682–11689. https://doi.org/10.1021/acsami.6b00924.
[160] P. Bertsch, P. Fischer, Adsorption and interfacial structure of nanocelluloses at fluid interfaces, Advances in Colloid and Interface Science. 276 (2020) 102089. https://doi.org/10.1016/j.cis.2019.102089.
[161] F. Azzam, L. Heux, J.-L. Putaux, B. Jean, Preparation By Grafting Onto, Characterization, and Properties of Thermally Responsive Polymer-Decorated Cellulose Nanocrystals, Biomacromolecules. 11 (2010) 3652–3659. https://doi.org/10.1021/bm101106c.
[162] R. Pichot, F. Spyropoulos, I.T. Norton, Competitive adsorption of surfactants and hydrophilic silica particles at the oil–water interface: Interfacial tension and contact angle studies, Journal of Colloid and Interface Science. 377 (2012) 396–405. https://doi.org/10.1016/j.jcis.2012.01.065.
[163] Vani Madan, Arsh Chanana, Mahesh Kumar Kataria, Ajay Bilandi, Emulsion technology and recent trends in emulsion application, Internation Research Journal of Pharmacy. 5 (n.d.) 533–542.
[164] D.J. French, A.T. Brown, A.B. Schofield, J. Fowler, P. Taylor, P.S. Clegg, The secret life of Pickering emulsions: particle exchange revealed using two colours of particle, Scientific Reports. 6 (2016) 31401. https://doi.org/10.1038/srep31401.
[165] J. Frelichowska, M.-A. Bolzinger, J. Pelletier, J.-P. Valour, Y. Chevalier, Topical delivery of lipophilic drugs from o/w Pickering emulsions, International Journal of Pharmaceutics. 371 (2009) 56–63. https://doi.org/10.1016/j.ijpharm.2008.12.017.
[166] T.N. Hunter, R.J. Pugh, G.V. Franks, G.J. Jameson, The role of particles in stabilising foams and emulsions, Advances in Colloid and Interface Science. 137 (2008) 57–81. https://doi.org/10.1016/j.cis.2007.07.007.
[167] Y. Gong, X. Zhao, Z. Cai, S.E. O'Reilly, X. Hao, D. Zhao, A review of oil, dispersed oil and sediment interactions in the aquatic environment: Influence on the fate, transport and remediation of oil spills, Marine Pollution Bulletin. 79 (2014) 16–33. https://doi.org/10.1016/j.marpolbul.2013.12.024.
[168] S.N. Molnes, A. Mamonov, K.G. Paso, S. Strand, K. Syverud, Investigation of a new application for cellulose nanocrystals: a study of the enhanced oil recovery potential by use of a green additive, Cellulose. 25 (2018) 2289–2301. https://doi.org/10.1007/s10570-018-1715-5.
[169] S.N. Molnes, I.P. Torrijos, S. Strand, K.G. Paso, K. Syverud, Sandstone injectivity and salt stability of cellulose nanocrystals (CNC) dispersions—Premises for use of CNC in enhanced oil recovery, Industrial Crops and Products. 93 (2016) 152–160. https://doi.org/10.1016/j.indcrop.2016.03.019.
[170] W. Du, J. Guo, H. Li, Y. Gao, Heterogeneously Modified Cellulose Nanocrystals-Stabilized Pickering Emulsion: Preparation and Their Template Application for the

Creation of PS Microspheres with Amino-Rich Surfaces, ACS Sustainable Chemistry & Engineering. (2017). https://doi.org/10.1021/acssuschemeng.7b00375.
[171] S.U. Pickering, Emulsions, J. Chem. Soc., Trans. 91 (1907) 2001–2021. https://doi.org/10.1039/CT9079102001.
[172] Ramsden W., Gotch Francis, Separation of solids in the surface-layers of solutions and 'suspensions' (observations on surface-membranes, bubbles, emulsions, and mechanical coagulation).—Preliminary account, Proceedings of the Royal Society of London. 72 (1904) 156–164. https://doi.org/10.1098/rspl.1903.0034.
[173] B.P. Binks, Chapter 1:Emulsions — Recent Advances in Understanding, in: 1998: pp. 1–55. http://pubs.rsc.org/en/content/chapter/bk9780854044399-00001/978-0-85404-439-9 (accessed February 8, 2017).
[174] H. Ma, M. Luo, L.L. Dai, Influences of surfactant and nanoparticle assembly on effective interfacial tensions, Physical Chemistry Chemical Physics. 10 (2008) 2207. https://doi.org/10.1039/b718427c.
[175] C. Miao, M. Tayebi, W.Y. Hamad, Investigation of the formation mechanisms in high internal phase Pickering emulsions stabilized by cellulose nanocrystals, Philosophical Transactions of the Royal Society A: Mathematical, Physical and Engineering Sciences. 376 (2018) 20170039. https://doi.org/10.1098/rsta.2017.0039.
[176] G. Barnes, I. Gentle, Interfacial Science: An Introduction, OUP Oxford, 2011.
[177] Nasrin Ghouchi Eskandar, Spomenka Simovic, Clive A. Prestidge, Synergistic effect of silica nanoparticles and charged surfactants in the formation and stability of submicron oil-in-water emulsions, Physical Chemistry Chemical Physics. 9 (2007) 6426–6434. https://doi.org/10.1039/b705094a.
[178] I. Akartuna, A.R. Studart, E. Tervoort, U.T. Gonzenbach, L.J. Gauckler, Stabilization of Oil-in-Water Emulsions by Colloidal Particles Modified with Short Amphiphiles, Langmuir. 24 (2008) 7161–7168. https://doi.org/10.1021/la800478g.
[179] A.J. Worthen, L.M. Foster, J. Dong, J.A. Bollinger, A.H. Peterman, L.E. Pastora, S.L. Bryant, T.M. Truskett, C.W. Bielawski, K.P. Johnston, Synergistic Formation and Stabilization of Oil-in-Water Emulsions by a Weakly Interacting Mixture of Zwitterionic Surfactant and Silica Nanoparticles, Langmuir. 30 (2014) 984–994. https://doi.org/10.1021/la404132p.
[180] B.P. Binks, J.A. Rodrigues, W.J. Frith, Synergistic Interaction in Emulsions Stabilized by a Mixture of Silica Nanoparticles and Cationic Surfactant, Langmuir. 23 (2007) 3626–3636. https://doi.org/10.1021/la0634600.
[181] A. Nesterenko, A. Drelich, H. Lu, D. Clausse, I. Pezron, Influence of a mixed particle/surfactant emulsifier system on water-in-oil emulsion stability, Colloids and Surfaces A: Physicochemical and Engineering Aspects. 457 (2014) 49–57. https://doi.org/10.1016/j.colsurfa.2014.05.044.
[182] Z. Hu, T. Patten, R. Pelton, E.D. Cranston, Synergistic Stabilization of Emulsions and Emulsion Gels with Water-Soluble Polymers and Cellulose Nanocrystals, ACS

Sustainable Chemistry & Engineering. 3 (2015) 1023–1031. https://doi.org/10.1021/acssuschemeng.5b00194.
[183] S.N. Molnes, K.G. Paso, S. Strand, K. Syverud, The effects of pH, time and temperature on the stability and viscosity of cellulose nanocrystal (CNC) dispersions: implications for use in enhanced oil recovery, Cellulose. 24 (2017) 4479–4491. https://doi.org/10.1007/s10570-017-1437-0.
[184] J.-P. Monclin, K. Nelson, Th. Retsina, Drilling fluid additives and fracturing fluid additives containing cellulose nanofibers and/or nanocrystals, US 2015/0368541 A1, 2015.
[185] T. Abitbol, E. Kloser, D.G. Gray, Estimation of the surface sulfur content of cellulose nanocrystals prepared by sulfuric acid hydrolysis, Cellulose. 20 (2013) 785–794. https://doi.org/10.1007/s10570-013-9871-0.
[186] H. Dong, K.E. Strawhecker, J.F. Snyder, J.A. Orlicki, R.S. Reiner, A.W. Rudie, Cellulose nanocrystals as a reinforcing material for electrospun poly(methyl methacrylate) fibers: Formation, properties and nanomechanical characterization, Carbohydrate Polymers. 87 (2012) 2488–2495. https://doi.org/10.1016/j.carbpol.2011.11.015.
[187] J.D. Berry, M.J. Neeson, R.R. Dagastine, D.Y.C. Chan, R.F. Tabor, Measurement of surface and interfacial tension using pendant drop tensiometry, Journal of Colloid and Interface Science. 454 (2015) 226–237. https://doi.org/10.1016/j.jcis.2015.05.012.
[188] U.P. Agarwal, 1064 nm FT-Raman spectroscopy for investigations of plant cell walls and other biomass materials, Front. Plant Sci. 5 (2014). https://doi.org/10.3389/fpls.2014.00490.
[189] S.A. Kedzior, H.S. Marway, E.D. Cranston, Tailoring Cellulose Nanocrystal and Surfactant Behavior in Miniemulsion Polymerization, Macromolecules. 50 (2017) 2645–2655. https://doi.org/10.1021/acs.macromol.7b00516.
[190] N. Dhar, D. Au, R.C. Berry, K.C. Tam, Interactions of nanocrystalline cellulose with an oppositely charged surfactant in aqueous medium, Colloids and Surfaces A: Physicochemical and Engineering Aspects. 415 (2012) 310–319. https://doi.org/10.1016/j.colsurfa.2012.09.010.
[191] B.P. Binks, A. Desforges, D.G. Duff, Synergistic Stabilization of Emulsions by a Mixture of Surface-Active Nanoparticles and Surfactant, Langmuir. 23 (2007) 1098–1106. https://doi.org/10.1021/la062510y.
[192] M.B. Mcbride, A critique of diffuse double layer models applied to colloid and surface chemistry. Clays Clay Miner, 1997.
[193] I. Kalashnikova, H. Bizot, B. Cathala, I. Capron, Modulation of Cellulose Nanocrystals Amphiphilic Properties to Stabilize Oil/Water Interface, Biomacromolecules. 13 (2012) 267–275. https://doi.org/10.1021/bm201599j.
[194] R. Aveyard, B.P. Binks, J.H. Clint, Emulsions stabilised solely by colloidal particles, Advances in Colloid and Interface Science. 100–102 (2003) 503–546. https://doi.org/10.1016/S0001-8686(02)00069-6.

[195] P. Pieranski, Two-Dimensional Interfacial Colloidal Crystals, Phys. Rev. Lett. 45 (1980) 569–572. https://doi.org/10.1103/PhysRevLett.45.569.
[196] R. Aveyard, J.H. Clint, T.S. Horozov, Aspects of the stabilisation of emulsions by solid particles: Effects of line tension and monolayer curvature energy, Phys. Chem. Chem. Phys. 5 (2003) 2398. https://doi.org/10.1039/b210687f.
[197] The packing density of 0.9 corresponds to hexagonally packed cylinders. In reality the CNC shape is closer to elongated particles with octagonal cross-sections. This value is only an upper limit., (n.d.).
[198] M.E.H. van den Berg, S. Kuster, E.J. Windhab, J. Adamcik, R. Mezzenga, T. Geue, L.M.C. Sagis, P. Fischer, Modifying the Contact Angle of Anisotropic Cellulose Nanocrystals: Effect on Interfacial Rheology and Structure, Langmuir. 34 (2018) 10932–10942. https://doi.org/10.1021/acs.langmuir.8b00623.
[199] K. Xu, P. Zhu, T. Colon, C. Huh, M. Balhoff, A Microfluidic Investigation of the Synergistic Effect of Nanoparticles and Surfactants in Macro-Emulsion-Based Enhanced Oil Recovery, SPE Journal. 22 (2017) 459–469. https://doi.org/10.2118/179691-PA.
[200] N. Kumar, T. Gaur, A. Mandal, Characterization of SPN Pickering emulsions for application in enhanced oil recovery, Journal of Industrial and Engineering Chemistry. 54 (2017) 304–315. https://doi.org/10.1016/j.jiec.2017.06.005.
[201] G. Chen, D. Tao, An experimental study of stability of oil–water emulsion, Fuel Processing Technology. 86 (2005) 499–508. https://doi.org/10.1016/j.fuproc.2004.03.010.
[202] B.P. Binks, A. Rocher, Effects of temperature on water-in-oil emulsions stabilised solely by wax microparticles, Journal of Colloid and Interface Science. 335 (2009) 94–104. https://doi.org/10.1016/j.jcis.2009.03.089.
[203] M.G. Barron, Ecological Impacts of the Deepwater Horizon Oil Spill: Implications for Immunotoxicity, Toxicol Pathol. 40 (2012) 315–320. https://doi.org/10.1177/0192623311428474.
[204] D.J. McClements, Advances in fabrication of emulsions with enhanced functionality using structural design principles, Current Opinion in Colloid & Interface Science. 17 (2012) 235–245. https://doi.org/10.1016/j.cocis.2012.06.002.
[205] M. Fingas, The Basics of Oil Spill Cleanup, CRC Press, 2012. https://doi.org/10.1201/b13686.
[206] M.B. Yakubu, Biological approach to oil spills remediation in the soil, African Journal of Biotechnology. 6 (2007). https://doi.org/10.5897/AJB2007.000-2437.
[207] C.M. Kao, C.Y. Chen, S.C. Chen, H.Y. Chien, Y.L. Chen, Application of in situ biosparging to remediate a petroleum-hydrocarbon spill site: Field and microbial evaluation, Chemosphere. 70 (2008) 1492–1499. https://doi.org/10.1016/j.chemosphere.2007.08.029.
[208] A. Pavía-Sanders, S. Zhang, J.A. Flores, J.E. Sanders, J.E. Raymond, K.L. Wooley, Robust Magnetic/Polymer Hybrid Nanoparticles Designed for Crude Oil Entrapment and

Recovery in Aqueous Environments, ACS Nano. 7 (2013) 7552–7561. https://doi.org/10.1021/nn401541e.
[209] S. Mirshahghassemi, J.R. Lead, Oil Recovery from Water under Environmentally Relevant Conditions Using Magnetic Nanoparticles, Environ. Sci. Technol. 49 (2015) 11729–11736. https://doi.org/10.1021/acs.est.5b02687.
[210] Q. Zhu, F. Tao, Q. Pan, Fast and Selective Removal of Oils from Water Surface via Highly Hydrophobic Core−Shell Fe2O3@C Nanoparticles under Magnetic Field, ACS Appl. Mater. Interfaces. 2 (2010) 3141–3146. https://doi.org/10.1021/am1006194.
[211] Q. Zhu, Q. Pan, Mussel-Inspired Direct Immobilization of Nanoparticles and Application for Oil–Water Separation, ACS Nano. 8 (2014) 1402–1409. https://doi.org/10.1021/nn4052277.
[212] C.A. Franco, F.B. Cortés, N.N. Nassar, Adsorptive removal of oil spill from oil-in-fresh water emulsions by hydrophobic alumina nanoparticles functionalized with petroleum vacuum residue, Journal of Colloid and Interface Science. 425 (2014) 168–177. https://doi.org/10.1016/j.jcis.2014.03.051.
[213] O. Laitinen, J. Ojala, J.A. Sirviö, H. Liimatainen, Sustainable stabilization of oil in water emulsions by cellulose nanocrystals synthesized from deep eutectic solvents, Cellulose. 24 (2017) 1679–1689. https://doi.org/10.1007/s10570-017-1226-9.
[214] J. Frelichowska, M.-A. Bolzinger, Y. Chevalier, Effects of solid particle content on properties of o/w Pickering emulsions, Journal of Colloid and Interface Science. 351 (2010) 348–356. https://doi.org/10.1016/j.jcis.2010.08.019.
[215] R. Prathapan, R. Thapa, G. Garnier, R.F. Tabor, Modulating the zeta potential of cellulose nanocrystals using salts and surfactants, Colloids and Surfaces A: Physicochemical and Engineering Aspects. 509 (2016) 11–18. https://doi.org/10.1016/j.colsurfa.2016.08.075.
[216] L. Zhong, S. Fu, X. Peng, H. Zhan, R. Sun, Colloidal stability of negatively charged cellulose nanocrystalline in aqueous systems, Carbohydrate Polymers. 90 (2012) 644–649. https://doi.org/10.1016/j.carbpol.2012.05.091.
[217] A.P. Sullivan, P.K. Kilpatrick, The Effects of Inorganic Solid Particles on Water and Crude Oil Emulsion Stability, Ind. Eng. Chem. Res. 41 (2002) 3389–3404. https://doi.org/10.1021/ie010927n.
[218] H. Gong, Y. Li, M. Bao, D. Lv, Z. Wang, Petroleum hydrocarbon degrading bacteria associated with chitosan as effective particle-stabilizers for oil emulsification, RSC Adv. 5 (2015) 37640–37647. https://doi.org/10.1039/C5RA01360G.
[219] M. Omarova, L.T. Swientoniewski, I.K.M. Tsengam, A. Panchal, T. Yu, D.A. Blake, Y.M. Lvov, D. Zhang, V. John, Engineered Clays as Sustainable Oil Dispersants in the Presence of Model Hydrocarbon Degrading Bacteria: The Role of Bacterial Sequestration and Biofilm Formation, ACS Sustainable Chem. Eng. 6 (2018) 14143–14153. https://doi.org/10.1021/acssuschemeng.8b02744.

[220] I. Gulec, B. Leonard, D.A. Holdway, Oil and dispersed oil toxicity to amphipods and snails, Spill Science & Technology Bulletin. 4 (1997) 1–6. https://doi.org/10.1016/S1353-2561(97)00003-0.
[221] G. Goodbody-Gringley, D.L. Wetzel, D. Gillon, E. Pulster, A. Miller, K.B. Ritchie, Toxicity of Deepwater Horizon Source Oil and the Chemical Dispersant, Corexit® 9500, to Coral Larvae, PLoS One. 8 (2013). https://doi.org/10.1371/journal.pone.0045574.
[222] J. Koyama, A. Kakuno, Toxicity of heavy fuel oil, dispersant, and oil-dispersant mixtures to a marine fish, Pagrus major, Fisheries Sci. 70 (2004) 587–594. https://doi.org/10.1111/j.1444-2906.2004.00845.x.
[223] X.M. Dong, J.-F.O. Revol, D.G. Gray, Effect of microcrystallite preparation conditions on the formation of colloid crystals of cellulose, Cellulose. 5 (1998) 19–32.
[224] S. Beck-Candanedo, M. Roman, D.G. Gray, Effect of reaction conditions on the properties and behavior of wood cellulose nanocrystal suspensions, Biomacromolecules. 6 (2005) 1048–1054. https://doi.org/10.1021/bm049300p.
[225] B.L. Peng, N. Dhar, H.L. Liu, K.C. Tam, Chemistry and applications of nanocrystalline cellulose and its derivatives: A nanotechnology perspective, The Canadian Journal of Chemical Engineering. 89 (2011) 1191–1206. https://doi.org/10.1002/cjce.20554.
[226] L. Chen, Q. Wang, K. Hirth, C. Baez, U.P. Agarwal, J.Y. Zhu, Tailoring the yield and characteristics of wood cellulose nanocrystals (CNC) using concentrated acid hydrolysis, Cellulose. 22 (2015) 1753–1762. https://doi.org/10.1007/s10570-015-0615-1.
[227] S. Beck, M. Méthot, J. Bouchard, General procedure for determining cellulose nanocrystal sulfate half-ester content by conductometric titration, Cellulose. 22 (2015) 101–116. https://doi.org/10.1007/s10570-014-0513-y.
[228] B.P. Binks, C.P. Whitby, Nanoparticle silica-stabilised oil-in-water emulsions: improving emulsion stability, Colloids and Surfaces A: Physicochemical and Engineering Aspects. 253 (2005) 105–115. https://doi.org/10.1016/j.colsurfa.2004.10.116.
[229] M. Bobra, SOLUBILTY BEHAVIOUR OF PETROLEUM OILS IN WATER, Environmental Protection Directorate, Canada, 1992.
[230] R. Pichot, F. Spyropoulos, I.T. Norton, Mixed-emulsifier stabilised emulsions: Investigation of the effect of monoolein and hydrophilic silica particle mixtures on the stability against coalescence, Journal of Colloid and Interface Science. 329 (2009) 284–291. https://doi.org/10.1016/j.jcis.2008.09.083.
[231] D.E. Tambe, M.M. Sharma, Factors Controlling the Stability of Colloid-Stabilized Emulsions: I. An Experimental Investigation, Journal of Colloid and Interface Science. 157 (1993) 244–253. https://doi.org/10.1006/jcis.1993.1182.
[232] I. Diddens, B. Murphy, M. Krisch, M. Müller, Anisotropic Elastic Properties of Cellulose Measured Using Inelastic X-ray Scattering, Macromolecules. 41 (2008) 9755–9759. https://doi.org/10.1021/ma801796u.

[233] T.J. Robichaux, N.H. Myrick, Chemical Enhancement of the Biodegradation of Crude-Oil Pollutants, Journal of Petroleum Technology. 24 (1972) 16–20. https://doi.org/10.2118/3392-PA.
[234] A. Panchal, L.T. Swientoniewski, M. Omarova, T. Yu, D. Zhang, D.A. Blake, V. John, Y.M. Lvov, Bacterial proliferation on clay nanotube Pickering emulsions for oil spill bioremediation, Colloids and Surfaces B: Biointerfaces. 164 (2018) 27–33. https://doi.org/10.1016/j.colsurfb.2018.01.021.
[235] H. Im, H. Kwon, G. Cho, J. Kwon, S.Y. Choi, R.J. Mitchell, Viscosity has dichotomous effects on Bdellovibrio bacteriovorus HD100 predation, Environmental Microbiology. 21 (2019) 4675–4684. https://doi.org/10.1111/1462-2920.14799.
[236] Z. Cybulski, E. Dziurla, E. Kaczorek, A. Olszanowski, The Influence of Emulsifiers on Hydrocarbon Biodegradation by Pseudomonadacea and Bacillacea Strains, Spill Science & Technology Bulletin. 8 (2003) 503–507. https://doi.org/10.1016/S1353-2561(03)00068-9.
[237] T.J. Silhavy, D. Kahne, S. Walker, The Bacterial Cell Envelope, Cold Spring Harb Perspect Biol. 2 (2010). https://doi.org/10.1101/cshperspect.a000414.
[238] M. Kakran, M.N. Antipina, Emulsion-based techniques for encapsulation in biomedicine, food and personal care, Current Opinion in Pharmacology. 18 (2014) 47–55. https://doi.org/10.1016/j.coph.2014.09.003.
[239] A. Timgren, M. Rayner, M. Sjöö, P. Dejmek, Starch particles for food based Pickering emulsions, Procedia Food Science. 1 (2011) 95–103. https://doi.org/10.1016/j.profoo.2011.09.016.
[240] A. Arzhavitina, H. Steckel, Foams for pharmaceutical and cosmetic application, International Journal of Pharmaceutics. 394 (2010) 1–17. https://doi.org/10.1016/j.ijpharm.2010.04.028.
[241] F. Nielloud, G. Marti-Mestres, Pharmaceutical Emulsions and Suspensions: Second Edition, Revised and Expanded, CRC Press, 2000. https://doi.org/10.1201/b14005.
[242] S.H. Talebian, R. Masoudi, I.Mohd. Tan, P.L.J. Zitha, Foam assisted CO2-EOR: A review of concept, challenges, and future prospects, Journal of Petroleum Science and Engineering. 120 (2014) 202–215. https://doi.org/10.1016/j.petrol.2014.05.013.
[243] N.K. Maurya, A. Mandal, Investigation of synergistic effect of nanoparticle and surfactant in macro emulsion based EOR application in oil reservoirs, Chemical Engineering Research and Design. 132 (2018) 370–384. https://doi.org/10.1016/j.cherd.2018.01.049.
[244] E.Z. Ron, E. Rosenberg, Biosurfactants and oil bioremediation, Current Opinion in Biotechnology. 13 (2002) 249–252. https://doi.org/10.1016/S0958-1669(02)00316-6.
[245] T. Sharma, G.S. Kumar, B.H. Chon, J.S. Sangwai, Thermal stability of oil-in-water Pickering emulsion in the presence of nanoparticle, surfactant, and polymer, Journal of Industrial and Engineering Chemistry. 22 (2015) 324–334. https://doi.org/10.1016/j.jiec.2014.07.026.

[246] C. Wen, Q. Yuan, H. Liang, F. Vriesekoop, Preparation and stabilization of d-limonene Pickering emulsions by cellulose nanocrystals, Carbohydrate Polymers. 112 (2014) 695–700. https://doi.org/10.1016/j.carbpol.2014.06.051.
[247] A.S. Elhag, Y. Chen, P.P. Reddy, J.A. Noguera, A.M. Ou, G.J. Hirasaki, Q.P. Nguyen, S.L. Biswal, K.P. Johnston, Switchable Diamine Surfactants for CO2 Mobility Control in Enhanced Oil Recovery and Sequestration, Energy Procedia. 63 (2014) 7709–7716. https://doi.org/10.1016/j.egypro.2014.11.804.
[248] H. (Gene) Koide, Z. Xue, Carbon microbubbles sequestration: A novel technology for stable underground emplacement of greenhouse gases into wide variety of saline aquifers, fractured rocks and tight reservoirs, Energy Procedia. 1 (2009) 3655–3662. https://doi.org/10.1016/j.egypro.2009.02.162.
[249] X. Chen, S.S. Adkins, Q.P. Nguyen, A.W. Sanders, K.P. Johnston, Interfacial tension and the behavior of microemulsions and macroemulsions of water and carbon dioxide with a branched hydrocarbon nonionic surfactant, The Journal of Supercritical Fluids. 55 (2010) 712–723. https://doi.org/10.1016/j.supflu.2010.08.019.
[250] D. Espinosa, F. Caldelas, K. Johnston, S.L. Bryant, C. Huh, Nanoparticle-Stabilized Supercritical CO2 Foams for Potential Mobility Control Applications, (n.d.) 13.
[251] J. Yu, N. Liu, L. Li, R.L. Lee, Generation of Nanoparticle-Stabilized Supercritical CO2 Foams, in: Carbon Management Technology Conference, Carbon Management Technology Conference, Orlando, Florida, USA, 2012. https://doi.org/10.7122/150849-MS.
[252] Z. Xue, A. Worthen, A. Qajar, I. Robert, S.L. Bryant, C. Huh, M. Prodanović, K.P. Johnston, Viscosity and stability of ultra-high internal phase CO2-in-water foams stabilized with surfactants and nanoparticles with or without polyelectrolytes, Journal of Colloid and Interface Science. 461 (2016) 383–395. https://doi.org/10.1016/j.jcis.2015.08.031.
[253] S. Lam, K.P. Velikov, O.D. Velev, Pickering stabilization of foams and emulsions with particles of biological origin, Current Opinion in Colloid & Interface Science. 19 (2014) 490–500. https://doi.org/10.1016/j.cocis.2014.07.003.
[254] H. Liu, C. Wang, S. Zou, Z. Wei, Z. Tong, Simple, Reversible Emulsion System Switched by pH on the Basis of Chitosan without Any Hydrophobic Modification, Langmuir. 28 (2012) 11017–11024. https://doi.org/10.1021/la3021113.
[255] W.W. Mwangi, K.-W. Ho, B.-T. Tey, E.-S. Chan, Effects of environmental factors on the physical stability of pickering-emulsions stabilized by chitosan particles, Food Hydrocolloids. 60 (2016) 543–550. https://doi.org/10.1016/j.foodhyd.2016.04.023.
[256] M.J. Kamlet, J.L.M. Abboud, M.H. Abraham, R.W. Taft, Linear solvation energy relationships. 23. A comprehensive collection of the solvatochromic parameters, .pi.*, .alpha., and .beta., and some methods for simplifying the generalized solvatochromic equation, J. Org. Chem. 48 (1983) 2877–2887. https://doi.org/10.1021/jo00165a018.

[257] P.G. Jessop, D.A. Jessop, D. Fu, L. Phan, Solvatochromic parameters for solvents of interest in green chemistry, Green Chem. 14 (2012) 1245. https://doi.org/10.1039/c2gc16670d.
[258] G.M. Schneider, High-pressure investigations of fluid mixtures — review and recent results, The Journal of Supercritical Fluids. 13 (1998) 5–14. https://doi.org/10.1016/S0896-8446(98)00028-X.
[259] C.L. Tucker III, P. Moldenaers, Microstructural Evolution in Polymer Blends, Annual Review of Fluid Mechanics. 34 (2002) 177–210. https://doi.org/10.1146/annurev.fluid.34.082301.144051.
[260] J.C. Berg, Introduction To Interfaces And Colloids, An: The Bridge To Nanoscience, WSPC, Singapore ; Hackensack, NJ, 2009.
[261] I. Kim, A.J. Worthen, K.P. Johnston, D.A. DiCarlo, C. Huh, Size-dependent properties of silica nanoparticles for Pickering stabilization of emulsions and foams, J Nanopart Res. 18 (2016) 82. https://doi.org/10.1007/s11051-016-3395-0.
[262] B.P. Binks, A. Desforges, D.G. Duff, Synergistic Stabilization of Emulsions by a Mixture of Surface-Active Nanoparticles and Surfactant, Langmuir. 23 (2007) 1098–1106. https://doi.org/10.1021/la062510y.
[263] R. Chanamai, G. Horn, D.J. McClements, Influence of Oil Polarity on Droplet Growth in Oil-in-Water Emulsions Stabilized by a Weakly Adsorbing Biopolymer or a Nonionic Surfactant, Journal of Colloid and Interface Science. 247 (2002) 167–176. https://doi.org/10.1006/jcis.2001.8110.
[264] B.P. Binks, Particles as surfactants—similarities and differences, Current Opinion in Colloid & Interface Science. 7 (2002) 21–41. https://doi.org/10.1016/S1359-0294(02)00008-0.
[265] Y. Maphosa, V.A. Jideani, Factors Affecting the Stability of Emulsions Stabilised by Biopolymers, in: S. Karakuş (Ed.), Science and Technology Behind Nanoemulsions, InTech, 2018. https://doi.org/10.5772/intechopen.75308.
[266] Z. Duan, R. Sun, An improved model calculating CO2 solubility in pure water and aqueous NaCl solutions from 273 to 533 K and from 0 to 2000 bar, Chemical Geology. 193 (2003) 257–271. https://doi.org/10.1016/S0009-2541(02)00263-2.
[267] A.J. Worthen, H.G. Bagaria, Y. Chen, S.L. Bryant, C. Huh, K.P. Johnston, Nanoparticle-stabilized carbon dioxide-in-water foams with fine texture, Journal of Colloid and Interface Science. 391 (2013) 142–151. https://doi.org/10.1016/j.jcis.2012.09.043.
[268] J.-L. Salager, M. Briceno, C.L. Bracho, Heavy Hydrocarbon Emulsions Making Use of the State of the Art in Formulation Engineering | Encyclopedic Handbook of Emulsion Technology | Taylor & Francis Group, in: Encyclopedic Handbook of Emulsion Technology, 2001: pp. 455–496. https://www.taylorfrancis.com/books/e/9781420029581/chapters/10.1201%2F9781420029581-20 (accessed July 5, 2018).

[269] L. Jiang, M. Rekkas, A. Wong, Comparing the Means of Two Log-Normal Distributions: A Likelihood Approach, (n.d.) 16.

LIST OF APPENDICES

APPENDIX A

Chemical Structures of the emulsifiers used

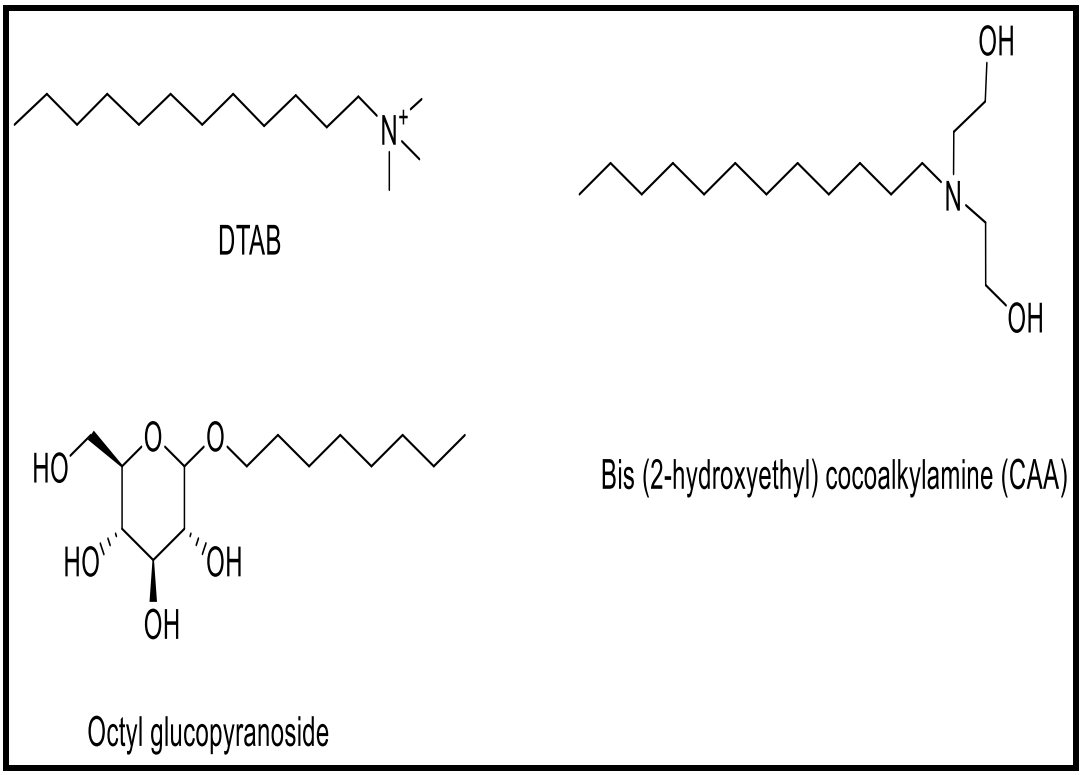

Figure S1.1: Chemical structure of emulsifiers.

Sulfur Content Measurements

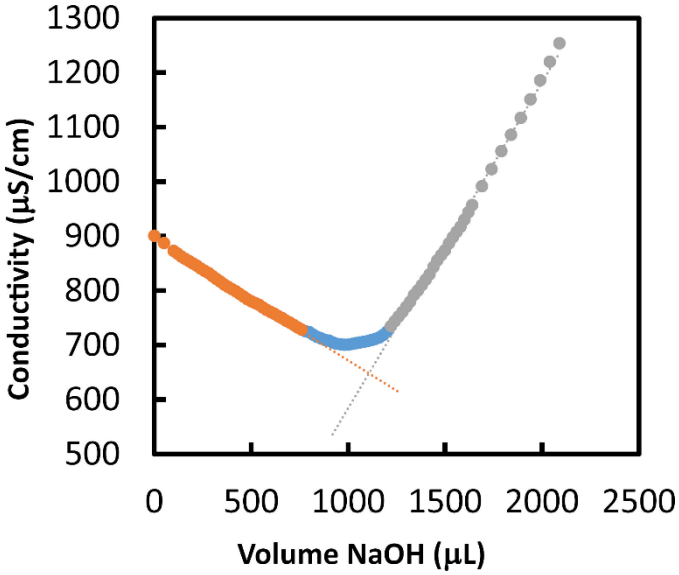

Figure S1.2: Conductometric titration of 2wt% CNC sample with 0.01 M NaOH.

The Sulphur content on the surface of CNCs was estimated using the equation (1) below. The pH of 2wt.% CNC suspension was adjusted to 2.4 and titrated against 0.01M NaOH.

$$\%S = \left(\frac{V_{NaOH} C_{NaOH} MW_{sulphur}}{m_{susp} C_{susp}}\right) \times 100 \qquad (1)$$

The result indicated that 0.045±0.018 g-Sulphur/g- cellulose was present on the surface of the CNC used in this study (Figure S3). Abitbol et al found the average sulfur content of cotton derived cellulose nanocrystals having a length of 131 nm to be approximately 0.058 g-S/g-cellulose.

Identification of Dispersed and Continuous Phases

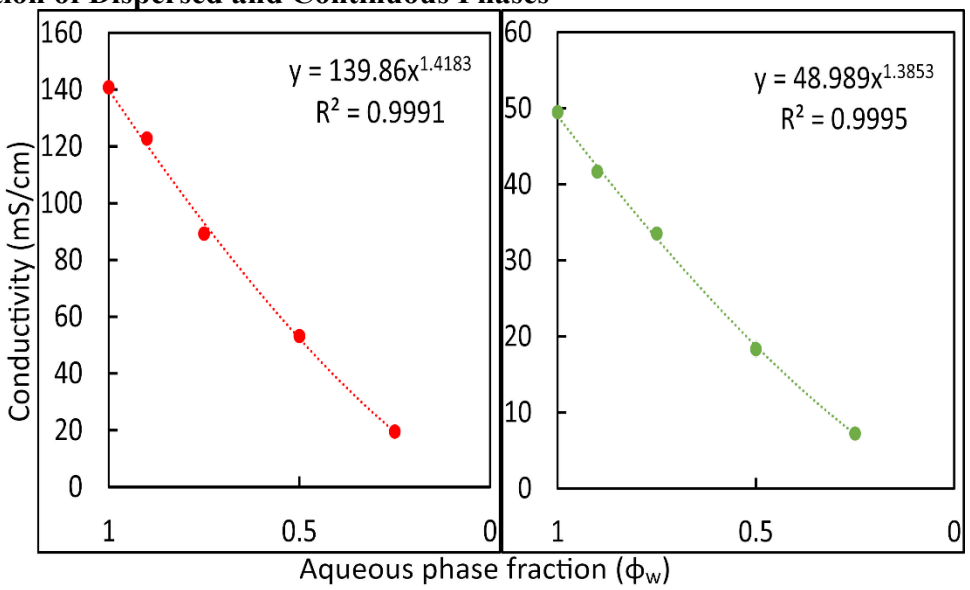

Figure S1.3: Conductivity measurement vs volume fraction of the aqueous phase of emulsions. The graph on the left represents CNC emulsions in API brine while the one on the right represents CNC emulsions in SSW. In both cases, no emulsifiers were used for preparing emulsions.

The types of emulsions formed were identified using conductivity experiments. The measured conductivity was fit to a power-law equation for O/W emulsions

$$K_{em} = K_{aq}\phi_{aq}^{m}$$

Where K_{em} is the conductivity of emulsion, K_{aq} is the conductivity of pure aqueous phase, ϕ_{aq} is the volume fraction of aqueous phase and m is a constant that ranges between 1 and 1.5 for all O/W emulsions. In emulsions prepared in API brine and SSW, the fitted value for K_{aq} was 139.86 and 49.99 respectively. The value-form was calculated at 1.4183 for API brine and 1.3853 for SSW.

Raman Spectra of OGP and DTAB in brines with and without CNC

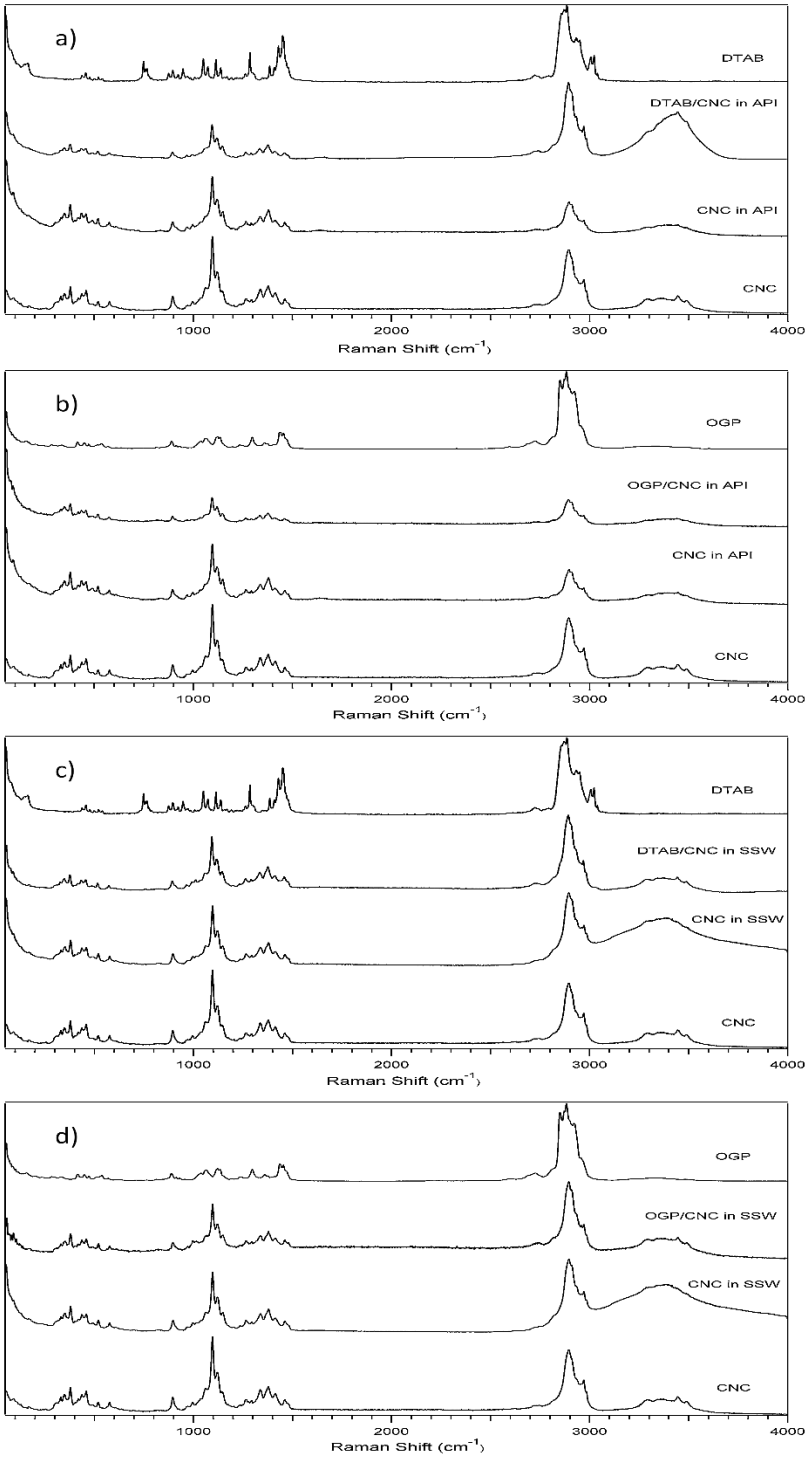

Figure S1.4: Full Raman spectra of a) DTAB in API w and w/o CNC, b) OGP in API w and w/o CNC, c) DTAB in SSW w and w/o CNC and d) OGP in SSW w and w/o CNC.

Raman Spectra of CNC and CAA at different pH

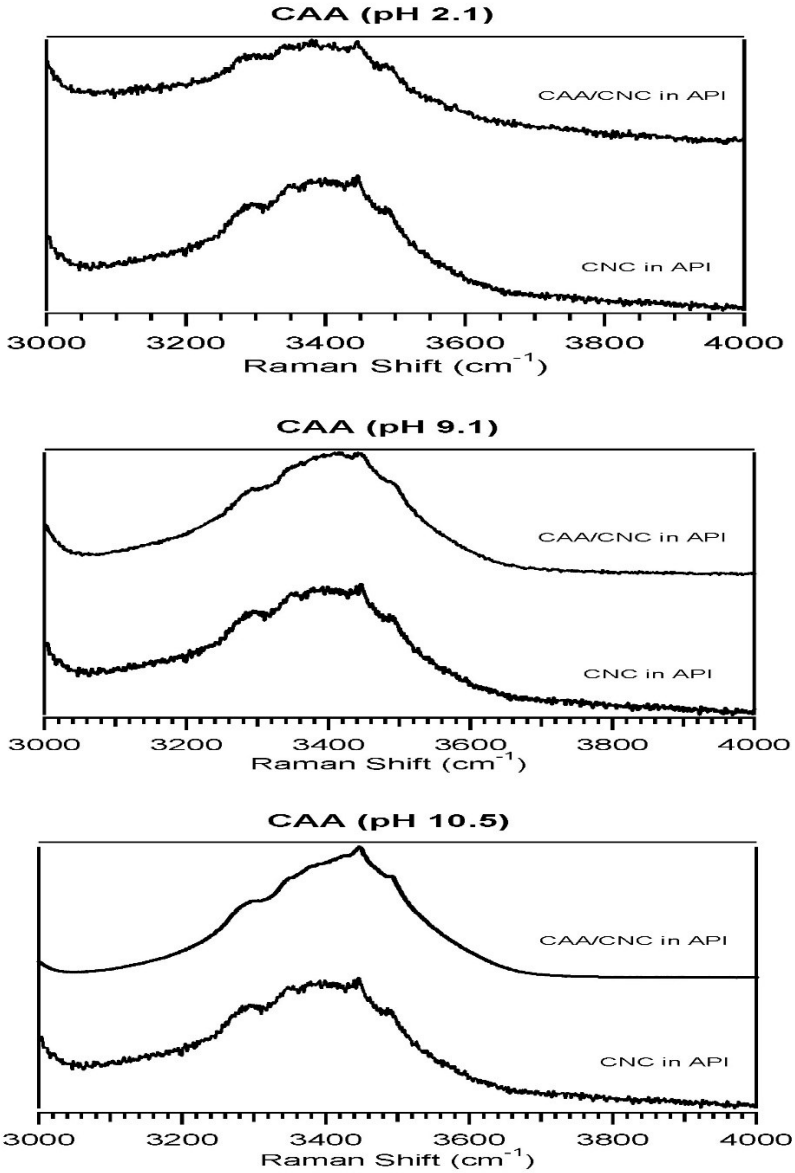

Figure S1.5: Raman Spectra of OH stretching region of CAA+CNC in API Brine at different pH

Figure S1.5 depicts the Raman spectra of CAA+CNC in API brine at different pH. The isoelectric point of CAA in DI water is at pH 9.2. The spectra in the above figure thus represent CAA with a positively charged head group (pH 2.1), uncharged head group (9.1) and negatively charged head group (10.5). Differences in peak structure within the OH stretching region indicates a prevalence of ionic interactions.

Zeta Potential

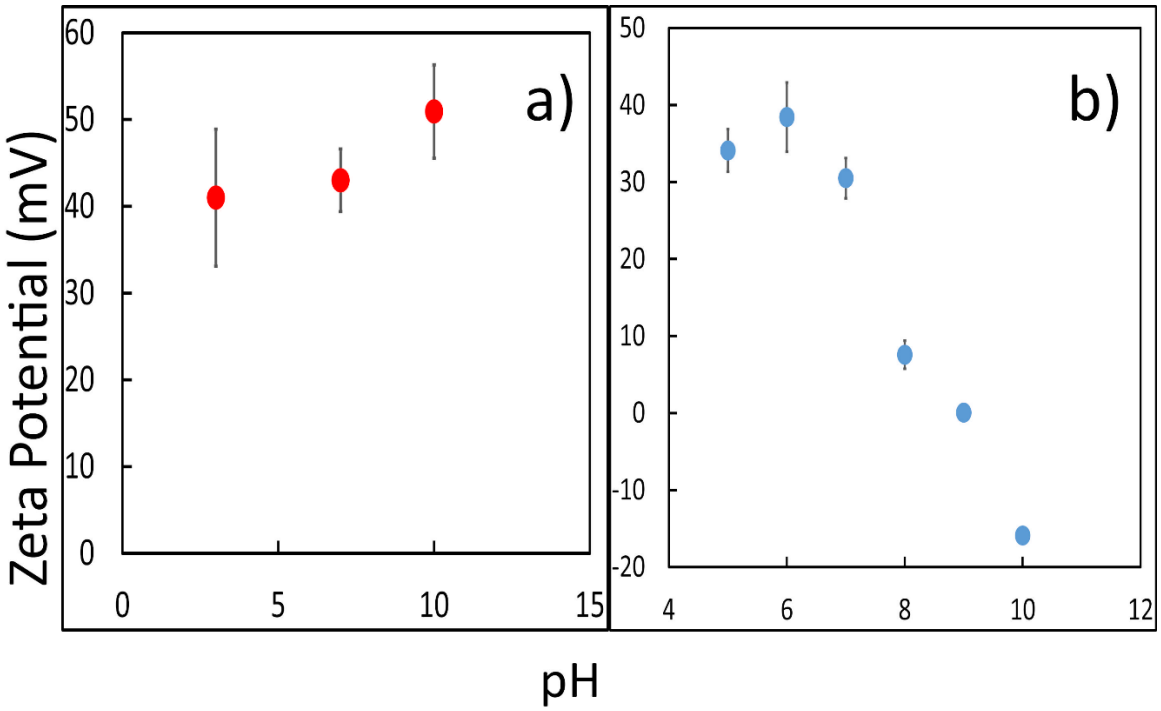

Figure S1.6: pH vs zeta potential curve for DTAB (red circles) and CAA (blue circles)

Zeta potential (ZP) of DTAB and CAA was measured using Malvern Zetasizer Nano S. Concentrated solutions of surfactant (at least higher than its CMC) were prepared in 10mM NaCl solution, the solution was then passed through 0.4 μm syringe filter. The filtered solution was then used to thoroughly rinse the zeta cell before measurements. The CMC of OGP is excessively large and the zeta potential could not be measured; however, it is well known to be a neutral surfactant.

Figure S1.6 shows the effect of pH on the net charge on the head of surfactants studied. In the pH range between 3 and 10, DTAB remained positively charged with zeta potential ranging between +40mV and +50mV. CAA, on the other hand, which has an amine group that can be protonated relatively was a negative charge (ZP= -20mV) at pH 10 and positively charged at lower pHs. The isoelectric point for CAA was measured at pH 9.

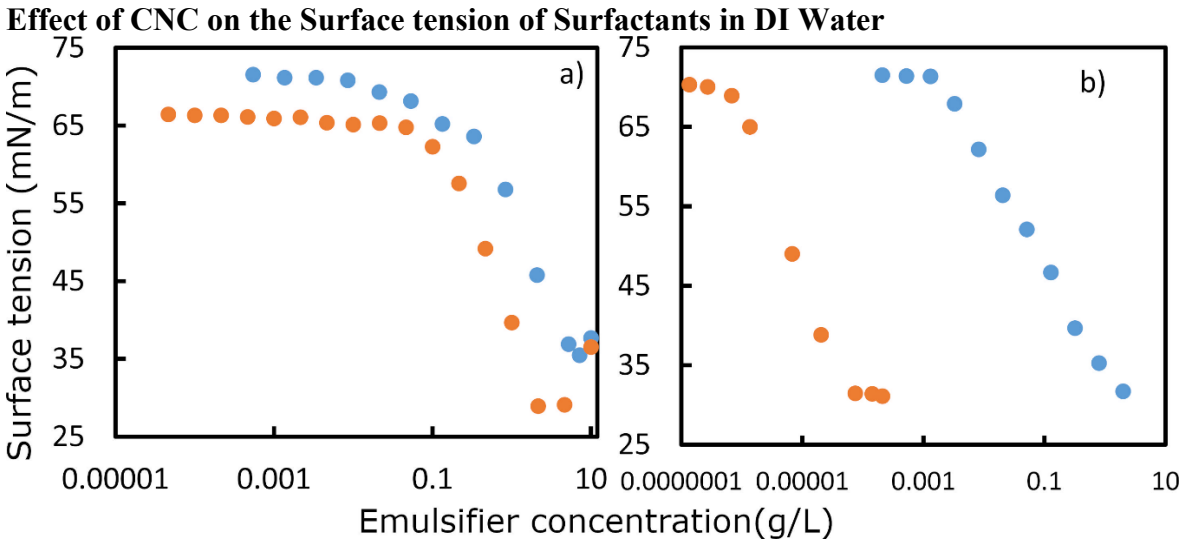

Figure S1.7: Air/DI water surface tensions (γ_{AW}) at various aqueous-phase concentrations of a) DTAB and b) CAA. The aqueous phase was either equilibrated with (blue circle ●) and without (orange circle ●) 0.5% w/w cellulose nanocrystals

Figure S1.7 indicates that in DI water DTAB and CAA interact with CNC in DI water while no change in surface tension was observed when Guar was added to the DI water solution. This indicates that in DI water the electrostatic interaction between negatively charged CNC and positively charged surfactants is the driving force for adsorption of surfactants onto the surface of CNC.

Derivation of adsorption energy for cylindrical nanoparticles

Derivation 1.1: ΔE calculated for CNCs in the presence of surfactants based on Pawel Pieranski's approach; assuming that CNCs are hydrophilic cylindrical particles (radius r and length L), lying flat on the oil-water interface.

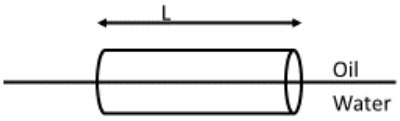

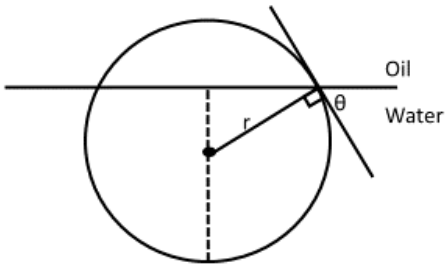

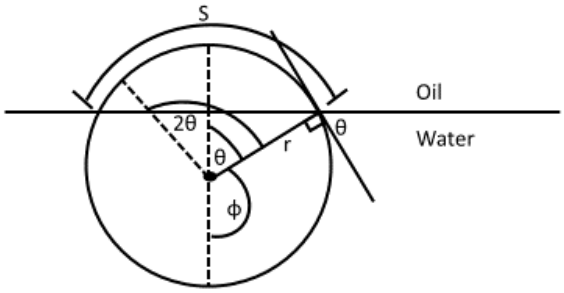

Solid-Oil

$S = arc\ length = 2\theta r = 2(\pi - \varphi)r$

Solid-Water

$arc\ length = 2\varphi r$

$\theta = \pi - \varphi$

Solid-oil interfacial area

$Lateral = 2\theta rL = 2(\pi - \varphi)rL$

$Ends = 2\{\theta r^2 - \frac{r^2}{2}\sin(2\theta)\}$

Solid-water interfacial area

$Lateral = 2\varphi rL$

$Ends = 2\{\varphi r^2 - \frac{r^2}{2}\sin(2\theta)\}$

Oil water area lost due to particle

$A_{OW,lost} = 2rsin\theta L = 2rsin\varphi L$

Assume that V represents top phase, L represents bottom phase and S represents solid phase, then interfacial energy related to particle flat (parallel to the interface) is given by:

$$E_{parallel} = \gamma_{VS}2(\pi - \varphi)rL + \gamma_{LS}2\varphi rL - \gamma_{VL}2r\sin(\varphi)\,L + \gamma_{VS}[2\{\theta r^2 - \frac{r^2}{2}\sin(2\theta)\}] + \gamma_{LS}\{2\{\varphi r^2 - \frac{r^2}{2}\sin(2\theta)\}\}$$

Interfacial energy related to particle completely submerged is given by:

$E_{sub} = \gamma_{LS}(2\pi rL + 2\pi r^2)$

$$\Delta E = \gamma_{VS} 2\theta r L + 2\gamma_{VS}\left\{\theta r^2 - \frac{r^2}{2}\sin(2\theta)\right\} + \gamma_{LS}\left[2\varphi r L - 2\pi r L - 2\pi r^2 + 2\left\{\theta r^2 - \frac{r^2}{2}\sin(2\theta)\right\}\right] - \gamma_{VL} 2r \sin\varphi\, L$$

$$= 2\theta r L\gamma_{VS} + 2\theta r^2\gamma_{VS} - r^2 \sin(2\theta)\gamma_{VS} + 2\varphi r L\gamma_{LS} - 2\pi r L\gamma_{LS} - 2\pi r^2\gamma_{LS} + 2\theta r^2\gamma_{LS} - r^2\sin(2\theta)\gamma_{LS} - \gamma_{VL} 2r \sin\varphi\, L$$

Replace $\theta = \pi - \varphi$

$$= 2\theta r L(\gamma_{VS} - \gamma_{LS}) + 2\theta r^2(\gamma_{VS} - \gamma_{LS}) - r^2 \sin 2\theta(\gamma_{VS} - \gamma_{LS}) - \gamma_{VL} 2r \sin\varphi\, L$$

Replace $\cos\theta = \frac{(\gamma_{VS} - \gamma_{LS})}{\gamma_{LV}}$ and $\sin\varphi = \sin(\pi - \theta) = \sin\theta$

$$= 2\theta r L(\gamma_{VS} - \gamma_{LS}) + 2\theta r^2(\gamma_{VS} - \gamma_{LS}) - r^2 \sin 2\theta(\gamma_{VS} - \gamma_{LS}) - \gamma_{VL} 2r \sin\theta\, L$$

$$= 2rL[\theta(\gamma_{VS} - \gamma_{LS}) - \gamma_{LV} \sin\theta] + r^2[(2\theta - \sin 2\theta)\,(\gamma_{VS} - \gamma_{LS})]$$

$$= 2rL[\gamma_{LV}\theta\cos\theta - \gamma_{LV}\sin\theta] + r^2[(2\theta - \sin 2\theta)\gamma_{LV}\cos\theta]$$

$$= 2rL\gamma_{LV}[\theta\cos\theta - \sin\theta] + r^2\gamma_{LV}\cos\theta\,(2\theta - \sin 2\theta)$$

$$\Delta E = 2rL\gamma_{LV}\cos\theta\,[\theta - \tan\theta + \frac{r}{2L}(2\theta - \sin 2\theta)]$$

Emulsion Stability in DI water and Brine

Figure S1.8: Representative emulsions prepared using dodecane in DI water and Brine. a) and b) are emulsions in DI water immediately before mixing and after 1 min respectively and c) and d) are emulsions in API brine immediately before mixing and after 1 min respectively

Emulsion with different volume ratios prepared using CNC only

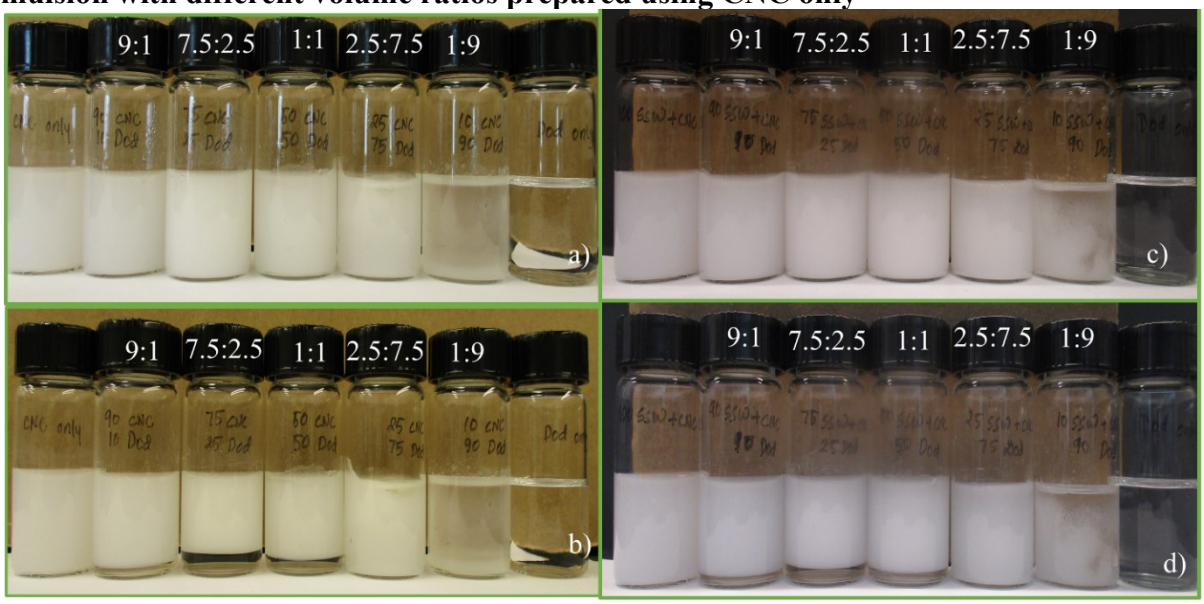

Figure S1.9: Representative samples of the emulsion prepared using CNC particles in API (left panel) and SSW (right panel) as the aqueous phase and dodecane as the organic phase. a) and c) are images were taken immediately after emulsification in API and SSW respectively and b) and d) are pictures of emulsion taken after 24 hours standing on the benchtop at room temperature. Numbers on the top of the vials indicate the ratio of aqueous phase to dodecane in the emulsion.

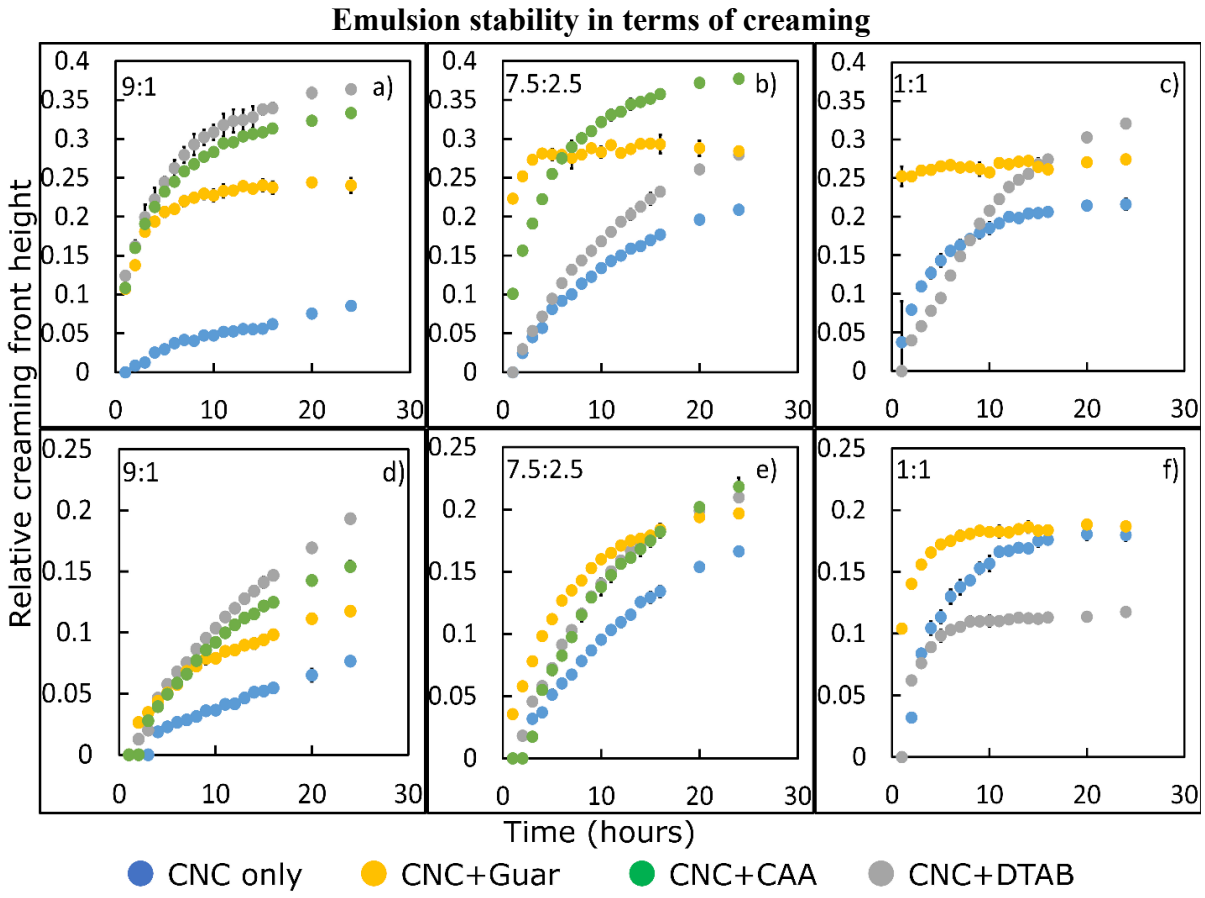

Figure S1.10: Creaming front of emulsions prepared in API Brine a), b) and c) and in SSW d), e) and f). The numbers on the top left corner of each graph indicate the volume ratio of the aqueous phase to the oil phase in a sample. Errors indicate standard deviation.

Among the emulsions prepared in API brine, the least stable to creaming was the one that had CNC and CAA with 25% v/v aqueous phase. Approximately 38% of the water eluted from the sample indicating that only 62% of the aqueous phase was retained in the emulsion. Similarly, among emulsions prepared in SSW, the emulsion most susceptible to creaming was also the one containing CNC and CAA with 25% v/v aqueous phase. However, in the latter case, only 22% of water eluted from the sample, retaining 78% of the aqueous phase in the emulsion after 24 hours.

Polymeric emulsifiers, like guar gum, have a different stabilization mechanism than small-molecule surfactants; they increase the viscosity of the aqueous continuous phase and can

provide steric repulsion between the oil droplets. However, adding guar to the CNC did not improve emulsion stability. Similar to CAA, the contact angle of guar solutions in brine was very low, indicating a high wettability on the CNC surface and thus preferential desorption from the dodecane/brine interface.

APPENDIX B

Sulfur content on CNC surface

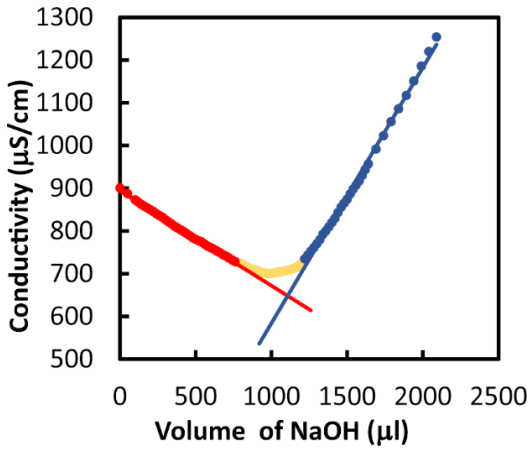

Figure S2.1: Conductometric titration of 2wt % CNC with 0.01M NaOH

The surface of CNC produced by sulfuric acid hydrolysis is covered with sulfonate -HSO_3 groups. The amount of sulfur on the surface of CNCs was estimated by titrating 2 wt% CNC with 0.01M NaOH and monitoring the conductivity. The endpoint of the titration is given by the point of intersection between 2 arms of the curve. The sulfur content can then be calculated using equation 1.[185] The pH of 2wt.% CNC suspension was adjusted to 2.4 and titrated against 0.01M NaOH.

$$\%S = \left(\frac{V_{NaOH}C_{NaOH}MW_{sulphur}}{m_{susp}C_{susp}}\right) \times 100 \qquad (1)$$

In equation (1) V_{NaOH} is the volume of base required to neutralize the -HSO_3, C_{NaOH} is the concentration of base used for titration, m_{susp}, and C_{susp} are mass and concentration of CNCsuspension used for titration respectively. The result indicated that 0.045±0.018 g-Sulphur/g- cellulose was present on the surface of the CNC used in this study (Figure S1).

Identification of emulsion type

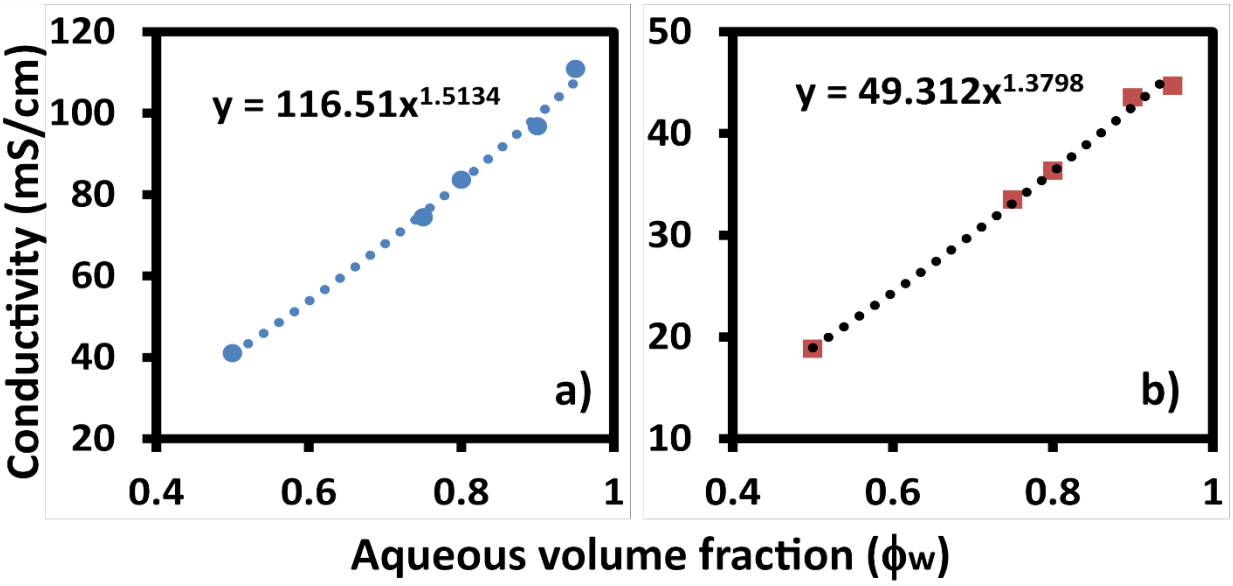

Figure S2.2: Conductivity of emulsions stabilized by 0.8wt % CNC plotted as the function of volume fraction of a) API brine and b) SSW.

The types of emulsions formed were identified using conductivity experiments. The measured conductivity was fit to a power-law equation for O/W emulsions

$$K_{em} = K_{aq}\phi_w^m \qquad (2)$$

Where K_{em} is the conductivity of emulsion, K_{aq} is the conductivity of pure aqueous phase, ϕ_w is the volume fraction of aqueous phase and m is a constant that ranges between 1 and 1.5 for all O/W emulsions.[268] In emulsions prepared in API brine and SSW, the fitted value for K_{aq} was 116.51 and 49.31 respectively. The value for m was calculated at 1.51 for API brine and 1.38 for SSW.

Sauter mean diameter (D[3,2]) and hypothesis test of emulsions prepared

Table S2.1: Sauter mean diameter of crude oil emulsion droplets under various physicochemical parameters

	0 hr		24 hr		
Samples	**D[3,2]**	**Standard deviation**	**D[3,2]**	**Standard deviation**	**Hypothesis test**
0.4% API CNC	36.0	12.5	32.5	11.2	Do not reject null hypothesis
0.8% API CNC	34.5	12.3	32.6	11.5	Reject null hypothesis
1% API CNC	29.4	10.4	33.1	11.4	Reject null hypothesis
0.8% CNC SSW CNC	32.8	11.0	33.2	11.2	Do not reject null hypothesis
0.8% CNC 1.9M NaCl	38.1	13.8	30.2	9.7	Do not reject null hypothesis
0.8% CNC 0.65 M NaCl	39.0	12.6	37.9	12.9	Do not reject null hypothesis
0.8% CNC 0.32M NaCl + CNC	36.3	13.3	35.2	12.8	Do not reject null hypothesis
0.8% CNC 0.95M NaCl+CNC	30.6	11.1	30.1	10.9	Do not reject null hypothesis

Table S2.1 provides a summary of D[3,2] values of emulsion droplets immediately after emulsification and after 24 hours under different physicochemical conditions. D[3,2] values were compared to examine the coalescence of droplets. In addition, statistical analysis was performed to verify changes in the means at 95% confidence The emulsion droplets were log-normally distributed, z statistics test was carried out for droplets population of 'n' and 'm' had the population mean of $\hat{\mu}_1$ and $\hat{\mu}_2$ at t=0 and t=24 hours respectively after emulsification. In order to verify the changes, the null hypothesis (H0) and alternate hypothesis (Ha) were defined as

$$H0: \hat{\mu}_1 = \hat{\mu}_2 \quad \text{vs} \quad Ha: \hat{\mu}_1 \neq \hat{\mu}_2$$

For log-normal distribution, the population mean ($\hat{\mu}_i$) was calculated using the equation (3).[269]

$$\hat{\mu}_1 = \frac{\sum \log x_1}{n} \text{ and } \hat{\mu}_2 = \frac{\sum \log x_2}{m} \qquad (3)$$

The z value for the log-normal distribution was calculated using equation 4.

$$z = \frac{\hat{\mu}_1 - \hat{\mu}_2 + \left(\frac{s_1^2 + s_2^2}{2}\right) - \psi_0}{\sqrt{\frac{s_1^2}{n} + \frac{s_2^2}{m} + \frac{1}{2}\left(\frac{s_1^4}{n-1} + \frac{s_2^4}{m-1}\right)}} \qquad (4)$$

where s_1^2 and s_2^2 are estimators of population standard deviation and ψ_0 is the difference between the $\hat{\mu}_1$ and $\hat{\mu}_2$ in the null hypothesis and is equal to zero in this case. In equation 4, the terms s_1^2 and s_2^2 are calculated using sets of equation 5.

$$s_1^2 = \frac{\sum(\log x_1 - \hat{\mu}_1)^2}{n-1} \quad \text{and} \quad s_2^2 = \frac{\sum(\log x_2 - \hat{\mu}_2)^2}{m-1} \qquad (5)$$

APPENDIX C

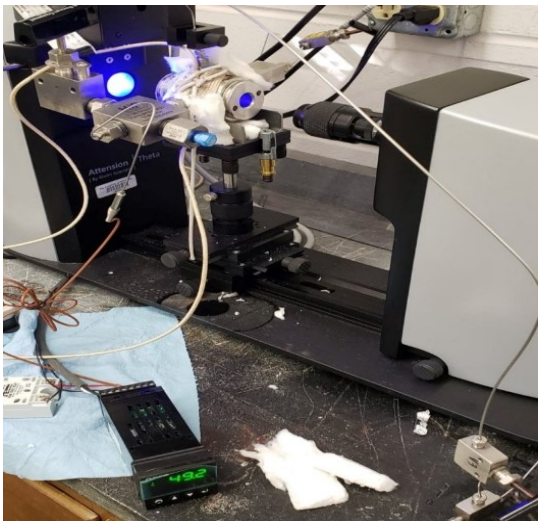

Figure S3.1: Cross-section of view cell attached to an apparatus for measuring g_{ow} at high temperature and pressure

The interfacial tension between oil phase/CO_2 and brine was measured at elevated temperatures and pressures using an apparatus fabricated in-house with a high-pressure view cell with a sapphire window attached to it to take images of the droplets for axisymmetric droplet analysis.

Properties of heptane emulsion droplets at 25°C

Table S3.1: Properties of heptane emulsion droplets prepared at 25°C

Sample	ϕ_w		Average (μm)	D[3,2] (μm)	D[4,3] (μm)	Std. dev (μm)
DTAB only	0.25	d0	12.6	30.0	41.8	9.3
		d1	--	--	--	--
	0.2	d0	12.7	23.8	32.7	7.5
		d1	--	--	--	--
	0.1	d0	9.8	33.6	53.5	9.2
		d1	--	--	--	--
CNC only	0.25	d0	24.6	79.3	108.9	19.7
		d1	26.9	13.7	80.9	25.0
	0.2	d0	21.4	59.4	80.1	19.5
		d1	21.8	45.8	56.0	16.5
	0.1	d0	17.5	56.8	73.4	17.8
		d1	31.7	82.4	102.6	29.1
CNC+DTAB	0.25	d0	14.5	27.0	34.5	9.1
		d1	20.9	58.0	81.0	17.9
	0.2	d0	14.9	32.4	40.9	11.0
		d1	17.1	99.0	136.1	22.5
	0.1	d0	16.0	22.7	25.5	7.5
		d1	17.5	42.0	68.3	12.4

Viscosities of CNC dispersions in API brine

The viscosities of CNC dispersions in API brine were measured in the presence and absence of cationic surfactant DTAB as the function of shear rate at ambient temperature and pressure using a rotational viscometer. The results indicate that the emulsification of heptane by CNC and/or CNC+DTAB increases the viscosity. Furthermore, emulsification appears to flip the viscosities with viscosities of CNC stabilized emulsions appearing to be higher than CNC+DTAB stabilized emulsion. The viscosity of aqueous phase CNC+DTAB appears to be slightly higher for all shear rate measured but the measured difference is not significant enough to draw clear conclusions. The results suggest that heptane-brine interfaces stabilized CNC only has a higher contribution to viscosity than interface stabilized by CNC+DTAB.

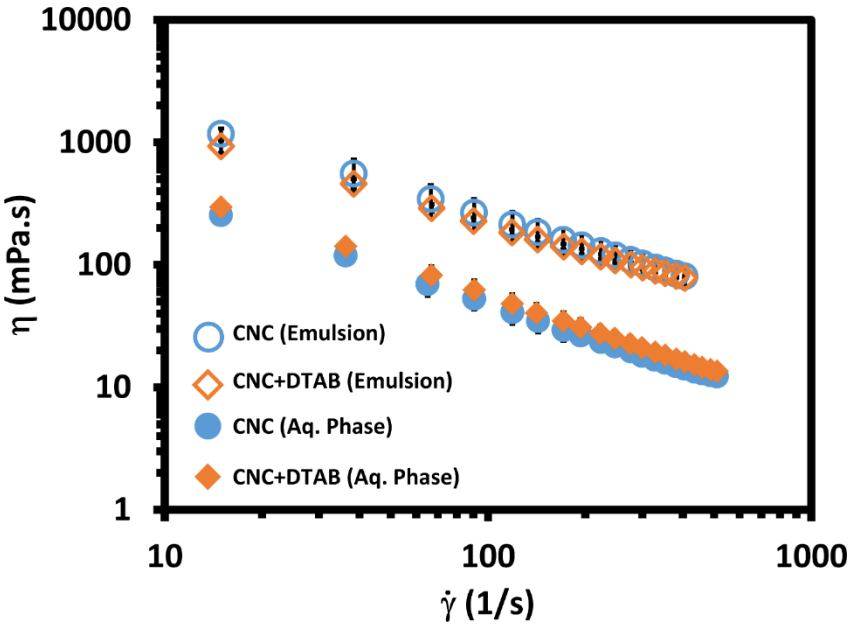

Figure S3.2: Viscosities of CNC dispersions in API brine with DTAB and without DTAB

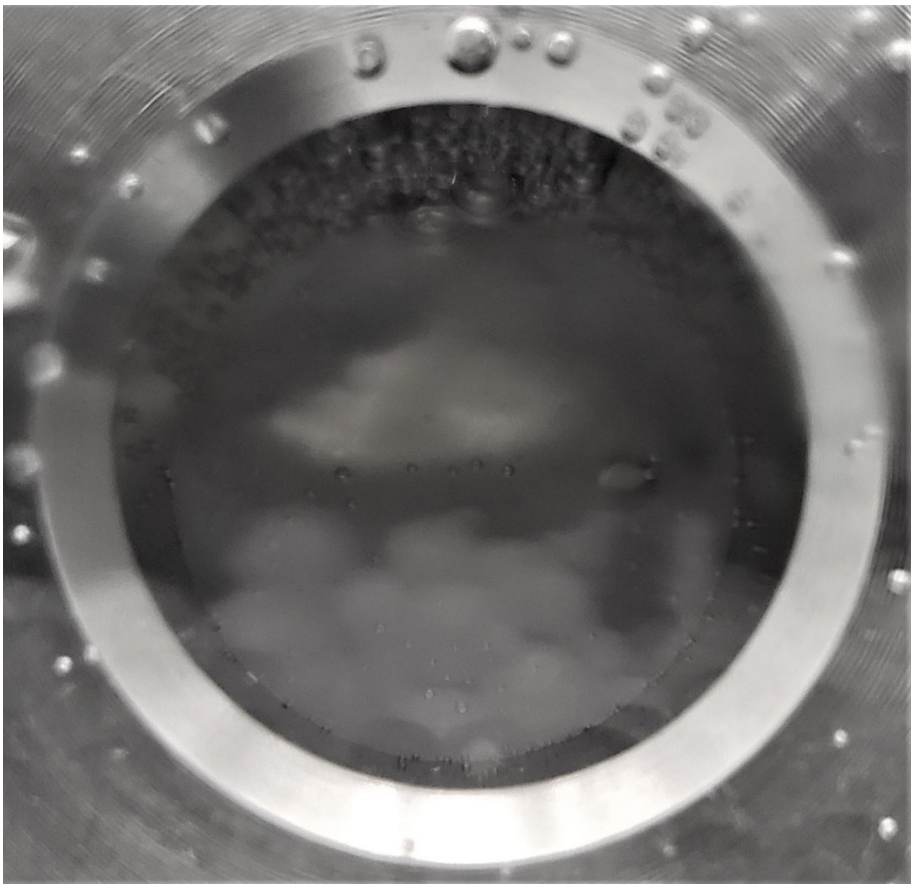

Figure S3.4: Phase-separated CO_2 and CNC suspension at 25ºC immediately after passing through the beadpack.

CNC dispersions were not able to stabilize scCO2 emulsions and foams at CO2 volume fractions higher than 0.75. Figure S3 is a representative picture of CO2 (ϕ_c =0.8) emulsion stabilized using CNC alone. Figure S3 shows that at ϕ_c higher than 0.75, CNC suspension was not able to stabilize CO2 emulsions. This could be because as the volume fraction of the discrete phase increases the amount of CNC available

VITAE

PROFESSIONAL SUMMARY

- Research Scientist with 3+ years' experience in colloidal and surface studies, excellent writing and verbal communication skills with great attention to detail resulting in 6+ manuscripts in scientific journals and delivering presentations at 5+ scientific conferences.
- Collaborative team member with leadership skills demonstrated by successfully driving and completing 3 projects with multidisciplinary research teams within allocated time and budget and mentoring a team of 2 graduate and 5 undergraduate students.

EDUCATION

University of Mississippi, USA May 2020

Ph.D. in Engineering Science, Chemical Engineering

Dissertation: Application of nanocellulosic materials for stabilization of liquid-liquid and gas-liquid interfaces in brine.

University of Warwick, UK July 2010

MS. Biotechnology, Bioprocessing, and Business Management

Thesis: A Feasibility study on using bacterial consortium for degradation of polyaromatic hydrocarbons in municipal wastes.

Kathmandu University, Nepal

BS. in Biotechnology July 2008

Thesis: The effect of Himalayan herbs on the growth of lactic acid bacteria for improving the shelf-life of dairy products.

EMPLOYMENT HISTORY

Graduate Research Assistant Aug 2015-Present

University of Mississippi, MS

- Successfully analyzed technical scientific concepts, designed standard test protocols, performed data analysis and lead studies involving novel formulation of materials using nanocellulosic material and polymers to study their surface and rheological properties resulting in 5+ manuscript for scientific journals and 5+ presentations at scientific conferences.
- Demonstrated ability to collaborate with multidisciplinary team members and project management skills by training and mentoring a team of 3 undergraduate and 3 graduate students from 3 different research labs to complete 2 separate research and graduation of students with Master's and Honors' degree.
- Self-driven with the ability to work independently and creative problem solver, demonstrated by successful initiation, securing of $1000 in external funding, and completion of a mini-project designed specifically to support findings and solve problems experienced by the team members.

Research Associate Sept 2014- July 2015

Kathmandu University, Nepal

- Designed experimental protocols, conducted experiments and data analysis and completed scientific report writing to study and optimize the process for bioethanol production industrial waste resulting in 2 presentations at scientific conferences.
- Demonstrated organizational and leadership skills by successfully co-chairing an organization and planning committee for the "Biofuel" conference in 2015.
- Demonstrated project management skills, drive and multidisciplinary collaboration skills by partnering with an external engineering firm resulting in completed pilot testing and secured additional funding of $3000 to further the project.

Project Coordinator Feb 2013- July 2014

Research Institute for Biosciences and Biotechnology, Nepal

- Used technical skills to facilitate the design and scaleup of waste management system in 2 cheese manufacturing companies of Nepal saving each company $3000+ in waste management cost and meeting waste disposal regulatory standards.
- Mobilized human and financial resources to complete the 6-month project designed to train dairy farmers in rural Nepal regarding modern farming technology and potential marketing and sales opportunities of dairy byproducts.
- Demonstrated organization and effective communication skills to align customer needs with the needs of project members resulting in successfully organizing 2 conferences and 2 customer training camps for dairy farmers.

AWARDS AND ACHIEVEMENTS

- 1st Runner Up, Graduate School 7th Annual Research Symposium, 2016
- University of Mississippi Graduate School Travel Grant, 2017
- Winner, Graduate Student Council (GSC) Research Grants, 2017. University of Mississippi, 2017
- Winner, Travel Grant Office of Research and Sponsored Program, University of Mississippi, 2018

PROFESSIONAL AFFILIATIONS/LICENCES

- Member: American Institute of Chemical Engineers (AIChE): 2016-Present
- Member: American Chemical Society (ACS): 2018-Present
- Associate member: Sigma Xi, The Scientific Research Society: 2017-Present
- Six Sigma Green Belt: LinkedIn: 2019-Present

PUBLICATIONS

1. Parajuli, S.; Dorris, A. L.; Middleton, C.; Rodriguez, A.; Haver, M. O.; Hammer, N. I.; Ureña-Benavides, E. Surface and Interfacial Interactions in Dodecane/Brine Pickering Emulsions Stabilized by the Combination of Cellulose Nanocrystals and Emulsifiers. *Langmuir* **2019**, *35* (37), 12061–12070. https://doi.org/10.1021/acs.langmuir.9b01218.

2. Parajuli, S.; Alazzam, O.; Wang, M.; Mota, L. C.; Adhikari, S.; Wicks, D.; Ureña-Benavides, E. E. Surface Properties of Cellulose Nanocrystal Stabilized Crude Oil Emulsions and Their Effect on Petroleum Biodegradation. *Colloids and Surfaces A: Physicochemical and Engineering Aspects* **2020**, 124705. https://doi.org/10.1016/j.colsurfa.2020.124705.

3. Parajuli, S. & Ureña-Benavides, E. Nanocellulose at interfaces: Fundamental Aspects of Nanocellulose Stabilized Pickering Emulsions and Foams*: Submitted*

4. Dao, MH; Pillai, AR; Thakkar, R; Parajuli, S; Ureña-Benavides, E; Jo, S. Near-Infrared Light-Induced Reversible Self-Assembly Polymeric Micelles based on Methylene Blue Conjugated Polyethylene Glycol: *Submitted*

5. Sharma, PK; Panda, A; Parajuli, S; Kundu, S; Repka, MA; Ureña-Benavides, E; Narasimha Murthy, S. Effect of Surfactant on Quality And Performance Attributes Of Topical Semi-Solids: *Submitted*

6. Dao HM, Parajuli S, Ureña-Benavides E, Jo S: Hemopressin Self-Assembly Fibril with pH and Ionic Strength Reversible Sensitive Surface Activity: *In Preparation*

7. Parajuli, S; Prater, LA; Heath, T; Green, K; Moyer, W; Ureña-Benavides, E. Improving Stability of Carbon Dioxide Foams and Emulsions in API Brine Using Cellulose Nanocrystals at High Temperature and Pressure. *In preparation*

CONFERENCE PRESENTATIONS

1. Parajuli, S. Interfacial and Molecular Interactions between Cellulose Nanocrystals and Surfactants in Brine and Responsible for Pickering Emulsion Stability. AIChE (2019), Orlando, FL.
2. Parajuli, S. Interfacial interactions between Cellulose nanocrystal and surfactants driving the stability of dodecane emulsions. ACS-Colloids and Surface Science Symposium, (2019), Atlanta, GA.
3. Parajuli, S. Cellulose nanocrystal stabilized emulsions in brine at high temperatures. Southern Schools in Chemistry and Engineering Conference (2018), Oxford, MS.
4. Parajuli, S. Surface and Interfacial Interactions in Dodecane/Brine Pickering Emulsions Stabilized by Combination of Cellulose Nanocrystals and Emulsion Stabilizers. ACS-Colloids and Surface Science Symposium, (2018), State College, PA.
5. Parajuli, S. Interfacial Interactions in Oil/Brine Emulsions Stabilized by Cellulose Nanocrystals and Emulsion Stabilizers. AIChE (2017), Minneapolis, MN.
6. Parajuli, S. Stabilization of oil/water interface by cellulose nanocrystals to prepare stable emulsions. Graduate Student Council Annual Research Symposium (2016), Oxford, MS.

PROFESSIONAL ACTIVITIES

Peer reviewer – Colloids and Surface A: Physicochemical and Engineering Aspects

SPECIAL SKILLS/PROFICIENCES

Atomic Force Microscopy	Material Science	Spectroscopy
Polymers	Surface chemistry	Rheology
Light Scattering	FTIR/UV-Vis	DSC/TGA
Colloidal Chemistry	Chromatography	Image Analysis
Project Management	Problem Solving	Scientific Writing
Mechanical characterization	Collaboration	Leadership

REFERENCES

AVAILABLE UPON REQUEST